EDDY FORCING OF THE MEAN CIRCULATION IN THE WESTERN NORTH ATLANTIC

Ellen Dunning Brown

B.A., Princeton University (1979)

SUBMITTED IN PARTIAL FULFILLMENT OF THE
REQUIREMENTS FOR THE DEGREE OF
DOCTOR OF PHILOSOPHY

at the

MASSACHUSETTS INSTITUTE OF TECHNOLOGY

and the

WOODS HOLE OCEANOGRAPHIC INSTITUTION

August, 1984

Signature of Author _____
Department of Earth, Atmospheric, and Planetary Sciences, Massachusetts Institute of Technology and the Joint Program in Oceanography, Massachusetts Institute of Technology/Woods Hole Oceanographic Institution, August, 1984

Certified by _____
Thesis Supervisor.

Accepted by _____
Chairman, Joint Committee for Physical Oceanography, Massachusetts Institute of Technology/Woods Hole Oceanographic Institution.

EDDY FORCING OF THE MEAN CIRCULATION IN THE WESTERN NORTH ATLANTIC

by

Ellen D. Brown

Submitted to the Joint Committee for Physical Oceanography,
Massachusetts Institute of Technology and
Woods Hole Oceanographic Institution, in August, 1984,
in Partial Fulfillment of the Requirements
for the Degree of Doctor of Philosophy

ABSTRACT

This thesis addresses several aspects of the problem of determining the effect of the low-frequency eddy variability on the mean circulation of the Western North Atlantic. A framework for this study is first established by scale analysis of the eddy and mean terms in the mean momentum, vorticity, and heat balances in three regions of the Western North Atlantic -- the northern recirculation, the southern recirculation, and the mid-ocean. The data from the last decade of field experiments suggest somewhat different conclusions from the earlier analysis of Harrison (1980). In the momentum balance we confirm that the eddy terms are negligible compared to the lowest order mean geostrophic balance. The eddy term may be an O(1) term in the vorticity balance only in the northern recirculation region where the mean flow is anisotropic.

In the mean heat balance, if the mean temperature advection is scaled using the thermal wind relation, then the eddy heat flux is negligible in the mid-ocean, but it may be important in the recirculation areas. For all the balances the eddy terms are comparable to or an order of magnitude larger than the mean advective terms. We conclude from the scale analysis that the eddy field is most likely to be important in the Gulf Stream recirculation region.

These balances are subsequently examined in more detail using data from the Local Dynamics Experiment (LDE). Several inconsistencies are first shown in McWilliams' (1983) model for the mean dynamical balances in the LDE. The sampling uncertainties do not allow us to draw conclusions about the long-term dynamical balances. However, it is shown that if we assume that the linear vorticity balance holds between the surface and the thermocline for a finite record, then the vertical velocity induced by the eddy heat flux divergence is non-zero.

The local effect of the mesoscale eddy field on the mean potential vorticity distribution of the Gulf Stream recirculation region is determined from the quasigeostrophic eddy potential vorticity flux. This flux is calculated by finite difference of current and temperature time series from the Local Dynamics Experiment. This long-term array of moorings is the only experimental data from which the complete eddy flux can be calculated. The total eddy flux is dominated by the term due to the time variation in the thickness of isopycnal layers. This thickness flux is an order of magnitude larger than the relative vorticity flux. The total flux is statistically significant and directed 217°T to the southwest with a magnitude of 1.57×10^{-5} cm/s^2.

The direction of the eddy flux with respect to the mean large scale potential vorticity gradient from hydrographic data indicates that eddies in

this region tend to reduce the mean potential vorticity gradient. The results are qualitatively consistent with numerical model results and with other data from the Gulf Stream recirculation region. We find that the strength of the eddy transfer in the enstrophy cascade is comparable to the source terms in the mean enstrophy balance. The Austauch coefficient for potential vorticity mixing is estimated to be $O(10^7 cm^2/sec)$. An order of magnitude estimate of the enstrophy dissipation due only to the internal wave field shows that other processes must be important in enstrophy dissipation.

The measured eddy potential vorticity fluxes are compared to the linear stability model of Gill, Green, and Simmons (1974). An earlier study (Hogg, 1984) has shown agreement between the empirical orthogonal modes of the data and the predicted wavenumbers, growth rates, and phase speeds of the most unstable waves. However, we show substantial disagreement in a comparison of the higher moments -- the eddy heat and potential vorticity fluxes. Because the critical layer of the model is located near the surface, the model predicts that most of the eddy potential vorticity and eddy heat flux should occur within about 300 meters of the surface. The data show much greater deep eddy heat flux than predicted by the model. It is suggested that the unstable modes in the ocean have a longer vertical scale because of the reduction in the buoyancy frequency near the surface.

The evidence for in situ instability is also examined in the decay region of the Gulf Stream from an array of current and temperature recorders. Although there is vertical phase propagation in the empirical orthogonal modes for some of the variables at some of the moorings, there is not much evidence for a strong ongoing process of wave generation.

Thesis Supervisor: W. Brechner Owens, Associate Scientist
Department of Physical Oceanography
Woods Hole Oceanographic Institution

Table of Contents

CHAPTER 1

INTRODUCTION

Much of the oceanographic research during the last decade has been directed towards understanding the importance of the mesoscale eddy field in the time-mean circulation. The term mesoscale eddy is defined here as the low-frequency variability at periods longer than one day. Even with more than a decade of field experiments, there has been little direct evidence that eddies contribute to the mean dynamical balances. Most of the data analyses have examined only the wave kinematics and energetics. The eddy statistics have been calculated from time series of current and temperature from moored arrays in the western North Atlantic deployed as part of the POLYMODE program. Analyses of data from these experiments (MODE, 1978; Schmitz, 1976, 1978; Dickson, 1983; Fu et al., 1982) have established only the general distribution of eddy energy and space-time scales. These studies show that the eddy energy level increases westward along 28°N from the center of the North Atlantic basin towards the Gulf Stream where it is comparable to the mean energy near the western boundary current. However, despite the intensity of the eddy field, the role of eddies in the dynamics of the mean circulation still has not been determined. In order to study this problem, it is necessary to first examine the magnitude of the eddy fluxes in the mean heat, vorticity, and momentum balances.

Several studies have suggested that the eddy momentum flux or Reynolds stress divergence may contribute to the mean momentum balance in certain geographic regions of the North Atlantic. Thompson (1977) postulated that the

convergence of momentum fluxes induced by topographic Rossby waves along the continental rise at 70°W could cause mean flow accelerations of 1 cm/sec over 10 days. Webster's (1965) analysis of the offshore flux of downstream eddy momentum in the surface Gulf Stream indicates a transfer of eddy to mean kinetic energy sufficient to double the mean kinetic energy in 21 days. Measurements (Schmitz, 1981) from the POLYMODE Array II moorings along 55°W show that the sign of $\overline{u'v'}$ changes from positive to negative as the Gulf Stream axis is crossed from the south. This meridional distribution of momentum fluxes would tend to accelerate the eastward Gulf Stream and might account for the observed downstream increase in transport. The observations are also consistent with the distribution of Reynolds stresses in numerical model experiments of the wind-driven circulation (Schmitz and Holland, 1982).

Although these types of comparisons based on Reynolds stress distributions suggest mean flow acceleration by the eddies, the net effect of the momentum flux distribution remains ambiguous because the fluxes can also produce an ageostrophic flow. This ambiguity can be most easily seen by examining the momentum equation for a zonally-averaged mean flow (denoted by an overbar). To zeroth order in a Rossby number expansion the mean flow is geostrophically balanced. The eddy Reynolds stress term $\overline{u'v'}$ enters the first order momentum balance:

$$\frac{\partial \overline{u_0}}{\partial t} - f\overline{v_1} = -\frac{\partial \overline{u'v'}}{\partial y}$$

where the subscripts denote the order in Rossby number expansion. Comparisons have been made between this balance and the locally zonal Gulf Stream along 55°W as measured in POLYMODE Array II although the analogy is not exact

because the observational data are time-averaged instead of zonally-averaged. From the Array II data a typical value for the Reynolds stress at 600 m depth is $\overline{u'v'} \sim 20\ cm^2/s^2$ and the eddy statistics vary over a length scale of about 300 km. A balance between the eddy divergence term and the mean flow acceleration would then imply a 21 cm/sec increase in the mean flow over a period of one year. This would have a substantial effect on the mean zonal transport. However, the eddy term could equally be balanced by a northward ageostrophic flow of only $\bar{v}_1 = .01$ cm/sec, a value which is below the significance level of present measurements. Although the vertically-integrated ageostrophic northward velocity must vanish over the basin, it is not possible to determine the effect of Reynolds stresses on the momentum balance from point measurements. Therefore, arguments about the effect of eddy Reynolds stresses on the Gulf Stream flow in this region remain speculative.

Budget analyses of mean and eddy kinetic and potential energy do not suffer from the type of ambiguity inherent in the momentum balance. Bryden (1982) calculated the balances from the current meter mooring array in the Local Dynamics Experiment located in the Gulf Stream recirculation region. For a 225 day period during the experiment he found a loss of eddy kinetic energy through an up-gradient flux of eddy momentum and a conversion of available potential energy to eddy potential energy by an eddy heat flux directed down the mean temperature gradient. The results are consistent with the production of eddy energy by baroclinic instability in the mean flow, although the combined energy conversion is not significantly different from zero. Moreover, these conversions do not indicate local energy exchange between the mean and eddy fields because they are not balanced by production of mean energy. The total effect of the eddy field on the mean energy balance cannot

be deduced from this type of analysis because the pressure-work terms cannot be estimated and because the eddy and mean energy conversions do not necessarily balance for open ocean regions within the model basin.

Because of the scarcity of observational data, ocean modelers have addressed the "eddy problem" by calculating mean and eddy balances from numerical eddy-resolving general circulation models. Eddy activity in these models has been evaluated using energy budgets (Robinson et al., 1977; Holland and Lin, 1975; Holland, 1978; Harrison and Robinson, 1978) computed as area-integrals over the model basins. Because the model flows are inhomogeneous, it is necessary to compute the energy budgets in subregions of the model balances, in order to identify regions where eddies may be transferring energy to the mean flow. Harrison and Robinson (1978) have shown that the conversions between the eddy and mean energy are meaningful only if the regions are chosen so that there is no divergence of eddy energy flux across the open boundaries. The eddy production of mean kinetic energy balances the conversion of mean kinetic to eddy kinetic energy only for regions where the flow satisfies this condition. Moreover, although the model results are useful for guiding the interpretation of ocean data, the direct application of these model studies is not clear given the dependence of the results on the specific model assumptions (Harrison, 1979).

More recent numerical studies (Holland and Rhines, 1980; Harrison and Holland, 1981) have concentrated on the dynamical role of eddies in the mean vorticity budgets. These models emphasize the importance of the eddy potential vorticity flux. The mesoscale eddies contribute to the mean vorticity balance through the potential vorticity flux - a combination of lateral momentum transfer and vertical pressure drag. According to the theory of

eddy-driven mean flows (Rhines and Holland, 1979), the direction of the eddy potential vorticity flux relative to the mean potential vorticity gradient indicates regions of growing or decaying eddy enstrophy. Holland and Rhines (1980) demonstrate this in their analysis of potential vorticity balances in a two-layer quasigeostrophic eddy resolving general circulation model. The model calculation shows that eddies gain energy by baroclinic instability from the mean flow in the Gulf Stream recirculation region of the upper layer. This conversion is characterized by a down-gradient flux of eddy potential vorticity. Because the model has no built-in stress between the fluid layers, the deep circulation is forced by the divergence of the eddy flux in the upper layer.

Experience with numerical model flows has shown that one must be cautious in interpreting point measurements of eddy fluxes. In Harrison and Holland's (1981) model, the magnitude of point estimates changed by as much as 100 percent when the averaging time was doubled from five to ten years. The spatial variation of the fluxes in the model of Holland and Rhines (1980) ranged from scales of O(100 km) for the relative vorticity flux to O(1000 km) for the thickness flux. Modelers have concluded from numerical experiments that these fluxes are statistically reliable only if they are area-integrated. At present, very little is known about the variation of these vorticity fluxes in the ocean. The only published observation (Harrison, 1980) is that the second order velocity statistics in POLYMODE Array II vary on spatial scales of O(100 km). Thus, part of the motivation for this analysis is to assess the reliability of eddy potential vorticity flux measurements in the ocean.

The first chapter of this thesis is a scale analysis of the mean and eddy terms in the time-mean momentum, vorticity, and heat balances in three

regions of the North Atlantic. A previous scale analysis (Harrison, 1980) of the mean dynamical balances indicated that the eddy term might be important only in the mean heat balance of the mid-ocean. Chapter 2 of this thesis is a detailed reexamination of this scale analysis using the more extensive data set available from the last ten years of POLYMODE experiments. We show that the eddy term may be lowest order in the vorticity balance of the northern recirculation region, where the mean flow has a short cross-stream length scale and large zonal speed. In the mean heat balance the eddy term is not important in the mid-ocean, but it may be a dominant term in the Gulf Stream recirculation region where the eddy heat fluxes are significant.

Chapter 3 of this thesis is a calculation of the eddy potential vorticity flux in the Gulf Steam recirculation region. As discussed above, recent theoretical models of the general ocean circulation have emphasized the effect of the eddy potential vorticity flux on the time-averaged vorticity field. Oceanic measurements of the eddy potential vorticity flux require long time series from an array of instruments which spatially resolves the mesoscale eddy field. The only data satisfying these requirements were recorded during the Local Dynamics Experiment in the Gulf Stream recirculation region. This region has been identified as a likely site for the generation of mesoscale waves through baroclinic instability of the mean flow. These measurements are used to estimate the flux of eddy potential vorticity and the conversion to eddy enstrophy from the large-scale vorticity field. The results are shown to be consistent with theoretical predictions of the potential vorticity flux due to unstable baroclinic waves.

The mean dynamical balances in the Local Dynamics Experiment are reexamined in Chapter 4. In particular, we show that a previous model (McWilliams,

1983) for the vertically-integrated mean vorticity balance is not consistent with the vertical velocity predicted by the mean heat equation. Our analysis suggests that although the eddy term does not seem important in the vorticity balance of the LDE, it may have an effect on the mean heat balance. While the sampling requirements prevent us from drawing conclusions about the long-term mean dynamical balances, the finite records are used to test the consistency of a linear mean vorticity balance.

The fifth chapter compares the predictions of a numerical stability model with the observed eddy potential vorticity and heat fluxes in the Array II region. A remarkable agreement has been shown previously by Hogg (1984) between the wavelengths, phase speeds, and growth rates predicted by a linear stability model of Gill, Green, and Simmons (1974) and the empirical orthogonal modes from the Array II data. However, the model predicts that the largest phase change and heat flux in the growing modes should occur at depths shallower than the instruments. We show that the surface intensification of the higher moments from the model is not supported by the observations. Since the vertical scale of the modes is proportional to the buoyancy frequency, the discrepancy may be due to the reduction in stratification near the surface.

Finally in Chapter 6 we discuss the vertical structure of the mesoscale eddy field in the Gulf Stream Extension Region located near 40°N, 45°W, downstream of the maximum velocities in the stream. The empirical modes are computed in frequency bands from the velocity and temperature cross-spectral matrix. Although there is upward phase propagation in some of the variables at a few of the moorings, there is not much evidence for strong in situ wave generation.

The eddy-mean flow problem is the uniting theme of the chapters of this thesis. The problem is examined from the standpoint of the mean dynamical balances and from the potential vorticity flux and its importance in stability theory. Over the last decade it has become clear that the meager observational base is insufficient to clearly establish direct eddy forcing of the mean circulation. Although the present observational data are nowhere sufficient to solve the "eddy problem", the topics addressed in this thesis imply that eddies do have a significant effect on the time-mean flow in the Gulf Stream recirculation region.

CHAPTER 2

SCALE ANALYSIS REVISITED: THE EDDY TERMS IN THE MEAN DYNAMICAL BALANCES

2.I. INTRODUCTION

A primary objective of research on oceanic eddies is to assess their effects on the mean dynamical balances. Since the data base is inadequate to fully answer this question, scale analysis has been used to estimate the relative importance of the eddy terms. Harrison (1980) examined the magnitude of the eddy terms in the quasigeostrophic mean momentum, vorticity, and heat balances using scale estimates from the MODE and POLYMODE I and II mooring array data sets. Two flow regimes were considered -- a near field of the Gulf Stream between 35°N and 38°N along 55°W a few hundred kilometers south of the stream axis and a mid-ocean region along 28°N to the east of 70°W. He concluded from these data that the eddy terms are at least an order of magnitude smaller than the mean contributions to the momentum and vorticity balances in both regions. In the mean heat balance the eddy heat flux divergence was found to be a dominant term only in the mid-ocean. Although there were large uncertainties in the scale estimates, this initial study concluded that the eddy terms are not important in the mean dynamical balances in most regions of the ocean.

Much additional data have been collected from the North Atlantic during the last five years since the experiments used in Harrison's analysis. Therefore, it seems timely to review the scale estimates after a full decade of field research. Because of instrumentation difficulties there still has not

been an array of moorings deployed in the most intense part of the Gulf Stream. Therefore, this analysis is again limited to the near field and mid-ocean regions. However, the new data suggest that the three mean dynamical balances -- momentum, vorticity, and heat -- should be evaluated in three distinct oceanic flow regimes. This chapter examines the magnitude of the eddy terms in each of these balances for each of these regions.

The majority of the instrument arrays have returned data from the largest geographical flow regime, the gyre interior. Data arrays from this region include MODE, POLYMODE I, and the southernmost mooring (07) from POLYMODE II which were examined by Harrison (1980). Since that time, the geographic variation in the mid-ocean mean and eddy energy has been further explored in the POLYMODE Array III Clusters A and B deployed eastward along 28°N from the site of Array I (Figure 2.1). These clusters were located on the flanks of the Mid-Atlantic Ridge at 28°N, 48°W (Cluster A) and 27°N, 41°W (Cluster B) from May 1977 to May 1978 with an additional 16 months from the site moorings. All of these data suggest that throughout the mid-ocean the eddy and mean energy are comparable. The mean flow has a broad length scale which is also comparable to the scale of variation of the eddy statistics.

A second distinct flow regime has been identified in data from POLYMODE Array II along 55°W between 35°N and 38°N. The mean position of the Gulf Stream at this longitude is approximately 200 km from the northernmost mooring with instruments at thermocline depth. Two characteristics of the mean flow in this region may have important consequences for the mean dynamical balances. First, the Array II measurements and the float data from this Gulf Stream recirculation region show an anisotropic mean flow with bands of intense zonal flow in reversing directions. It has been suggested (Schmitz, 1976) that

eddies drive the westward recirculating flow in this region south of the Gulf Stream. Therefore, for the scale analysis it is necessary to include the anisotropy of the mean flow in order to obtain correct estimates for each dynamical balance. The second important characteristic of this region is the presence of baroclinic instability of the mean flow (Hogg, 1984). The eddy heat fluxes generated by the instability process could have an important effect on the mean heat balance. In quasigeostrophic numerical models (Harrison, 1980) the vertical velocity in the recirculation region is driven by the divergence of the eddy heat fluxes. Although the scale analysis cannot prove that either of these processes occurs, it is useful to check their plausibility.

The third region identified in this chapter as a distinct mean flow regime contains the POLYMODE Local Dynamics Experiment (LDE) (31°N, 69.5°W). Like Array II the LDE was deployed in the Gulf Stream recirculation region, but some characteristics of the mean flow are significantly different. The eddy heat fluxes are comparable to those observed in Array II, but the mean flows are more nearly isotropic and less intense. The eddy field is also less energetic by almost a factor of 3. When compared to the Array II data, one would be inclined to categorize the LDE as part of the mid-ocean regime. However, the LDE is also distinctly different from the MODE region located only 300 km to the southwest (28°N, 70°W). The eddy field in the LDE is a factor of 3 more energetic than that in the MODE data. This is true for the LDE record averages as well as for the period excluding the intense baroclinic jets (Owens et al., 1982). In addition, the heat fluxes in the LDE are significantly non-zero, unlike those in the mid-ocean. Because the LDE data differs from both the Array II and mid-ocean observations, it is identified as a third distinct flow regime.

The other data set, the Gulf Stream Extension (GSE), discussed later in this thesis (Chapter 6) was centered at (40°N, 45°W), downstream of the maximum Gulf Stream surface velocities. The GSE measurements show some similarities to the PMII data. For example, the eddy kinetic energy and its spatial decay are comparable in both regions. The eddy heat fluxes in the GSE are also comparable but with large statistical uncertainties. However, the GSE region differs from the Array II region because the mean flow is not well determined. It is unclear from the available surface drifter and satellite data whether the Gulf Stream at this location is a broad system of branching currents or an unstable jet which meanders around the Grand Banks. Although the GSE array does not resolve the mean flow in this region, it provides scale information about the eddy field. Thus, the data from the GSE will be used only to compare the magnitude of the eddy contribution in the balances.

Additional data from surface drifters (Richardson, 1983) and SOFAR floats (Owens, 1984) provide a check on several of the scale parameters from the current meter array data. The float data give better areal coverage than the point measurements, although the spatial averaging necessary to achieve statistical reliability limits their use in this study. Since the float data are averaged into bins over several degrees of latitude and longitude to reduce the statistical uncertainty, they do not resolve length scales smaller than a few hundred kilometers. However, the float data still provide a useful check on the scales for the velocities and for the variation in eddy kinetic energy.

This chapter reassesses the scale estimates of the mean dynamical balances in light of these new data sets. Since the purpose of this analysis is to evaluate the in situ effect of the eddy field, only scale estimates from

the thermocline and shallower depths will be discussed. The moorings in Cluster A were instrumented with current meters only at 200 and 1500 m depth, while the other data summarized here are from 500 to 600 m depths. We caution that topography can have a large effect on both the mean and eddy fields. In Clusters III A and B, for example, there is a striking decrease in deep eddy kinetic energy over rough topography. Therefore, the conclusions of this chapter pertain only to thermocline flow fields where the eddy kinetic energy is maximum in depth and where processes like baroclinic instability will have the largest signature.

The following three sections of this chapter contain the scale analysis for the mean momentum, vorticity, and heat balances. For each balance the three regions are discussed in separate sections. For each region the dynamical balance is first scaled, then the regional data is examined to chose the proper scale parameters, and finally the balance is evaluated.

2.II. THE MEAN MOMENTUM BALANCE

(A) The Mid-Ocean

In order to facilitate comparison with Harrison's (1980) estimates, the same notation will be used here for scaling the momentum and vorticity balances. The scale parameters for each term in the mean momentum equation for the mid-ocean are shown in the first column of Table 2.1(a). The momentum scaling requires two velocity parameters -- the scale u_o for the eddy field and U_o for the mean flow. The eddy velocity scale will be estimated from the rms eddy kinetic energy assuming that the correlation coefficient between the eddy velocity components is O(1). Appendix A, Tables A.1 and A.2 show that in Array I and Cluster III B $\overline{u'^2} > \overline{v'^2}$, while in Cluster III A $\overline{v'^2} > \overline{u'^2}$. In

most of these cases, the difference in energy is less than a factor of two, so the difference in rms zonal and meridional velocity scales is even smaller. Thus we use the rms average eddy kinetic energy $\sqrt{(u_0^2)}$ to scale the eddy velocity. The ratio of eddy to mean terms (Table 2.1(b), column 1) shows that the important velocity scales are the ratio u_0/U_0 and the value of u_0.

In addition to the velocity scales, two length scales are necessary: the horizontal scale (L) for the mean flow and the scale of variation ($\mathcal{L}$) for the quadratic eddy velocity statistics. In general, $\mathcal{L}$ will differ from the scale of individual eddies and from the mean length scale. The ratios in Table 2.1(b), column 1 depend on the ratios of length scales ($L/\mathcal{L}$) and on the value of the scale of variation .

The mid-ocean velocity and length scales from POLYMODE Array III Clusters A and B (Appendix A) do not differ much from the earlier data at thermocline depths. From the earlier measurements Harrison (1980) chose to evaluate the ratios of eddy to mean terms with the ratio $u_0/U_0 = O(10)$ and the value u_0 = 1-7 cm/sec. The more recent measurements from PM III show eddy and mean velocity scales in the thermocline that are comparable to the Array I and MODE values. Fu et al. (1982) report that the eddy kinetic energy at 500 m decreases eastward along 28° N from 40 cm^2/sec^2 at MODE Center (68°W) to 9 cm^2/sec^2 at POLYMODE Array I (55°W). The eddy kinetic energy then increases again to 36 cm^2/sec^2 at 41°W in Cluster B. Thus we have chosen a typical value of 30 cm^2/sec^2 for the eddy kinetic energy u_0^2 in the mid-ocean as listed in Table 2.2, column 1. Harrison reported mean speeds of typically 1 cm/sec from the gyre interior between 70°W and 40°W along 28°N. The mean velocity from the PM III arrays is also about 1 cm/sec, although individual

record means may be up to a factor of seven larger. The length scale of variation of the mean fields in the gyre interior is about L = 1000 km. In Figure 2.2 the eddy kinetic energy has been plotted along 28°N from MODE Center, MODE East, PMI, and PMIII A and B. This figure shows that the eddy kinetic energy also varies over a broad spatial scale. Thus, as shown in Table 2.2, column 1, both the mean and the eddy length scales are taken to be $L = \mathcal{L} = 1000$ km in the mid-ocean.

The evaluated ratios of eddy to mean terms in the mid-ocean mean momentum balance are given in Table 2.3, column 1. For this balance our conclusions are basically the same as in Harrison (1980). The eddy term is an order of magnitude larger than the mean advective term. However, since the ratio of the eddy term to the Coriolis term is only .004, the eddy term has negligible effect on the mean geostrophic balance. Although the horizontal pressure gradient cannot be directly estimated, we assume that it balances the Coriolis term because the other terms in the momentum balance are much smaller.

2.II. (B) POLYMODE Array II

The scaling for the zonal and meridional mean momentum balances in the Array II region are tabulated in the second column of Table 2.1(a). Since the mean flow in the Array II region is anisotropic, it is necessary to identify both a zonal (L_x) and a meridional (L_y) length scale in addition to different scales for the zonal U_o and meridional V_o velocity components. The observational data do not suggest anisotropic scaling for the eddy field. Appendix A shows that in Array II $\overline{u'^2}$ is greater than $\overline{v'^2}$ by less than a factor of two, so the eddy velocity component scales are comparable. In the second column of Table 2.1(b) the relative importance of the eddy term depends on the

ratios of scales u_o/U_o, u_o/V_o, $L_x/\mathcal{L}$, and $L_y/\mathcal{L}$ for an anisotropic flow instead of u_o/U_o and $L/\mathcal{L}$ for an isotropic flow. Since these sets of ratios can be significantly different, the importance of the eddy term may be underestimated in the Array II region by scale estimates for an isotropic flow. Moreover, the errors are compounded in evaluating the ratios in Table 2.1(b).

To evaluate the ratios in Table 2.1(b), column 2 we require observational estimates for the anisotropic velocity and length scales of the mean flow along 55°W. Figure 6 from Owens (1984) shows the record average of the three settings of current meters at 600 and 1500 m depth (Schmitz, 1980). A typical half width for the peak amplitude of the mean zonal flow is ~ 100 km. Richardson (1984) has presented a comprehensive intercomparison of the zonal velocity field from the Array II data with several years of float data from this region. The float data were treated like Eulerian measurements and averaged into bins over one degree of latitude and 10 degrees of longitude. The average direction of the surface floats is 93°T, so the surface flow along 55°W is directed nearly to the east. Although the measurements were made at different time periods, the subsurface float measurements like the current meter data show a narrow zonal jet flanked by two countercurrents. Thus the float data give independent confirmation that the zonal Array II data is representative of the long-term mean flow in this region. From the current meter measurements the scale parameters are chosen to be L_y = 100 km and U_o = 5 → 9 cm/sec.

If the flow across 55°W is purely zonal, then the advective terms in the mean balances are zero. A recent analysis (Richardson, 1983) of surface drifter data clearly shows that in the near field of the Gulf Stream the mean meridional speeds are an order of magnitude smaller than the zonal speeds.

However, we do not assume that the flow is strictly zonal because the current meter data show a typical mean meridional speed of V_0 = 2 cm/sec. The downstream length scale (L_x) is estimated to be at least 500 km from the mean velocity vectors from surface drifters plotted in Richardson (1983), Figure 8.

The eddy scales in the ratios in Table 2.1(b) are the eddy kinetic energy u_0^2 and its length scale of variation. Appendix A shows that for the Array II data from the thermocline the eddy kinetic energy for the composite record is $u_0^2 = 200\ cm^2/sec^2$ as listed in Table 2.2. The estimates of the near field length scale ($\mathcal{L}$) for the variation in eddy velocity statistics suggest a value of 300 km in both the meridional and zonal directions. The meridional variation is shown in Figure 8 from Owens (1984) of eddy kinetic energy from SOFAR float data plotted along 55°W together with the current meter data from Array II. The half-width for the peak amplitude is $\mathcal{L}$ = 300 km at both thermocline and deeper depths. Data analyzed from surface drifters along 65°W (Richardson, 1983) also suggest a 300 km e-folding scale for eddy kinetic energy.

The zonal variation in eddy kinetic energy can be estimated from the GSE mooring array data. Figure 2.2 shows the thermocline eddy kinetic energy from the GSE array plotted as a function of longitude and the Array II data plotted as a function of latitude. The horizontal scale is a mercator projection so that the two axes have the same scale in kilometers. Although the eddy kinetic energy variation in the GSE array might be related to the local topography, the zonal length scale is comparable to the meridional scale. Since the moorings in the GSE array were not located at the same latitude, there is some spread among the points. However, it is clear that the zonal GSE data curve has the same slope and amplitude as the meridional 55°W data. Thus, the recent

data from regions close to the Gulf Stream support Harrison's choice of $\mathcal{L}$ = 300 km for the scale of variation in quadratic eddy statistics.

With the substitution of these observed scales in the ratios of Table 2.1(b), column 2, we obtain the values in Table 2.3, column 2. Each of the ratios of eddy to mean terms in the mean momentum balance is at least an order of magnitude larger than Harrison's (1980) estimates shown in Table 2.3, column 3. The eddy term is comparable to or larger than the mean advection term. However, the eddy term in the Array II momentum balance signifies only a 4 percent deviation from the mean geostrophic zonal balance. Thus, the eddy term is probably not important in the lowest order momentum balance for the Array II region.

2.II. (C) LOCAL DYNAMICS ARRAY

The scaling of the mean momentum balance in the LDE region is problematic because the array does not resolve the mean length scales. Since there is no evidence for choosing anisotropic scales and since the observed zonal and meridional mean speeds are comparable, the LDE balances (Table 2.1(a,b), column 1) are scaled like those for the mid-ocean. The mean and eddy variation length scales must be inferred from other observations. McWilliams' (1983) 200 km mean length scale based on schematic flow diagrams will be used in this analysis. We estimate the spatial scales of variation in the eddy kinetic energy to be about 300 km because the LDE eddy field is a factor of three more energetic than that observed during the MODE experiment 300 km to the southeast (28°N, 69.6°W). The mean speeds at 600 m depth are 2 cm/sec for both the zonal and meridional components and the eddy kinetic energy is approximately

80 cm^2/sec^2. From these observations we scale the LDE balance using L = 200 km, $\mathcal{L}$ = 300 km, U_o = 2 cm/sec, and u_o^2 = 80 cm^2/sec^2 as shown in column 4 of Table 3.

The eddy field in the LDE region is less energetic than that in Array II but more energetic than in the mid-ocean. In Figure 2.2 the LDE eddy kinetic energy is plotted at 70°W. Although the LDE data is from nearly the same latitude (30°N) as the mid-ocean data (28°N), it is significantly more energetic. In this sense, the LDE represents a transition between the more energetic recirculation region measured in Array II and the less energetic mid-ocean region. However, even though the LDE region is less energetic than the Array II region, the choice u_o/U_o = O(1) would still underestimate the eddy effect by nearly a factor of five. The assumption that eddy and mean energies are comparable near the Gulf Stream was based in part on data from ship drift measurements like Wyrtki et al. (1976). A more recent analysis of data from surface drifting buoys (Richardson, 1983) demonstrates that the spatial averaging of these measurements over scales comparable to the eddy length scale causes an underestimate in near field eddy kinetic energy. The order of magnitude value u_o/U_o = O(1) now appears to be based on an underestimate of the eddy energy.

The ratios of eddy to mean terms in the momentum balance from the LDE data (Table 2.3, column 4) give the same results found for Array II. The eddy term may be an order of magnitude larger than mean advection, but the dominant mean balance remains geostrophic.

2.III. THE MEAN VORTICITY BALANCE

(A) The Mid-Ocean

The scaling for the mean vorticity balance (Table 2.4(a,b)) differs from the momentum balance only by a length scale. Direct estimates of the mean terms in this balance can be made only for the planetary and mean advection terms which depend on horizontal velocity and length scales. It is not possible to estimate the vortex stretching term fw_z because the vertical velocity cannot be measured for low-frequency motion. Thus, this analysis must concentrate on comparison of the eddy terms with $\beta\bar{v}$ and $\bar{u} \cdot \nabla\bar{\zeta}$. Nonetheless, some conclusions are still possible about the dominant balance of terms even without direct scale estimates of the magnitude of vortex stretching.

Harrison (1980) scaled the vertical velocity from the continuity equation but allowed the flow to be horizontally non-divergent to order γ by writing $w = \gamma U_0 H/L$. The value of γ was inferred from the lowest order vorticity balance by scale analysis. In both the near field of the Gulf Stream and the mid-ocean regions it was found that the linear, geostrophic vorticity balance dominated:

$$\beta\bar{v} = f \frac{\partial \bar{w}}{\partial z} .$$

Traditional arguments about the size of the mean vertical velocity imply that the vortex stretching will have the same scale as the planetary advection or as the mean advection of vorticity. Whether these two mean terms are also the same magnitude depends only on the length and velocity parameters of the mean flow. For a mean velocity field that is horizontally non-divergent to within order Rossby number (R_0) the vertical velocity scales as:

$$\bar{w}_{ro} = \frac{R_0 U_0 H}{L}$$

where $R_o \equiv U_o/f_oL$ and H is the mean depth scale. The stretching term will then scale like the mean advection of vorticity. In the interior ocean, however, the mean advection of vorticity is small compared to planetary advection. A lowest order linear vorticity balance between vortex stretching and planetary advection would require that the vertical velocity be scaled like:

$$\bar{w}_{ge} = \frac{\beta H U_o}{f_o} \quad .$$

This scaling implies that the ratio of w_{ge} to w_{ro} is equal to the ratio of planetary to mean advection $\beta L^2/U_o$. In the mid-ocean where the mean flow is weak and broad the vertical velocity may be several orders of magnitude larger than the Rossby number.

The consistency of these scale arguments must be verified if there is an induced vertical velocity due to flow across topographic contours. Wunsch (1984) and Bryden (1980) have suggested that these contributions can invalidate the vertically integrated Sverdrup balance between the northward planetary advection and the wind stress curl. Furthermore, the magnitude of the vortex stretching term must also be consistent with the vertical velocity in the mean heat balance. The magnitude of the vertical velocity implied by the lowest order vorticity and heat balances and from topographic forcing will be compared in section V.

The ratios of eddy to mean terms in the mean vorticity balance for the mid-ocean are given in the first column of Table 2.5. In the vorticity balance like in the momentum balance, the eddy term is an order of magnitude larger than the mean advection term. However, planetary advection is the dominant term and it must be balanced by vortex stretching if there is to be a lowest

order balance. From these estimates we conclude like Harrison (1980) that in the mid-ocean the eddy term probably does not upset the linear vorticity balance.

2.III. (B) POLYMODE Array II

The scaling for the vorticity balance in the Array II region is given in the second column of Table 2.4(a,b). The vortex stretching term can be scaled by assuming a balance with planetary advection (βV_o). Alternatively, if the vertical velocity is scaled by the Rossby number, then there are two different Rossby numbers:

$$R_{ox} = \frac{U_o}{f_o L_y} \qquad \text{and} \qquad R_{oy} = \frac{V_o}{f_o L_x} \quad .$$

for the zonal and meridional balances. For the observational scales in Array II (Table 2.2, column 2) $R_{ox} = .01$ and $R_{oy} = .001$ are assumed to be sufficiently small parameters for the quasigeostrophic approximation to remain valid. With these Rossby numbers the vertical velocity scaling is given by

$$\bar{w}_{ro} = \max\left[R_{ox} \frac{U_o H}{L_x} , R_{oy} \frac{V_o H}{L_y} \right] .$$

The stretching term would then be the same order as the mean advection of relative vorticity. Thus for the anisotropic case as well as the isotropic case, the vortex stretching term could be the same order as the planetary or mean advection terms.

Our scale estimates for the vorticity balance in Array II are evaluated in Table 2.5, column 2 and compared to Harrison's (1980) results in column 3. We find that the eddy term is in each comparison an order of magnitude larger

than estimated by Harrison. All three terms -- the eddy relative vorticity flux divergence, the planetary vorticity, and the mean advection of relative vorticity -- could be important in the lowest order vorticity balance. The eddy term is comparable to mean advection of vorticity and it is 60 percent of planetary advection. Verification of the magnitude of this term, however, must await direct measurements of the eddy relative vorticity flux and its spatial variation. Since these estimates are only based on scale analysis, it is possible that the divergence terms have been overestimated. However, these data suggest that both the eddy term and the mean advection terms are significant in the mean vorticity balance in the Array II region.

2.III. (C) LOCAL DYNAMICS ARRAY

The scaling for the vorticity balance in the LDE (Table 2.4(a), column 1) is identical to that for the mid-ocean and the scale parameters have already been discussed for the momentum balance. From the LDE data we can calculate the eddy relative vorticity flux (Chapter 3) and the associated error directly so that there is more confidence in this scale estimate. The eddy term scale estimate based on the eddy kinetic energy $u_o^2 = 80$ cm^2/sec^2 and the length scale $\mathcal{L} = 300$ km agrees with the measured eddy relative vorticity flux $O(10^{-6}$ cm/sec$^2)$. The divergence should be smaller by a factor of $1/\mathcal{L}$. The last column of Table 2.5 shows the evaluated ratios of the eddy to mean terms for the LDE data. The eddy term is less important compared to βv in the LDE than in Array II because of the lower eddy kinetic energy. However, in the LDE, since $U_o/\beta L^2$ is small, the eddy term is an order of magnitude larger than the mean advection of vorticity. The scale analysis suggests that the linear vorticity balance holds in the LDE region as well as in the mid-ocean.

In these regions the eddy term is not important because the mean flow is isotropic and both the mean and eddy fields are less energetic than in Array II.

2.IV. THE MEAN HEAT BALANCE

The terms in the heat balance are particularly difficult to evaluate because of the uncertainty in the observational data. Harrison (1980) scaled the equations directly by estimating the horizontal (θ_0) and vertical (T_0) mean temperature variations. The eddy heat flux was scaled with the eddy velocity (u_0), the horizontal eddy temperature variation (θ'_0), and the correlation coefficient (C_T) between the two variables. With this type of scaling shown in the third column of Table 2.6, the ratios of eddy to mean terms depend on the ratios of u_0/U_0, $L/\mathcal{L}$, θ'_0/θ_0, and θ'_0/T_0. Although this type of scaling emphasizes the relative order of magnitudes of the eddy and mean variables, it tends to obscure the uncertainties in the ratios.

The horizontal temperature scales θ_0 and θ'_0 in the mean horizontal temperature advection and eddy heat flux divergence are very difficult to estimate from experimental data. For this reason, there are several differences in our scale analysis of the mean heat balance. First, in section 2.II it was shown that the mean momentum balance is geostrophic to within 4 percent in both the near field and mid-ocean. If the mean flow is both geostrophic and hydrostatic, then the mean horizontal temperature advection term can be re-written using the thermal wind relation and evaluated from the mean velocity scale U_0 which is more easily evaluated than the horizontal mean temperature variation θ_0. Second, the eddy heat flux divergence term will be scaled with the observed heat fluxes and the length scale of variation of eddy statistics introduced in section 2.II. Although the length scale $\mathcal{L}$ pertains to the

variation in eddy kinetic energy, the observational data do not indicate that the eddy heat fluxes vary over a significantly different scale. The third difference between this analysis and the previous one is in the scaling of the vertical temperature advection. The discussion of the vortex stretching term in the vorticity equation showed that the vertical velocity can be scaled assuming either a field which is of order Rossby number (w_{ro}) or in geostrophic balance (w_{ge}). These alternatives for w are listed in Table 2.6. Whether either of these is the proper scaling will be determined by requiring that there be a lowest order balance in the mean heat equation.

2.IV. (A) The Mid-Ocean

With these chosen scale parameters the terms in the mean heat balance for the mid-ocean are tabulated as in the first column of Table 2.6. Mean horizontal temperature advection depends on the mean kinetic energy U_o^2, the mean vertical scale H, and the constants f_o, g, and α. The constant α is the parameter relating temperature and density fluctuations according to:

$$\rho = \left(\frac{\partial \rho}{\partial T} + \frac{\partial \rho}{\partial S}\frac{dS}{dT}\right)T = -\alpha T \ .$$

The variation of density with temperature for typical oceanic salinities is of order 10^{-4}gm/(cm^3°C) as shown in Appendix A, Table V of Neumann and Pierson (1966). The variation due to salinity is an order of magnitude smaller. Thus, it will be assumed that $\alpha = 1 \times 10^{-4}$gm/(cm^3°C) for all the balances evaluated herein.

Scaling the mean vertical temperature advection term involves a choice since w again is not known. If there is a linear vorticity balance, then vertical temperature advection is of order $U_o \beta T_o / f_o$ where T_o is the

amplitude of mean vertical temperature variations. Rossby number scaling for vertical velocity gives a vertical advection differing in magnitude from the previous scaling by the factor $U_0/\beta L^2$. It will be necessary to compare the magnitudes of the vortex stretching term in the vorticity balance and the vertical temperature advection in the heat balance in order to check the consistency of the vertical velocity estimates.

The observed values of the mean vertical temperature amplitude T_0 and the eddy heat flux $\overline{u't'}$ at mid-thermocline depths in the mid-ocean are given in Table 2.7, column 1. In the Clusters A and B and Array I mooring data only one of the correlation coefficients between a velocity component and temperature is statistically significant at the 90 percent level. A typical value for the eddy heat flux in the mid-ocean (Appendix A) is .1°C cm/sec, although the range of values is as much as two orders of magnitude larger in one nine month record (Array I, mooring 549). The mean temperature is varies from 14°C to a maximum of 18°C at 200 m depth in Cluster A (28°N, 48°W). To evaluate the mean heat balance in mid-ocean we use the scale parameters $\overline{v't'}$ = .1°C cm/sec and T_0 = 14→18°C.

The magnitude of the terms in the mean heat equation evaluated with these scales are given in the first column of Table 2.8. The terms have not been evaluated as ratios of eddy to mean terms because of the possible uncertainties. For the mid-ocean, the values in the first column suggest that the eddy term is negligible compared to the lowest order balance between mean horizontal and vertical temperature advection. This type of balance was used by Bryden (1980) to calculate the vertical velocity from the mean horizontal advection using the thermal wind relation. In the mid-ocean the eddy heat flux

correlation coefficients are small so the eddy term does not contribute to the lowest order balance.

These results differ from those of Harrison (1980) who found the eddy term to be comparable to both mean horizontal and vertical temperature advection in the mid-ocean. Those scale estimates from the POLYMODE Array I data (Spencer et al., 1979) are listed in Table 2.7, column 2. The reason for our different conclusions is not immediately apparent. Both the eddy heat flux divergence ($.1 \rightarrow .4 \times 10^{-8}$°C sec^{-1}) and the mean horizontal temperature advection (2×10^{-8}°C sec^{-1}) from the values in column 2 are comparable to our estimates. However, Harrison's (1980) result is based on the ratio of the eddy term to the mean horizontal advection or in terms of his scaling:

$$c_T(\frac{u_o}{U_o})(\frac{L}{\mathcal{L}})(\frac{\mathcal{O}_o}{\theta_o}) \ .$$

This ratio was found to be equal to 1 using $c_T = .1$, $u_o/U_o = O(10)$, $L/\mathcal{L} = O(1)$, and $\mathcal{O}_o/\theta_o = O(1)$. The values in Table 2.7, column 2 show that these ratios are both smaller ($u_o/U_o = 1 \rightarrow 7$ and $\mathcal{O}_o/\theta_o = .3$ at 500 m) so that the ratio of the eddy term to the mean horizontal temperature advection should be $.03 \rightarrow .21$ instead of order 1. Thus, the difference in our conclusions seems related to the compounded errors in overestimating these ratios.

2.IV. (B) POLYMODE Array II

The scaling of the mean heat balance for Array II (Table 2.6, column 2) incorporates the anisotropy of the mean scales in the mean horizontal and vertical temperature advection. The parameters for evaluating these estimates are given in column 3 of Table 2.7. In Array II the heat fluxes are large,

but so are the associated errors. Only the two moorings closest to the Gulf Stream axis measured significant correlation coefficients for the eddy heat fluxes. Typical values for the heat flux ($\overline{v't'}$ = 2 → 9 °C cm/sec) and its divergence are comparable to those in Harrison's (1980) analysis.

From these estimates we conclude that all three terms -- the mean horizontal and vertical advection of temperature and the eddy heat flux divergence -- may be of the same order in the mean heat balance (Table 2.8, column 2) for Array II. This conclusion differs from Harrison (1980) who found that in the Array II region the eddy heat flux divergence was an order of magnitude less than the mean horizontal temperature advection. Harrison evaluated these ratios using the values listed in Table 2.7, column 4 from Fuglister's (1960) atlas and Tarbell et al. (1978). We estimate from scaling by the thermal wind relation that the mean horizontal temperature advection is of order 10^{-7} °C sec^{-1}. Harrison's scaling would predict that this term is an order of magnitude larger using the parameters:

$U = 5 \rightarrow 10$ cm/sec

$L = 100$ km

and $\theta = 2°C$ at 500 m.

This is not consistent with the turning of the mean velocity vector in the Array II moorings between 600 and 1000 m depth. From the average turning of about .1 radian and the average speed of 7 cm/sec, the mean horizontal temperature advection is $O(10^{-7}$ °C $sec^{-1})$. If the mean horizontal advection were an order of magnitude larger, the mean velocity vector would turn through a 60 degree instead of a 6 degree angle between the two depths. Thus we conclude that in the Array II region the eddy heat flux term is the same order of magnitude as the mean horizontal and vertical temperature advection.

2.IV. (C) LOCAL DYNAMICS ARRAY

Since the mean flow is assumed to be isotropic in the LDE region, the scaling of the mean temperature balance (Table 2.6, column 1) is the same as in the mid-ocean. Unlike the mid-ocean, however, the meridional thermocline eddy heat fluxes are significant with larger correlation coefficient than in the Array II data. The scale estimates for the mean heat balance are evaluated using the mean temperature scale $T_o = 15°C$ and the array average meridional heat flux at 700 m, $\overline{v't'} = 2°C$ cm/sec. The lowest order balance at thermocline depth in the LDE (Table 2.8, column 3) is between the mean vertical temperature advection and the eddy heat flux divergence. The mean horizontal temperature advection may also be important although the scale analysis suggests that it is a factor of two smaller. These scale estimates are verified in Chapter 4 by direct computation of the mean advection and eddy terms from the LDE data.

2.V. SUMMARY AND CONCLUSIONS

Because the new data do not suggest radically different scale parameters, it is surprising that some of the results differ significantly from those of Harrison (1980). In part this is a reflection of the possible errors in the scale parameters and especially in the ratios of these quantities. In the momentum balance (Table 2.3) for all three regions, the eddy terms are not likely to upset the mean geostrophic momentum balance although they may be comparable to or larger than mean advection. The importance of the eddy term relative to the Coriolis term decreases in the less energetic mid-ocean region, while it increases relative to mean advection. In the vorticity balance (Table 2.5) the eddy term is negligible compared to βv except in the Array II

region where both the eddy term and the horizontal advection of vorticity may also be important. The eddy term in the LDE and mid-ocean regions is an order of magnitude larger than mean advection. This reflects the increase in mean length scale and decrease in mean velocity scale in these two regions compared to the Array II region.

Our conclusions from the mean heat balance differ in all regions from the previous scale analysis. In the mid-ocean the eddy term is negligible so that the mean horizontal temperature advection balances vertical temperature advection. Vertical velocity can then be estimated using the thermal wind relation from the turning of the velocity vector with depth. In the Array II and LDE regions the eddy heat flux divergence may be comparable to both mean horizontal and vertical advection at thermocline depth. The vertical velocity in all three regions is consistent with a scaling based on the linear vorticity balance while Rossby number scaling underestimates the mean vertical temperature advection by several orders of magnitude in the mid-ocean and LDE regions. In Array II the vertical velocity scale w_{ro} is more nearly equal to w_{ge} because the ratio $\beta L^2/U_o$ approaches one. The magnitude of the vertical velocity $w = 10^{-4}$ cm/sec based on geostrophic scaling is consistent with both the vorticity and heat balances in all three regions.

We conclude from these scale estimates that the thermocline eddy field should not affect classical mid-ocean dynamics. The linear vorticity balance should remain valid and the mean temperature balance will be between mean horizontal and vertical temperature advection. In the Array II region the eddy terms as well as the mean advective terms are not negligible in the mean vorticity and heat balances. The scale estimates suggest that the divergence of the eddy relative vorticity flux $\overline{u'\zeta'}$ may be the same order as planetary

advection and mean advection of vorticity in the mean vorticity balance. The eddy term may also be important in the mean heat balance of this region where significant eddy heat fluxes are generated by baroclinic instability of the mean flow. The balances in the LDE region show some similarity to both the Array II and mid-ocean regions. In the LDE region like in the mid-ocean the linear vorticity balance should not be upset by either the eddy term or by mean advection of vorticity. However, both the eddy heat flux divergence and the mean horizontal temperature advection may be significant in the mean heat balance. These conclusions are significantly different from the previous scale analysis. They suggest that eddies are most likely to have an effect on the mean dynamical balances of the Gulf Stream recirculation region.

TABLES AND FIGURES

Figure 2.1: Western North Atlantic map showing the locations of the arrays referred to in this paper: (MODE) Mid-Ocean Dynamics Experiment, (LDE) Local Dynamics Experiment, (PMI) POLYMODE Array I, (PMII) POLYMODE Array II, (PMIII A&B) POLYMODE Array III Clusters A and B, (GSE) Gulf Stream Extension. Also shown in this figure is the historical mean position of the 15°C isotherm at 200 m depth from Fisher (1977).

Figure 2.2: Summary of the geographic variation of eddy kinetic energy in the near field and mid-ocean from current meter data. The MODE East, Center, PMI, PMIIIA, and PMIIIB values are the cluster averages reported in Fu et al. (1982), Table 3. These arrays have been plotted as a function of longitude along 28°N (bottom scale). The other data from the LDE, PMII, and GSE arrays are tabulated in Appendix A. The data from the LDE and the GSE have been plotted as a function of longitude (bottom scale). Since Array II was deployed meridionally along 55°W, those data have been plotted as a function of latitude (top scale). The projection of the latitude and longitude scales has been chosen so that they have equal distances in kilometers.

Appendix A

Table A.1: Near field statistics from POLYMODE Array II, LDE, and GSE.

Table A.2: Mid-ocean statistics from POLYMODE Array I and III Clusters A and B.

TABLE 2.1: MEAN MOMENTUM BALANCE

(a) Scaling

	Mid-ocean and LDE regions	Array II zonal balance	Array II meridional balance
$\bar{u} \cdot \nabla \bar{u}$	$\frac{U_o^2}{L}$	$\max\left[\frac{V_o U_o}{L_y}, \frac{U_o^2}{L_x}\right]$ *	$\max\left[\frac{U_o V_o}{L_x}, \frac{V_o^2}{L_y}\right]$
$f_o \bar{v}$	$f_o U_o$	$f_o V_o$	$f_o U_o$
$\nabla \cdot \overline{u_i' u_j'}$	$\frac{u_o^2}{\mathcal{L}}$	$\frac{u_o^2}{\mathcal{L}}$	$\frac{u_o^2}{\mathcal{L}}$

* Max (a,b) denotes the maximum value of a and b.

(b) Ratio of Eddy to Mean Terms

	Mid-ocean and LDE regions	Array II zonal balance	Array II meridional balance
$\frac{\nabla \cdot \overline{u_i' u_j'}}{f_o \bar{v}}$	$\frac{u_o}{U_o}\left(\frac{u_o}{f_o \mathcal{L}}\right)$	$\frac{u_o}{V_o}\left(\frac{u_o}{f_o \mathcal{L}}\right)$	$\frac{u_o}{U_o}\left(\frac{u_o}{f_o \mathcal{L}}\right)$
$\frac{\nabla \cdot \overline{u_i' u_j'}}{\bar{u} \cdot \nabla \bar{u}}$	$\left(\frac{u_o}{U_o}\right)^2 \left(\frac{L}{\mathcal{L}}\right)$	$\frac{u_o^2/\mathcal{L}}{\max\left(\frac{V_o U_o}{L_y}, \frac{U_o^2}{L_x}\right)}$	$\frac{u_o^2/\mathcal{L}}{\max\left(\frac{U_o V_o}{L_x}, \frac{V_o^2}{L_y}\right)}$

TABLE 2.2: SCALE PARAMETERS

	Mid-Ocean	Array II (this paper)	Array II (Harrison, 1980)	LDE	GSE
U_o (cm/sec)	1	$U_o = 5 \rightarrow 9$ $V_o = 2$	$5 \rightarrow 10$	2	
L (km)	1000	$L_y = 100$ $L_x = 500$	100	200	
$\mathcal{L}$ (km)	1000	300	300	300	300
u_o^2 (cm^2/sec^2)	30	200	49–144	80	200
f_o (sec^{-1})	6.8×10^{-5} (at 28°N)	8.7×10^{-5} (at 36.5°N)	10^{-4}	7.5×10^{-5} (at 30°N)	
β ($cm^{-1} sec^{-1}$)	1.9×10^{-13}	1.7×10^{-13}	2×10^{-13}	1.9×10^{-13}	

TABLE 2.3: EVALUATED MOMENTUM BALANCE RATIOS

	Mid-Ocean	Array II (this paper) zonal	Array II (this paper) meridional	Array II (Harrison, 1980)	LDE
$\frac{\nabla \cdot \overline{u_i' u_j'}}{f_o \bar{v}}$	.004	.04	.02 → .01	.002 → .004	.02
$\frac{\nabla \cdot \overline{u_i' u_j'}}{\bar{u} \cdot \nabla \bar{u}}$	30	4	20	.3	10

TABLE 2.4: MEAN VORTICITY BALANCE

(a) Scaling

	Mid-ocean and LDE regions	Array II
$\bar{\underset{\sim}{u}} \cdot \nabla\bar{\zeta}$	$\frac{U_o^2}{L^2}$	$\max\left[\frac{U_oV_o}{L_x^2}, \frac{V_oU_o}{L_y^2}, \frac{U_o^2}{L_xL_y}, \frac{V_o^2}{L_xL_y}\right]$
$\beta\bar{v}$	βU_o	βV_o
$\nabla \cdot \overline{\underset{\sim}{u}'\zeta'}$	$\frac{u_o^2}{\mathcal{L}^2}$	$\frac{u_o^2}{\mathcal{L}^2}$
$f\frac{\partial\bar{w}}{\partial z}$	βU_o if $\bar{w} = \bar{w}_{ge}$ or $\frac{U_o^2}{L^2}$ if $\bar{w} = \bar{w}_{ro}$	βV_o if $\bar{w} = \bar{w}_{ge}$ or $\max\left[\frac{U_oV_o}{L_y^2}, \frac{U_oV_o}{L_x^2}\right]$ if $\bar{w} = \bar{w}_{ro}$

* max(a,b) denotes the maximum value of a and b.

b) Ratio of Eddy to Mean Terms

	Mid-ocean and LDE regions	Array II
$\frac{\nabla \cdot \overline{\underset{\sim}{u}'\zeta'}}{\beta\bar{v}}$	$\frac{u_o}{U_o}\left(\frac{u_o}{\beta\mathcal{L}^2}\right)$	$\frac{u_o}{V_o}\left(\frac{u_o}{\beta\mathcal{L}^2}\right)$
$\frac{\nabla \cdot \overline{\underset{\sim}{u}'\zeta'}}{\bar{\underset{\sim}{u}} \cdot \nabla\bar{\zeta}}$	$\left(\frac{u_o}{U_o}\right)^2\left(\frac{L}{\mathcal{L}}\right)^2$	$\frac{u_o^2/\mathcal{L}^2}{\max\left(\frac{U_oV_o}{L_x^2}, \frac{V_oU_o}{L_y^2}, \frac{U_o^2}{L_xL_y}, \frac{V_o^2}{L_xL_y}\right)}$

TABLE 2.5: EVALUATED VORTICITY BALANCE RATIOS

	Mid-Ocean	Array 2 (this paper)	Array II (Harrison, 1980)	LDE
$\frac{\nabla \cdot \overline{u'\zeta'}}{\beta \bar{v}}$	.02	.6	.04 → .07	.2
$\frac{\nabla \cdot \overline{u'\zeta'}}{\bar{u} \cdot \nabla \bar{\zeta}}$	30	2 → 1	.1	9

TABLE 2.6: MEAN HEAT BALANCE

	Mid-Ocean and LDE	Array II (this paper)	Array II (Harrison, 1980)
$\bar{u} \cdot \nabla \bar{T}$	$\frac{U_o^2 f_o \rho_o}{\alpha g H}$	$\frac{U_o V_o f_o \rho_o}{\alpha g H}$	$\frac{U_o \theta_o}{L}$
$\nabla \cdot \overline{u't'}$	$\frac{\overline{u't'}}{\mathscr{L}}$	$\frac{\overline{u't'}}{\mathscr{L}}$	$\frac{c_T u_o \rho_o}{\mathscr{L}}$
$\bar{w} \frac{d\bar{T}}{dz}$	$\frac{U_o \beta T_o}{f_o}$ if $\bar{w} = \bar{w}_{ge}$ or $\frac{U_o^2}{L^2} \frac{T_o}{f_o}$ if $\bar{w} = \bar{w}_{ro}$	$\frac{V_o \beta T_o}{f_o}$ if $\bar{w} = \bar{w}_{ge}$ or $\max\left(\frac{U_o V_o}{L_y^2}, \frac{U_o V_o}{L_x^2}\right) \frac{T_o}{f_o}$ if $\bar{w} = \bar{w}_{ro}$	$\frac{\bar{\gamma} U_o T_o}{L}$

TABLE 2.7: SCALE ESTIMATES FOR THE MEAN HEAT BALANCE

	Mid-Ocean (this paper)	Mid-Ocean (Harrison, 1980)	Array II (this paper)	Array II (Harrison, 1980)	LDE	GSE
T_0 (°C)	14→18 (at 200/m)	20	14	10	15	10→13
$\overline{u't'}$ (°C cm/sec)	.1	.1→.4**	2→9	2→4*	2	2→6
θ_0(°C)		2 at 500m .1 at 2000m		2 at 500m .1 at 2000m		
$\mathcal{O}_0$(°C)		.6 at 500m .1 at 2000m .05 at 4000m		3 at 600m .2 at 2500m .1 at 4000m		
H(m)			1000			

* assuming u_0 = 7–12 cm/sec, $\mathcal{O}_0$ = 3° at 600m, and C_T = .1

** assuming u_0 = 1– 7 cm/sec, $\mathcal{O}_0$ = .6 at 500m, and C_T = .1

TABLE 2.8: EVALUATED TERMS IN THE MEAN HEAT BALANCE

All quantities have units of 10^{-8} °C sec^{-1}

	Mid-Ocean (this paper)	Array II (this paper)	LDE	GSE
$\bar{u} \cdot \nabla\bar{T}$	.8	9 → 20	3	
$\nabla \cdot \underset{\sim}{\overline{u't'}}$	.1	7 → 30	7	7 → 20
$\bar{w}_{ro} \frac{d\bar{T}}{dz}$	.002 → .003	2 → 3	.2	
$\bar{w}_{ge} \frac{d\bar{T}}{dz}$	4 → 5	6	8	

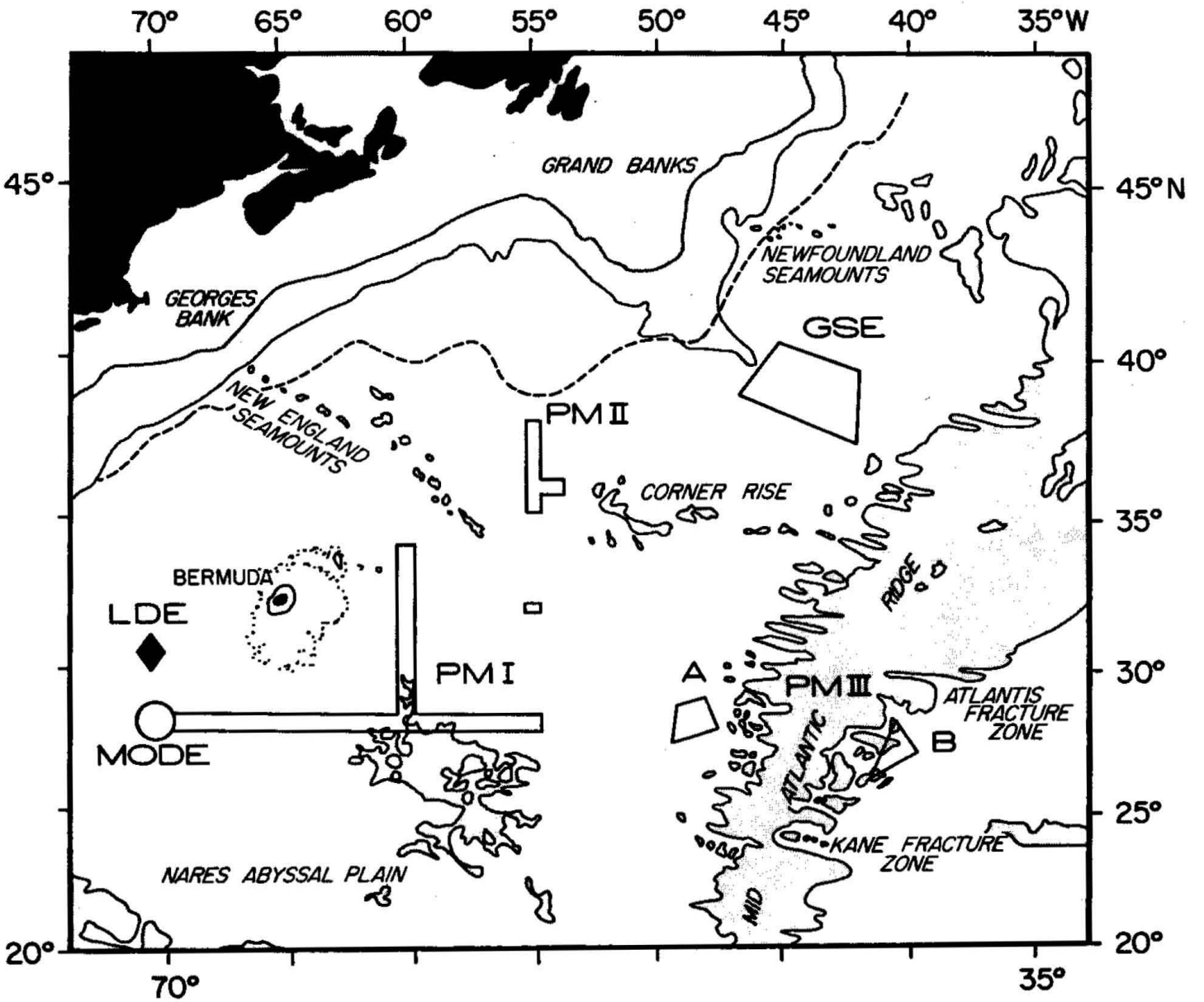
70°
65°
60°
55°
50°
45°
40°
35°W
45°
45°N
40°
35°
30°
25°
20°
70°
35°
GRAND BANKS
NEWFOUNDLAND SEAMOUNTS
GEORGES BANK
GSE
NEW ENGLAND SEAMOUNTS
PM II
CORNER RISE
BERMUDA
LDE
PM I
MODE
A
PM III
ATLANTIS FRACTURE ZONE
B
MID ATLANTIC RIDGE
KANE FRACTURE ZONE
NARES ABYSSAL PLAIN

Figure 2.1

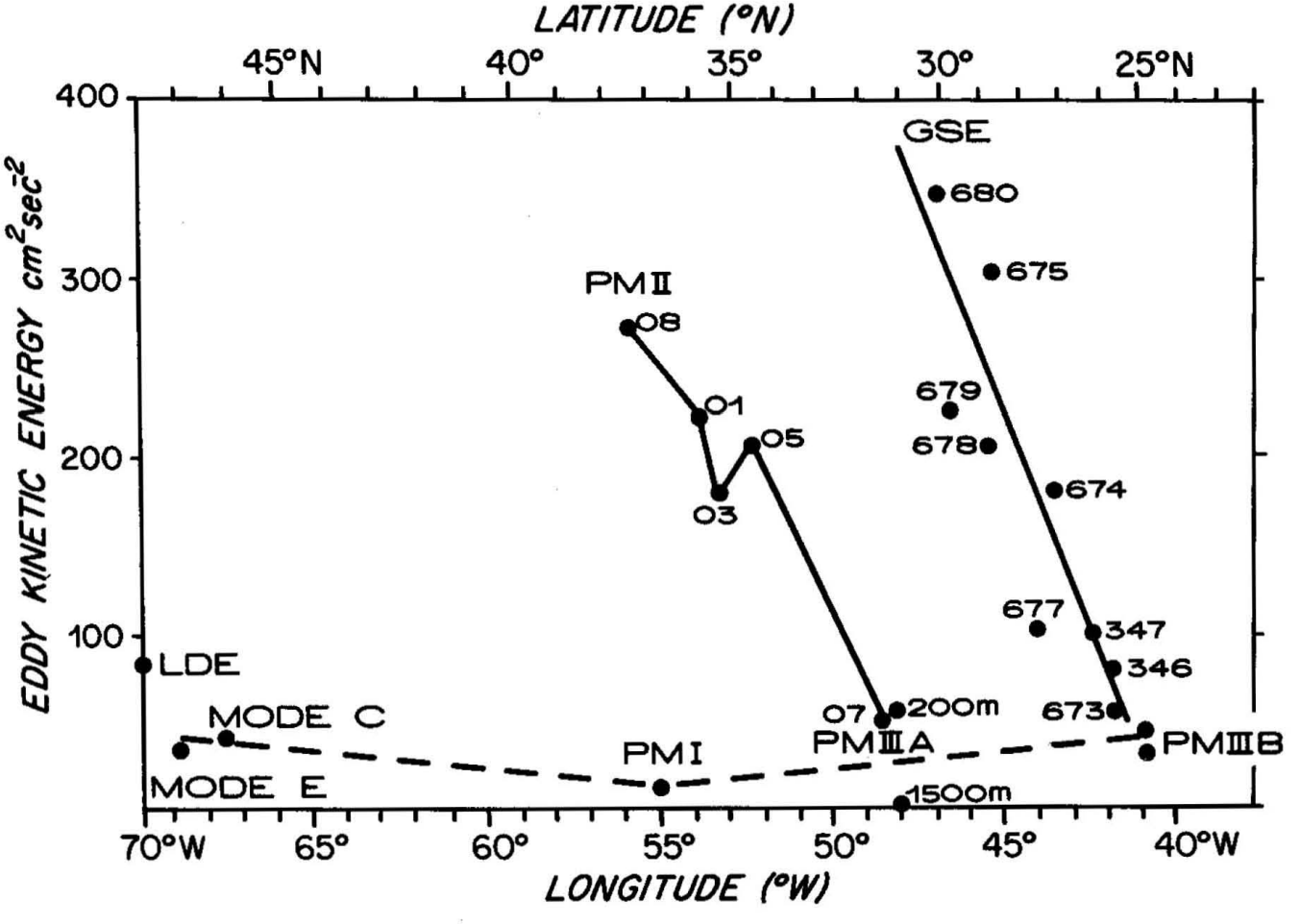
LATITUDE (°N)
45°N
40°
35°
30°
25°N
400
300
200
100
EDDY KINETIC ENERGY cm²sec⁻²
GSE
680
675
PMII
08
679
01
05
678
674
03
677
347
346
LDE
MODE C
07
200m
673
PMIIIA
PMIIIB
PMI
MODE E
1500m
70°W
65°
60°
55°
50°
45°
40°W
LONGITUDE (°W)

Figure 2.2

APPENDIX A:

Table A.1: Near Field Statistics

DATA SOURCE	Depth (m)	Duration days	$\bar{u}$ cm/sec	$\bar{v}$ cm/sec	T °C	$\overline{u'^2}$ cm^2/sec^2	$\overline{v'^2}$ cm^2/sec^2	$\overline{u't'}$ °C cm/sec	$\overline{v't'}$ °C cm/sec
POLYMODE II									
08 (37.5°N, 55°W)	600	779	7.98	3.11	14.31	273.82	260.89	-10.39* (-.28)*	- 9.63* (-.27)*
04 (36°, 53.8°)	600	697	-2.72	.93	14.39	298.37	241.67	-.26 (-.01)	- 4.70* (-.20)*
02 (35.9°, 54.8°)	600	527	-10.14	-2.85	14.96	248.56	208.38	-.98 (-.06)	- 2.03 (-.13)
01 (35.9°, 55.1°)	600	557	-8.71	-2.03	14.12	249.18	189.96	-.74 (-.03)	- 3.29 (-.16)
03 (35.6°, 55.1°)	600	776	-7.14	-1.56	13.26	184.08	172.20	1.67 (.07)	- 2.13 (-.09)
05 (34.9°, 55.1°)	600	724	-5.09	1.71	13.91	256.25	167.69	-1.06 (-.05)	.19 (.01)
Mooring 06 is not tabulated because the record length is only 284 days.									
LOCAL DYNAMICS EXPERIMENT (31°N, 70°W)	~600	array average	-2.84	-1.88	14.88	65.49	89.15	-.41 (-.06)	-2.08* (-.37)*

APPENDIX A:
Table A.1 (continued)
Near Field

DATA SOURCE	Depth (m)	Duration days	$\bar{u}$ cm/sec	$\bar{v}$ cm/sec	T °C	$\overline{u'^2}$ cm^2/sec^2	$\overline{v'^2}$ cm^2/sec^2	$\overline{u'T'}$ °C cm/sec	$\overline{v'T'}$ °C cm/sec
GULF STREAM EXTENSION									
680 (38.9°N, 46.9°W)	521	383	5.85	-.42	11.85	316.10	360.24	- 1.32 (-.13)	- 4.32 (-.39)
679 (38.0°, 46.6°)	519	383	-7.57	-9.61	12.26	259.33	202.83	- 6.21 (-.75)*	3.13 (.43)
678 (38.7°, 45.6°)	516	383 (152 for temperature)	-5.59	3.06		225.21	185.12		
677 (39.0°, 44.1°)	560	383	1.38	3.49	12.42	147.68	66.80	- 2.41 (-.21)	.67 (.09)
675 (40.4°, 45.3°)	569	383	-7.79	-4.21	11.19	145.77	452.76	6.15 (.29)	- 6.89 (-.19)
674 (39.8°, 43.9°)	550	383	6.51	2.18	11.28	215.66	149.05	-.36 (-.07)	- 2.28 (-.57)*
673 (37.0°, 42.0°)	641	383	-6.00	.21	10.14	39.85	69.77	- 1.72 (-.43)	- .82 (-.15)
347 (38.5°, 42.5°)	500	347	- .48	1.55	12.83	113.26	85.87	1.13 (.19)	2.50 (.47)
346 (39.6°, 42.2°)	500	214	1.42	-7.20	12.50	189.69	172.38	2.65 (.25)	- 2.41 (-.24)

* Significant at the 90 percent confidence level. Significance levels for the heat flux were computed assuming a time scale of 10 days in Array II, 14 days in the LDE, and 30 days in the GSE.

APPENDIX A:

Table A.2: Mid-Ocean Statistics Along 28°N

DATA SOURCE	Depth (m)	Duration days	$\bar{u}$ cm/sec	$\bar{v}$ cm/sec	T °C	$\overline{u'^2}$ cm^2/sec^2	$\overline{v'^2}$ cm^2/sec^2	$\overline{u'T'}$ °C cm/sec	$\overline{v'T'}$ °C cm/sec
POLYMODE I									
542 (28°N, 69.6°W) (MODE C)	495	267	- .13	-1.80	16.38	78.81	45.30	.42 (.21)	-.16 (-.11)
543 (28°, 65°)	498	265	1.57	1.87	16.23	5.80	16.78	.06 (.12)	.14 (.15)
548 (31°, 60.1°)	500	274	-3.33	- .77	16.16	445.64	301.41	- 1.29 (-.13)	- 2.15 (-.26)
549 (34°, 60°)	512	262	4.15	- .82	16.05	137.90	116.73	- 9.35 (-.78)*	3.53 (.32)
545 (27.8°, 55.6°)	492	272	.56	- .21	15.49	8.70	4.20	.31 (.59)	-.17 (-.47)
546 (27.9°, 54.9°)	526	276	1.07	.65	14.91	17.61	5.71	.37 (.44)	-.21 (-.43)
547 (28.2°, 54.9°)	496	280	2.43	.17	14.82	10.62	7.29	-.002 (-.003)	-.31 (-.59)
POLYMODE II									
07 (31.6°N, 55°W)	600	380	-1.21	.48	14.04	54.09	44.92	.94 (.34)	.13 (.05)

APPENDIX A:
Table A.2 (continued)

DATA SOURCE	Depth (m)	Duration days	$\bar{u}$ cm/sec	$\bar{v}$ cm/sec	T °C	$\overline{u'^2}$ cm^2/sec^2	$\overline{v'^2}$ cm^2/sec^2	$\overline{u'T'}$ °C cm/sec	$\overline{v'T'}$ °C cm/sec
POLYMODE III Cluster A									
632 (26.9°N, 49.2°W)	190	334	-6.89	-.01	18.68	35.12	52.23	.48 (.28)	.30 (.14)
631 (27.9°, 48.9°)	212	334	2.20	.56	18.25	50.81	66.87	.11 (.07)	-.03 (-.02)
630 (27.9°, 48.7°)	200	334	.39	.14	18.26	44.45	77.49	-.38 (-.24)	-.05 (-.02)
629 (28°, 48.1°)	203	334	3.41	-.98	18.62	49.70	66.47	-.62 (-.20)	.41 (.12)
648 (27.9°, 48.7°) site mooring	178	490	.63	-4.08	17.94	75.90	73.85	.75 (.31)	.86 (.35)
POLYMODE III Cluster B									
623(27.4°N, 41.1°W)	128	342	-3.22	-1.69	18.30	76.61	72.89	.28 (.10)	.88 (.31)
624 (27.3°, 40.8)	529	342	-2.30	- .05	13.78	41.03	30.77	.83 (.31)	-.44 (-.19)
625 (27.2°, 40.4°)	189	342	-2.10	- .72	18.38	94.32	60.74	.01 (.003)	.31 (.12)
627 (26.2°, 41.7°)	206	341	- .41	- .74	18.35	72.17	65.11	-.09 (.04)	.07 (.03)
649 (27.4°, 41.2°) site mooring	216	483	2.39	-3.05	17.90	58.16	41.42	.48 (.26)	.26 (.17)

* Significant at the 90 percent confidence level. Significance levels for the heat flux were computed assuming a time scale of 43 days in MODE C and in PMI, 33 days in Cluster A, and 44 days in Cluster B. These time scales are the average of the u, v, and t autocorrelation time scales as reported in Fu et al. (1982).

CHAPTER 3

EDDY POTENTIAL VORTICITY FLUXES IN THE GULF STREAM RECIRCULATION

3.I. INTRODUCTION

Recent analytical and numerical models have emphasized the importance of the eddy potential vorticity flux in the time-averaged potential vorticity balance. The eddy flux has been interpreted (Rhines and Holland, 1979) as a force-like quantity which allows the mean circulation to cross planetary contours. It is composed of a relative vorticity flux representing lateral momentum transfer and a thickness flux due to fluctuations in the thickness of isopycnal layers which causes vertical transfers of momentum. In two-layer quasigeostrophic numerical model flows the role of the eddy potential vorticity flux has been examined using either streamline (Holland and Rhines, 1980) or regional integrals (Harrison and Holland, 1981) of the terms in the mean potential vorticity balance. These vorticity budget analyses suggest that in certain regions of the model flows the area-integrated eddy flux can be a significant term in the mean dynamical balances.

The paucity of observational data prevents a detailed comparison of ocean measurements with the theoretical predictions. The fundamental problem is the difficulty in drawing conclusions from the few point measurements which are available. Other specific inadequacies are the large uncertainties in both the mean fields and the eddy fluxes and the insufficient knowledge of the spatial distribution of these quantities. The present observational data base

is nowhere sufficient for the type of analyses carried out on the numerical model flows.

Even after a decade of long-term moored array experiments only the Local Dynamics Experiment array deployed in the Gulf Stream recirculation region provides data that can be used to calculate the total eddy potential vorticity flux. Estimates of eddy potential vorticity flux require both long time-series for statistical stability and adequate resolution for horizontal and vertical spatial derivatives. Since the numerical model calculations also suffer from these uncertainties, part of the motivation for this study is to determine whether the fluxes can be reliably estimated from mooring data. Of the available observational data the Local Dynamics Experiment (LDE) moored instrument array provides the most accurate spatial resolution because it was designed to sample optimally the instantaneous mesoscale eddy vorticity field. Furthermore, it is the only array from which all the terms in the flux can be calculated. In this chapter the eddy potential vorticity flux is estimated from velocity and temperature time-series recorded from this array and compared to the local mean potential vorticity gradient.

Despite the severe limitations of interpreting the observational data, the measured eddy potential vorticity flux is still a useful quantity because it characterizes the effect of the eddy field on the mean potential vorticity distribution in the LDE region. The eddy flux in the mid-thermocline of the Local Dynamics region is found to be dominated by the baroclinic eddy contribution which is directed down the mean potential vorticity gradient. This result is consistent with both Hogg's (1983) approximate calculation based on the POLYMODE Array II data set and, in some respects, with the predictions of numerical model results. The interpretation of the observational results is

much more limited than in the numerical models because we cannot calculate the divergence of the eddy flux which appears in the mean potential vorticity balance. Since only a single point value can be calculated, our result describes only the tendancy of the eddy field to affect the distribution of mean potential vorticity. We can, however, estimate the strength of the local cascade of mean enstrophy from the magnitude of the potential vorticity flux and the mean potential vorticity gradient.

3.II. METHODOLOGY: THE EDDY POTENTIAL VORTICITY FLUX

The mean potential vorticity equation (Pedlosky, 1979) contains the total effect of the eddy field on the mean circulation because it incorporates the heat equation into the vorticity equation. For a continuously stratified inviscid fluid the quasigeostrophic potential vorticity equation is given by

$$\left[\frac{\partial}{\partial t} + u\frac{\partial}{\partial x} + v\frac{\partial}{\partial y}\right]\left[\zeta + f + f_o\frac{\partial}{\partial z}\left(\frac{\rho}{\rho_z^s}\right)\right] = S - D \qquad (3.1)$$

where $\zeta = v_x - u_y$ is the vertical component of relative vorticity,

ρ is the perturbation density $\rho_{total} = \rho_o + \rho^s(z) + \rho(x,y,z,t)$

ρ^s is the density in an unperturbed reference state

$f = f_o + \beta y$ is the Coriolis parameter

(u,v) are the east and north velocity components of the horizontal velocity vector $\underset{\sim}{u}$

$q = \zeta + f + f_o\frac{\partial}{\partial z}\left(\frac{\rho}{\rho_z^s}\right)$ is the potential vorticity.

The source term S has been included to represent the wind input of vorticity at the surface. It takes the form $S=w_{Ek}\delta(z)$ where w_{Ek} is the Ekman velocity

at the base of the mixed layer. Smaller scale dissipation by internal waves and other processes is subsumed into the term D. The equation for the mean potential vorticity is derived by separating the variables into time-mean (denoted by an overbar) and time-dependent components (primed variables) and averaging the equation to obtain

$$\underset{\sim}{\bar{u}} \cdot \nabla \bar{q} = -\nabla \cdot \overline{\underset{\sim}{u'q'}} + \bar{S} - \bar{D} \tag{3.2}$$

where the mean potential vorticity is defined as

$$\bar{q} = \beta y + \bar{v}_x - \bar{u}_y + f_o \overline{\frac{\partial}{\partial z}\left(\frac{\rho}{\rho_z}\right)_s} \tag{3.3}$$

planetary vorticity | relative vorticity | vortex stretching

and the total eddy potential vorticity flux vector is given by

$$\overline{\underset{\sim}{u'q'}} = \overline{\underset{\sim}{u'}(v'_x - u'_y)} + f_o \overline{\underset{\sim}{u'} \frac{\partial}{\partial z}\left(\frac{\rho'}{\rho_z}\right)_s} \tag{3.4}$$

The mean potential vorticity balance in Equation (3.2) equates the advection of the mean potential vorticity by the mean circulation with the horizontal divergence of the eddy potential vorticity flux and with other sources and sinks. The eddy potential vorticity flux divergence acts like a force in the basin interior which drives the mean flow across contours of mean potential vorticity.

The total eddy potential vorticity flux contains two components -- the relative vorticity flux and the thickness flux which represent respectively

the lateral and vertical transfers of mean potential vorticity. The eddy relative vorticity flux $\overline{u'\zeta'}$ is defined to be

$$\underset{\sim}{\overline{u'\zeta'}} \equiv [\overline{u'(v'_x - u'_y)} \quad , \quad \overline{v'(v'_x - u'_y)}] \ , \tag{3.5}$$

while the eddy thickness flux $\overline{u'\eta'}$ is given by

$$\underset{\sim}{\overline{u'\eta'}} \equiv [f_o \overline{u' \frac{\partial}{\partial z}(\frac{\rho'}{\rho_z})} \quad , \quad f_o \overline{v' \frac{\partial}{\partial z}(\frac{\rho'}{\rho_z})}] \quad . \tag{3.6}$$

If the Rossby number for the eddy field is small, the eddy velocity is nearly horizontally non-divergent and the components of Equation (3.5) can be rewritten in terms of derivatives of the quadratic eddy velocity components $\overline{u'^2}$, $\overline{v'^2}$, and $\overline{u'v'}$:

$$\overline{u'\zeta'} = \frac{\partial}{\partial x} \overline{u'v'} + \frac{\partial}{\partial y} \frac{\overline{v'^2 - u'^2}}{2} \tag{3.7}$$

$$\overline{v'\zeta'} = -\frac{\partial}{\partial y} \overline{u'v'} + \frac{\partial}{\partial x} \frac{\overline{v'^2 - u'^2}}{2} \quad . \tag{3.8}$$

In the numerical model experiment (Holland and Rhines, 1980) the eddy relative vorticity flux is larger than the thickness flux in the western boundary current and jet separation regions, but the thickness flux dominates vertical transfers of potential vorticity in the gyre interior.

Although the thickness flux in the two-layer model can locally transfer potential vorticity from the top to the bottom layer, the vertically-integrated thickness flux is zero. The proof of this is trivial for a two-layer model with layer thicknesses H_1 and H_3 and interface height η_2 because the thickness fluxes in the upper and lower layers are $\frac{-f_o \eta_2}{H_1}$ and

$\frac{f_o \eta_2}{H_3}$ respectively. For the continuously stratified case the problem is more subtle. The depth-integral of the thickness flux is:

$$\int_{-H}^{0} \overline{u' \frac{\partial}{\partial z}\left(\frac{\rho'}{\rho_z}_s\right)} \, dz = \left.\overline{\frac{u'\rho'}{\rho_z}_s}\right|_{-H}^{0} + \int_{-H}^{0} \frac{\partial}{\partial y} \overline{\frac{\rho'^2}{2\rho_z}_s} \, dz$$

$$\int_{-H}^{0} \overline{v' \frac{\partial}{\partial z}\left(\frac{\rho'}{\rho_z}_s\right)} \, dz = \left.\overline{\frac{v'\rho'}{\rho_z}_s}\right|_{-H}^{0} + \int_{-H}^{0} \frac{\partial}{\partial x} \overline{\frac{\rho'^2}{2\rho_z}_s} \, dz \quad , \tag{3.9}$$

where the thermal wind relation has been used to rewrite the velocity shear in terms of the lateral density gradient. Equation (3.9) relates the total thickness flux to the heat flux at the boundaries plus the lateral gradient of the eddy potential energy. In the special case of a zonally-averaged flow, Bretherton (1966) has shown that the volume-integrated northward eddy potential vorticity flux vanishes. While this theorem does not hold for a time-averaged flow, the thickness flux still has no net effect on the vertically-integrated mean potential vorticity equation. This can be shown by integrating Equation (3.2):

$$\int_{-H}^{0} \bar{\underset{\sim}{u}} \cdot \nabla\bar{\zeta} \, dz + \int_{-H}^{0} \beta\bar{v} dz + f_o \int_{-H}^{0} \bar{\underset{\sim}{u}} \cdot \nabla \frac{\partial}{\partial z}\left(\frac{\bar{\rho}}{\rho_z}_s\right) dz$$

$$= \int_{-H}^{0} \nabla \cdot \overline{\underset{\sim}{u}'\zeta'} \, dz - f_o \int_{-H}^{0} \nabla \cdot \overline{\underset{\sim}{u}' \frac{\partial}{\partial z}\left(\frac{\rho'}{\rho_z}_s\right)} \, dz \quad . \tag{3.10}$$

The last terms on both sides of this equation are integrated by parts according to:

$$\int_{-H}^{0} \bar{\underset{\sim}{u}} \cdot \nabla \frac{\partial}{\partial z}\left(\frac{\bar{\rho}}{\rho_z}_s\right) dz = -\int_{-H}^{0} \frac{\partial \bar{\underset{\sim}{u}}}{\partial z} \cdot \nabla \left(\frac{\bar{\rho}}{\rho_z}_s\right) dz + \left.\frac{\bar{u} \cdot \nabla \bar{\rho}}{\rho_z}_s\right|_{-H}^{0} \tag{3.11}$$

and

$$\int_{-H}^{0} \nabla \cdot \overline{\underset{\sim}{u}' \frac{\partial}{\partial z}\left(\frac{\rho'}{\rho_z}_s\right)} dz = -\int_{-H}^{0} \frac{\partial \underset{\sim}{u}'}{\partial z} \cdot \frac{\nabla \rho'}{\rho_z}_s dz + \left.\frac{\overline{u' \cdot \nabla \rho'}}{\rho_z}_s\right|_{-H}^{0} , \tag{3.12}$$

where the horizontal nondivergence of the eddy velocity has been used in Equation (3.12). In Equations (3.11) and (3.12) the first terms on the right side vanish because of the thermal wind relation for both the mean and the eddy fields. The boundary terms are evaluated with the conditions

$$\bar{w} = \frac{-\hat{k}}{f} \cdot \text{curl} \ \underset{\sim}{\tau} \qquad \text{at the surface } z = 0$$

and (3.13)

$$\bar{w} = \bar{u} \cdot \nabla h \qquad \text{at the bottom } z = -H+h(x,y)$$

where the total mean vertical velocity is

$$\bar{w} = \frac{-1}{\rho_z}_s \left(\bar{\underset{\sim}{u}} \cdot \nabla \bar{\rho} + \nabla \cdot \overline{u'\rho'}\right) . \tag{3.14}$$

With these substitutions, Equation (3.10) simplifies to:

$$\int_{-H}^{0} [\bar{u} \cdot \nabla \bar{\zeta} + \beta \bar{v} + \nabla \cdot \overline{u' \zeta'}] dz = \hat{k} \cdot \text{curl} \ \underset{\sim}{\tau} - f_o \bar{u} \cdot \nabla h \Big|_{z=-H} \tag{3.15}$$

which shows that the thickness flux does not contribute to the vertically-integrated mean potential vorticity balance. However, as demonstrated in the layer model experiments, the thickness flux can still be locally important in transferring mean potential vorticity between isopycnal layers.

The comparative magnitudes of the relative vorticity flux and the thickness flux is determined from scale analysis using the parameters:

$\mathcal{L}$ horizontal scale for the variation in quadratic eddy velocity statistics,

ℓ_e horizontal eddy length scale,

u_o horizontal eddy velocity scale,

h vertical eddy scale,

N buoyancy frequency,

f_o Coriolis parameter.

From Equations (3.7) and (3.8) the relative vorticity flux can be scaled in two ways. If the correlation coefficient $C_{u\zeta}$ between the eddy velocity and vorticity is known, then $\overline{u'\zeta'}$ scales as

$$C_{u\zeta} \frac{u_o^2}{\ell_e} \tag{3.16}$$

Alternatively, this term can be scaled from Equations (3.7) and (3.8) by the large-scale horizontal variation in quadratic eddy velocity statistics:

$$\underset{\sim}{\overline{u'\zeta'}} = \frac{u_o^2}{\mathcal{L}} \tag{3.17}$$

where we have assumed the correlation coefficient between eddy velocity components to be O(1). To express the eddy thickness flux Equation (3.6) in terms of the scale parameters, the pressure is scaled geostrophically and hydrostatically:

$$\underset{\sim}{\overline{u'\eta'}} \sim \frac{f_o^2 u_o^2 \ell_e}{N^2 h^2} . \tag{3.18}$$

The ratio of the thickness flux to the relative vorticity flux thus depends on the square of the ratio of the eddy length scale to the Rossby deformation radius $R_d = Nh/f_o$ and on the ratio of the length scales $\mathcal{L}$ and ℓ_e:

$$\frac{\overline{u'\eta'}}{\overline{u'\zeta'}} = \frac{f_o^2 \ell_e^2}{N^2 h^2} \times \frac{\mathcal{L}}{\ell_e} = \left(\frac{\ell_e}{R_d}\right)^2 \times \frac{\mathcal{L}}{\ell_e} \tag{3.19}$$

The most energetic eddies observed during the Local Dynamics Experiment have a scale ($\ell_e \sim 100$ km) based on the zero crossing of the transverse velocity autocorrelation function which is slightly larger than the deformation radius ($R_d \sim 45$ km). Although the eddy statistics do not vary over the dimensions of the LDE array, an estimate of $\mathcal{L} \sim 300$ km is suggested by other data (Chapter 2). The ratio in Equation (3.19) thus implies that in the Local Dynamics region the thickness flux could be an order of magnitude larger than the relative vorticity flux.

To interpret the size of the eddy potential vorticity flux which will be calculated from the data, it is useful to examine the mean enstrophy equation. The governing equation for mean potential enstrophy $\overline{q^2}$ is obtained by multiplying Equation (3.2) by the mean potential vorticity $\overline{q}$:

$$\frac{\bar{\underset{\sim}{u}} \cdot \nabla \overline{q}^2}{2} + \nabla \cdot (\overline{q}\ \overline{\underset{\sim}{u}'q'}) = \overline{\underset{\sim}{u}'q'} \cdot \nabla \overline{q} + \overline{Sq} - \overline{Dq} \tag{3.20}$$

Over the total volume of the fluid the mean enstrophy can be changed by the flux of eddy potential vorticity with respect to the mean potential vorticity gradient and by sources and sinks of mean enstrophy. Therefore, the importance of the eddy potential vorticity flux in the enstrophy cascade is shown by estimating the wind input of enstrophy. In a layer model the enstrophy

input due to a zonal wind stress which vanishes at the north and south basin boundaries is given by the area integral of

$$\frac{\tau}{\rho_0 h} \frac{\partial \bar{q}}{\partial y} \tag{3.21}$$

where h is the layer thickness and τ is the wind stress magnitude. Therefore, the rate of conversion of mean enstrophy due to the eddy field should be compared to the estimated enstrophy input (Equation 3.21) into the wind-driven circulation.

Holland and Rhines (1980) parametrize the eddy potential vorticity flux forcing by defining an Austauch coefficient A_{pv} for potential vorticity

$$A_{pv} = - \frac{\overline{\underset{\sim}{u}' q'} \cdot \nabla \bar{q}}{| \nabla \bar{q} |^2} \quad . \tag{3.22}$$

In their model experiments this coefficient varies between $-9.6 \times 10^7 cm^2 s^{-1}$ in the eastern part of the basin to a maximum of $+4 \times 10^7 cm^2 s^{-1}$ in the intense western boundary current. A positive Austauch coefficient indicates a region of countergradient flux of eddy potential vorticity and increasing eddy enstrophy. Since the experimental data only allow estimates of the eddy potential vorticity flux at a single location, these two quantities (Equations 3.13 and 3.14) are useful in interpreting the strength of eddy vorticity mixing. The magnitude and direction of the eddy potential vorticity flux with respect to the large scale potential vorticity gradient can be used to calculate the vorticity Austauch coefficient and the rate of conversion of mean enstrophy by the eddy field.

3.III. DATA AND MEASUREMENTS

The POLYMODE Local Dynamics Array was deployed by the Woods Hole Oceanographic Buoy Group at 31°N, 69°30'W, in the Gulf Stream recirculation region from May 1978 until July 1979. The maximum observational record length is fifteen months although for this analysis the failure of certain instruments reduce this useable data record to ~ 225 days. The array (Figure 3.1) consists of eight moorings arranged in two crosses at spacings of approximately 25-40 km with current and temperature recorders in the thermocline and a central mooring instrumented throughout the water column. The configuration was specifically designed using objective mapping principles for calculating optimal estimates of mesoscale dynamics (McWilliams and Owens, 1984). A more complete description of the low frequency and mean flow components of this data set is given in Mills et al. (1981) and in Owens et al. (1982).

The potential vorticity fluxes are calculated from the time-series of velocity and temperature and from hydrographic data. A mean hydrographic profile for the vertical temperature gradient was obtained by averaging 13 CTD profiles taken during an intensive survey of the Local Dynamics area in July-August 1978. The time-series of velocity and temperature from the moored array were low-pass filtered with a 24 hour half-width Gaussian window. In addition, the temperature records were corrected for vertical mooring motion by using the pressure time series to estimate the excursions of the instruments from nominal depth (Mills et al., 1981). This correction is necessary to avoid spurious correlations between velocity and temperature caused by mooring motion. The terms in the eddy potential vorticity fluxes were calculated by finite difference from the velocity and temperature records. As shown in section II, the eddy potential vorticity flux is the sum of two

components -- the relative vorticity flux and the thickness vorticity flux which have different sampling and measurement requirements.

The relative vorticity flux calculation from Equation (3.7) requires velocity measurements at a single depth from an array of at least three moorings. From Equations (3.5) and (3.7) and (3.8) the flux can be calculated by two methods which should be equivalent for an eddy field with small Rossby number. For an eddy resolving array of current meters, time-series of vorticity can be computed and the correlation of these vorticity time series with the velocity components is the relative vorticity flux. Alternatively, if the array is not eddy-resolving, then Equations (3.7) and (3.8) can be used to compute the relative vorticity flux vector components from horizontal derivatives of the horizontal velocity correlations. Since the Local Dynamics Experiment array contains nine moorings which spatially resolve the eddy field, these data also permit accurate estimates of the sampling and measurement errors.

3.IV. THE MEASURED EDDY POTENTIAL VORTICITY FLUX

The first method for calculating the relative vorticity flux is from differencing the horizontal velocity correlations according to Equations (3.7) and (3.8). The uniform velocity data record in the mid-thermocline for the nine moorings covers 225 days between May 1 and December 13 of 1978. The horizontal velocity correlations (Table 3.1) at the nine moorings were first adjusted to a common depth (637 m) by using the average vertical gradients of these quantities computed at moorings 1, 2, and 3. The measurement error in these velocity correlations was estimated by Bryden (1982) from the sum of the residuals to a least squares planar regression through the nine values. The

error in $\overline{u'v'}$ and $(\overline{v'^2-u'^2})/2$ are 3.21 cm^2/s^2 and 4.27 cm^2/s^2 respectively. The relative vorticity flux can then be calculated by a least squares regression to a planar fit through the nine values of the velocity correlations. As shown in Table 3.2 the individual gradients are comparable in magnitude within the statistical error and tend to cancel in the expression for the relative vorticity flux.

The sampling error in the relative vorticity flux is the combined error in the slopes for least-squares planar regressions through the velocity correlations at the nine moorings. The confidence limits for the slope of a planar regression through the nine values is determined from Student's t-distribution with six degrees of freedom as described in Gutman et al. (1971). According to this method, the relative vorticity flux components for the 225 day records are determined to be

$$\overline{u'\zeta'} = -1.57 \times 10^{-6} \pm 1.51 \times 10^{-6} \quad cm/s^2$$

$$\overline{v'\zeta'} = 1.95 \times 10^{-6} \pm 1.54 \times 10^{-6} \quad cm/s^2 \qquad (3.23)$$

where the 90 percent error estimate gives a statistically significant result but with large uncertainties. Table 3.2b shows the effect of longer averaging time on the stability of these estimates. A 434 day record length from moorings 1, 6, 8, 9 can be used to calculate finite difference derivatives of the momentum fluxes. For the longer record length there is a significant increase in the zonal component of the relative vorticity flux. The meridional component also increases but still remains within the estimated error for the 225 day record.

Since the horizontal non-divergence of the eddy velocity field has been used to obtain the relative vorticity flux in terms of the divergence of the momentum fluxes, the momentum flux derivatives tend to cancel in the relative vorticity flux expression Equations (3.7) and (3.8). The Rossby number for the LDE mesoscale eddy field is $R_o = U/fL = O(.01)$ assuming a length scale of 100 km and a scaling velocity of 7 cm/sec. Thus, the assumption of horizontal non-divergence should be satisfactory. Since the LDE array spatially resolves the eddy variability, this relative vorticity flux can also be calculated directly from the correlations between time series of velocity and vorticity. Time series of vorticity and spatially-averaged velocity are calculated from each of the triangles of three moorings -- an inner cross composed of triangles 123, 134, 145, and 152, and an outer cross composed of triangles 167, 178, 189, and 196 where the digits represent the moorings shown in Figure 3.1. The relative vorticity flux for the 225 day record length averaged over the eight triangles is $-1.37 \times 10^{-6} \pm 3.05 \times 10^{-6}$ cm/s^2 for the zonal component and $3.86 \times 10^{-6} \pm 3.83 \times 10^{-6}$ cm/s^2 for the meridional component. The estimated 90 percent confidence limits are based on the standard deviation of the correlation between velocity and vorticity assuming a 13 day time scale for independent data values. The 13 day time scale is the average of the integral time scales for the zonal (10 day) and meridional (15 day) velocity components. Because of the tendancy for terms to cancel in Equations (3.7) and (3.8), the direct method Equation (3.5) for computing the relative vorticity flux gives values larger than but not significantly different from the previous result in Table 3.2.

Estimates of the thickness flux require velocity and temperature records from only a single mooring. Since there is a tight correlation between

temperature and salinity in the mid-thermocline of the western North Atlantic, the thickness flux is evaluated using temperature in place of density in Equation (3.6). The LDE thickness fluxes (Table 3.3) are calculated at mid-thermocline depths from velocity records at 567-728 meters and from temperature measurements at 469-625 and 665-839 meters divided by the mean vertical temperature gradient from the averaged CTD profile. The average instrument depths for the six moorings are 525 and 743 m for temperature and 623 m for velocity so the array averaged thickness flux is calculated at nearly the same level (637 m) as the relative vorticity flux.

In order to make statistically reliable estimates of the thickness flux, the data record must be long compared to the time scale of the eddy field. As discussed in Section III of Chapter 4, the average integral correlation times for the nine instruments at 600 m depth are 10 days for u and 15 days for both v and t. Six of the LDE moorings -- 1, 2, 4, 5, 6, 9 -- have 225 day records (No. 4 is short with only 178 days) while a longer 434 record length is available at moorings 1, 5, 6, and 9. The temperature/pressure sensors on moorings 7 and 8 (Mills et al., 1981) failed, so that these moorings cannot be used in this calculation. Table 3 shows that doubling the record length tends to decrease the absolute value of the thickness flux components at a given mooring although the changes in the average values are not statistically significant. At least in this data set from the recirculation region, a 225 day record seems sufficient to estimate the thickness term. The estimated error is the 90 percent confidence level computed from the sample variance and a Student's t-distribution assuming a 15 and 13 day time scale for the meridional and zonal velocity components. The eddy thickness flux components averaged over the six moorings with 225 day records are determined to be

$$\overline{u'\eta'} = -.79 \times 10^{-5} \pm .53 \times 10^{-5} \quad cm/s^2$$

$$\overline{v'\eta'} = -1.45 \times 10^{-5} \pm .71 \times 10^{-5} \quad cm/s^2 \qquad (3.24)$$

The thickness flux is significant according to our error estimate and it is directed to the southwest.

The total eddy potential vorticity flux (Table 3.4) in the mid-thermocline LDE region is dominated by the thickness flux which is an order of magnitude larger than the relative vorticity flux. In addition, the two vectors differ in direction. The magnitude of the thickness flux vector is $1.65 \times 10^{-5} cm/s^2$ with a range due to the errors of between $.78 \times 10^{-5} cm/s^2$ and $2.53 \times 10^{-5} cm/s^2$. The direction of this vector is to the southwest at 209°T. From the possible errors in the components this direction could lie between 187°T and 241°T. The relative vorticity flux is an order of magnitude smaller with a greater percentage of uncertainty. The magnitude of the relative vorticity flux vector is $.25 \times 10^{-5} cm/s^2$ with a range due to the errors of between $.04 \times 10^{-5} cm/s^2$ and $.47 \times 10^{-5} cm/s^2$. The direction of this vector is to the northwest at 321°T with a possible range of 278°T to 359°T. The sum of these two vectors, the total eddy potential vorticity flux, has components:

$$\overline{u'q'} = -.95 \times 10^{-5} \pm .55 \times 10^{-5} \ cm/s^2$$

$$\overline{v'q'} = -1.25 \times 10^{-5} \pm .73 \times 10^{-5} \ cm/s^2 \qquad (3.25)$$

In terms of magnitude and direction the total flux is to the southwest at 217°T with a range of 191° to 251°. The magnitude is $1.57 \times 10^{-5} cm/s^2$ with a range of $.66 \times 10^{-5} cm/s^2$ to $2.48 \times 10^{-5} cm/s^2$.

The direction of the total eddy potential vorticity flux relative to the mean potential vorticity gradient indicates the sign of enstrophy transfer between the time-dependent eddy field and the mean flow. In the LDE region where the mean velocity is typically $U_o = 2$ cm/s and the length scale of the mean flow is L = 200 km, the advection of mean relative vorticity ($\bar{u} \cdot \nabla\bar{\zeta}$) is small compared to the advection of planetary vorticity ($\beta\bar{v}$) . Therefore, the potential vorticity gradient can be approximated as the sum of the planetary vorticity gradient β and the effective β_{eff} due to the northward thickening of the isopycnal layer. This can also be expressed in terms of the vertical shear of the mean velocity by using the thermal wind relation. In this form the mean potential vorticity gradients are:

$$\frac{\partial\bar{q}}{\partial x} = f_o^2 \frac{\partial}{\partial z}\left(\frac{\bar{v}_z}{N^2}\right)$$

$$\frac{\partial\bar{q}}{\partial y} = \beta - f_o^2 \frac{\partial}{\partial z}\left(\frac{\bar{u}_z}{N^2}\right) \qquad (3.26)$$

The errors in the point measurements of the mean velocities in the LDE are too large to permit a significant finite-difference estimate of the mean potential vorticity gradient. McWilliams (1983) calculated the mean gradients from differencing smoothed vertical profiles of the mean velocities from each instrument at the LDE central mooring. Because the instruments on the central mooring have different record lengths the mean velocity profile can be estimated either by using a uniform record length for all the instruments or by using the longest available record for each instrument. McWilliams' estimates (his Figure 12) for the north-south gradient of mean potential vorticity at 650 m depth are comparable to β, between $1.5 \times 10^{-13}\text{cm}^{-1}\text{s}^{-1}$ and $2.5 \times 10^{-13}\text{cm}^{-1}\text{s}^{-1}$,

while the east-west gradient is an order of magnitude smaller with the range between $-2 \times 10^{-14} cm^{-1} s^{-1}$ and $4.0 \times 10^{-14} cm^{-1} s^{-1}$. It is difficult, however, to have much confidence in these estimates given the basic uncertainties in the data values from which the smoothed profiles are generated.

An alternate estimate of the large scale potential vorticity gradient can be calculated using hydrographic data from two sources -- the January-March 1957-58 IGY section along 65°W and a compilation of historical data. McWilliams (1983) used McDowell et al.'s (1982) calculation of isopycnal thickness gradients from the IGY sections as a qualitative check on his estimates. A more complete hydrographic data set has recently been compiled by Levitus (1982) from the NODC historical data averaged for each degree square in the North Atlantic. Although the NODC data set includes the IGY data, there are more than 1000 additional mid-thermocline observations in the ten degree square centered around the LDE site. The NODC data set has been smoothed using an objective analysis scheme with a half-width filtering over about 1000 km. Sgouros and Keffer (1983) calculated mean potential vorticity defined as

$$\bar{q}_\theta = \frac{f}{\rho} \frac{\partial \rho_\theta}{\partial z} \tag{3.27}$$

from finite-differencing the potential density ρ_θ between constant density surfaces. This $\bar{q}_\theta$ differs from the quasigeostrophic potential vorticity q because it does not include the relative vorticity and it is divided by the thickness of the density layer. An effective β_{eff} due to the northward thickening of isopycnal layers can be calculated using the definition (3.27):

$$\beta_{eff} = \frac{\rho \frac{\partial \bar{q}_\theta}{\partial y}}{\frac{\partial \rho_\theta}{\partial z}} = \frac{f \frac{\partial \bar{q}_\theta}{\partial y}}{\bar{q}_\theta} \qquad (3.28)$$

Figure 3.2 shows the latitudinal variation along 70°W longitude of the potential vorticity $\bar{q}_\theta$ in the layer centered at the σ_θ = 26.75 density anomaly surface. This density layer lies between 400 and 700 m depth in the subtropical gyre. It intersects the sea surface to the north of the LDE region, but at 30°N it is deeper than the influence of direct wintertime convective mixing. The IGY section along 65°W shows general agreement with the climatological data although the local potential vorticity maximum at 32°N in the NODC data is not evident in the 65°W section. However, it is plotted as a local maximum on the contoured 65°W section shown in Figure 10 of McDowell et al. (1982). Since the zonal derivative of mean potential vorticity is much smaller than the meridional change, the total gradient will be approximated as the sum of the planetary term $\beta = 2 \times 10^{-13} cm^{-1} s^{-1}$ and the isopycnal thickening β_{eff}. At the LDE latitude the NODC data estimate for the contribution due to the northward isopycnal thickening in the mid-thermocline is $\beta_{eff} \tilde{\approx} 5 \times 10^{-13} cm^{-1} s^{-1}$, while for the 65°W data $\beta_{eff} \tilde{\approx} 3 \times 10^{-13} cm^{-1} s^{-1}$. Thus the combined mean potential vorticity gradient is approximately $5\text{-}7 \times 10^{-13} cm^{-1} s^{-1}$ in the north-south direction. The mean potential vorticity gradient is shown in Figure 3.3 along with the eddy potential vorticity flux.

3.V. DISCUSSION

The observational data from the Local Dynamics Experiment show that the eddy potential vorticity flux at 31°N, 69.5°W is directed to the southwest

with most of this term due to the thickness flux. Although the LDE is the only data from which the exact form of the total eddy potential vorticity flux (Equation 3.4) can be computed, a partial comparison can be made with another data set from the recirculation region by using the two-layer approximation. In the layer model representation (Holland and Rhines, 1980) the interface height perturbation is analagous to minus the temperature fluctuation divided by the mean vertical temperature gradient T_z^s. The thickness flux with this approximation is proportional to the heat flux at the interface:

$$\overline{\underset{\sim}{u'\eta'}} = \frac{f_o}{H_1} \frac{\overline{\underset{\sim}{u't'}}}{T_z^s} \tag{3.29}$$

In the LDE only the meridional component of the heat flux is significant with the maximum values in the thermocline. The spatially-averaged meridional heat flux at ~ 700 m for a uniform 225 day record at the nine moorings is $-1.89°C$ cm/s which gives a thickness flux of $\overline{v'\eta'} = -.91 \times 10^{-5} cm/s^2$ using an upper layer thickness of 700 m and a mean vertical temperature gradient, $T_z^s = 2.22 \times 10^{-4} °C\ cm^{-1}$, calculated from the average CTD profile. Thus, the two-layer approximation gives a value for the upper layer thickness flux which is comparable to the exact LDE calculation from Equation (3.24).

The two-layer approximation also gives values from Array II which are consistent with the LDE results. Hogg (1983) estimated the meridional lower layer thickness flux at 600 and 1000 m from the POLYMODE Array II data using a two-layer model approximation to the continuous form. Although the Array II data is longer (500-700 days) than the LDE data, the total relative vorticity flux cannot be calculated because of the array configuration. In the Array II data there is a large spatial variation in the heat fluxes, but at 600 and

1000 m depths all of the thickness fluxes in the moorings (with the exception of mooring 6 at 600 m) north of 35°N are southward (Table 3.4). However, as pointed out by Hogg (1983), the 600 m record from mooring 6 is only nine months long and it contains the signal due to two Gulf Stream rings. The magnitude of the correlation coefficients is less than .4, so there are large uncertainties even in the two year records. The amplitudes of the meridional components vary by an order of magnitude between a maximum of $-8 \times 10^{-5} cm/s^2$ at 600 m at 37.5°N to a minimum of $.99 \times 10^{-6} cm/s^2$ at 31.6°N. Although the two-layer approximation estimates are basically consistent with our result, the LDE data and the associated errors can be much better evaluated.

The LDE eddy potential vorticity flux estimates can also be qualitatively compared with the results from numerical model experiments although the LDE result is only a single point measurement. In the numerical model flows (Holland and Rhines, 1980; Harrison and Holland, 1981) the relative vorticity flux dominates the western boundary current and jet separation regions, but the thickness flux is largest in the gyre interior. The magnitude and direction of the eddy potential vorticity flux with respect to the mean potential vorticity gradient indicates the effect of the eddy field on the mean potential vorticity balance. The thickness fluxes in the near field of the model western boundary current are directed opposite to the mean potential vorticity gradient. This down-gradient flux is consistent with eddy generation by baroclinic instability.

The direct application of these model results to the real ocean is not immediate because buoyancy forcing is likely to be equally important as wind or eddy forcing of the mean flow in certain regions. For example, Hogg (1983) divided the North Atlantic abyssal circulation into two types of flow. The

Deep Western Boundary Undercurrent is generated by overflows of bottom water from the Norwegian-Greenland Sea, but there may also be deep recirculating gyres in the interior driven by the thermocline eddy field. While numerical models can a priori restrict the model physics, the oceanic measurement of the eddy potential vorticity flux is only one possible mechanism for mixing of potential vorticity.

The cascade of mean enstrophy by the eddy field can also be compared to the enstrophy input by the wind stress curl. For a wind stress amplitude of 1 dyne/cm^2 acting over a layer 700 m deep, the wind input is

$$\frac{\tau}{\rho_0 h} \sim 1.4 \times 10^{-5} \text{cm s}^{-2}$$

as compared to the eddy flux of $\overline{v'\eta'} = O(1 \times 10^{-5} \text{cm/s}^2)$. The wind input value is not very sensitive to the exact choice of upper layer thickness. A thickness of 1000 m instead of 700 m would not change the magnitude of the wind-input of enstrophy. Thus the eddy forcing of the mean potential vorticity field in the interior is a significant percentage of the wind forcing at the surface. The strength of eddy mixing can also be expressed in terms of the Austauch coefficient (Equation 3.14) for potential vorticity. Using the value $\beta_{eff} \sim 5 \times 10^{-13} \text{cm}^{-1}\text{sec}^{-1}$ estimated from the climatological data, we obtain a mixing coefficient for potential vorticity of

$$A_{pv} = 2 \times 10^{7} \text{cm}^2\text{s}^{-1}$$

which is comparable to the eddy diffusivity of heat estimated by Bryden (1982).

The enstrophy input by the wind and the cascade through potential vorticity mixing by the eddy field must be balanced by dissipation at smaller scales. The wind-input of enstrophy ($\overline{Sq}$) is estimated by

$$\frac{\tau}{\rho_0 h} \frac{\partial \bar{q}}{\partial y}$$

which has a value of $1 \times 10^{-17} sec^{-3}$ using an upper layer thickness of 700 m. The dissipation of the mesoscale eddy field by the internal wave field can be estimated using the viscosity coefficient calculated by Brown and Owens (1981) from the LDE data. They found that only the horizontal viscosity coefficient $\nu_h = 2 \times 10^{-6} cm^2 sec^{-1}$ at 600 m was statistically significant. If the vertical viscosity is neglected, then the wave-induced dissipation of potential vorticity is (from their Equation 1) of order

$$\frac{\nu_h}{2} \frac{1}{L^2} \left(\frac{\partial u}{\partial y} + \frac{\partial v}{\partial x}\right)$$

where L is the length scale of the eddy field and the term in parenthesis is the horizontal mesoscale shear. To estimate the magnitude of the internal wave enstrophy dissipation ($\overline{Dq}$), we use the values L=100 km, and an rms horizontal eddy shear of $2 \times 10^{-6} sec^{-1}$, and multiply by an estimate of the mean potential vorticity $q \sim f_0$. The result is of order $O(10^{-18}\ sec^{-3})$ which suggests that the internal wave field alone cannot account for enstrophy dissipation in the ocean.

Tables and Figures

TABLE 3.1

Eddy Velocity Correlation Gradients

(a) 225 day record from moorings 1-9

$$\frac{\partial}{\partial x}\overline{u'v'} = -1.38 \times 10^{-6} \pm 1.21 \times 10^{-6} \quad cm/s^2$$

$$\frac{\partial}{\partial y}\overline{u'v'} = .78 \times 10^{-6} \pm .85 \times 10^{-6}$$

$$\frac{\partial}{\partial x}\frac{\overline{v'^2 - u'^2}}{2} = 2.73 \times 10^{-6} \pm 1.29 \times 10^{-6}$$

$$\frac{\partial}{\partial y}\frac{\overline{v'^2 - u'^2}}{2} = -.19 \times 10^{-6} \pm .91 \times 10^{-6}$$

$$\overline{u'\zeta'} = -1.57 \times 10^{-6} \pm 1.51 \times 10^{-6} \quad cm/s^2$$

$$\overline{v'\zeta'} = 1.95 \times 10^{-6} \pm 1.54 \times 10^{-6} \quad cm/s^2$$

(b) 434 day record from moorings 1, 6, 8, 9

$$\frac{\partial}{\partial x}\overline{u'v'} = .53 \times 10^{-6} \ cm/s^2$$

$$\frac{\partial}{\partial y}\overline{u'v'} = .36 \times 10^{-6}$$

$$\frac{\partial}{\partial x}\frac{\overline{v'^2 - u'^2}}{2} = 3.05 \times 10^{-6}$$

$$\frac{\partial}{\partial y}\frac{\overline{v'^2 - u'^2}}{2} = .33 \times 10^{-6}$$

$$\overline{u'\zeta'} = .86 \times 10^{-6} \ cm/s^2$$

$$\overline{v'\zeta'} = 2.69 \times 10^{-6} \ cm/s^2$$

TABLE 3.2

Eddy Thickness Flux

(a) 225 day record length

Mooring	Depths	Length	$\overline{u'\eta'}$	$\overline{v'\eta'}$
1	516, 616, 839 m	225 days	$-.62 \times 10^{-5}$ cm/s^2	-1.16×10^{-5} cm/s^2
2	514, 611, 706	225	$-.87 \times 10^{-5}$	-1.73×10^{-5}
4	531, 634, 734	178	-1.66×10^{-5}	-1.89×10^{-5}
5	469, 567, 665	225	$-.92 \times 10^{-5}$	$-.46 \times 10^{-5}$
6	625, 728, 830	225	$-.20 \times 10^{-5}$	-2.86×10^{-5}
9	492, 587, 681	225	$-.48 \times 10^{-5}$	$-.62 \times 10^{-5}$

averages $\overline{u'\eta'} = -.79 \times 10^{-5} \pm .53 \times 10^{-5}$ cm/s^2

$\overline{v'\eta'} = -1.45 \times 10^{-5} \pm .71 \times 10^{-5}$ cm/s^2

(b) 434 day record length

Mooring	Length	$\overline{u'\eta'}$	$\overline{v'\eta'}$
1	434 days	$.18 \times 10^{-5}$ cm/s^2	$-.72 \times 10^{-5}$ cm/s^2
5	434	$.23 \times 10^{-5}$	$-.27 \times 10^{-5}$
6	434	$-.40 \times 10^{-5}$	-1.78×10^{-5}
9	434	$-.35 \times 10^{-5}$	$-.50 \times 10^{-5}$

averages $\overline{u'\eta'} = -.09 \times 10^{-5} \pm .56 \times 10^{-5}$ cm/s^2

$\overline{v'\eta'} = -.82 \times 10^{-5} \pm .57 \times 10^{-5}$ cm/s^2

TABLE 3.3

Eddy Potential Vorticity Flux

225 day records

$\overline{u'q'}$ =	$\overline{u'\zeta'}$ +	$\overline{u'\eta'}$	
$-.95 \times 10^{-5}$	$-.16 \times 10^{-5}$	$-.79 \times 10^{-5}$	cm/s^2
estimated errors			
$.55 \times 10^{-5}$	$.15 \times 10^{-5}$	$.53 \times 10^{-5}$	

$\overline{v'q'}$ =	$\overline{v'\zeta'}$ +	$\overline{v'\eta'}$	
-1.25×10^{-5}	$.20 \times 10^{-5}$	-1.45×10^{-5}	cm/s^2
estimated errors			
$.73 \times 10^{-5}$	$.15 \times 10^{-5}$	$.71 \times 10^{-5}$	

Table 3.4

* 90 percent level of correlation

Mooring	Lat./Long.	Record Length (days)	Depth (m)	Correlation Coefficients ρ_{ut}	ρ_{vt}	$\overline{u't'}$ °C cm/sec	$\overline{v't'}$ °C cm/sec	$\overline{u'n'} \times 10^{-6}$ cm/sec^2	$\overline{v'n'} \times 10^{-6}$ cm/sec^2
7	31.6°N,55°W	380	600	.34*	.05	.94	.13	7.16*	.99
		762	1000	.18	-.18	.35	-.33	2.66	-2.51
5	34.9°,55.1°	724	600	-.05	.01	-1.06	.19	-9.51	1.70
		724	1000	-.18	-.19	-1.05	-.95	-6.57	-5.94
3	35.6°,55.1°	776	600	.07	-.09	1.67	-2.13	15.01	-19.15
		476	1000	.05	-.19	.27	-1.02	1.98	-7.48
1	35.9°,55.1°	557	600	-.03	-.16	-.74	-3.29	-7.67	-34.09
		663	1000	-.002	-.21*	-.02	-1.72	-.10	-8.42*
2	35.9°,54.8°	527	600	-.06	-.13	-.98	-2.03	-11.21	-23.22
		744	1000	-.19*	-.26*	-2.00	-2.28	-1.07*	-1.47*
4	36.0°,53.8°	697	600	-.01	-.20*	-.26	-4.70	-2.41	-43.56*
		480	1000	-.22	-.20	-1.98	-1.10	-10.49	-5.83
6	35.9°,59.0°	284	600	-.10	.40*	-3.51	18.70	-31.92	+170.08*+
		648	1000	-.06	-.13	-.43	-1.32	-2.38	-7.30
8	37.5°,55.0°	779	600	-.28*	-.27*	-10.39	-9.63	-86.40*	-80.08*
		516	1000	-.40*	-.30*	-4.70	-3.63	-37.93*	-29.30*

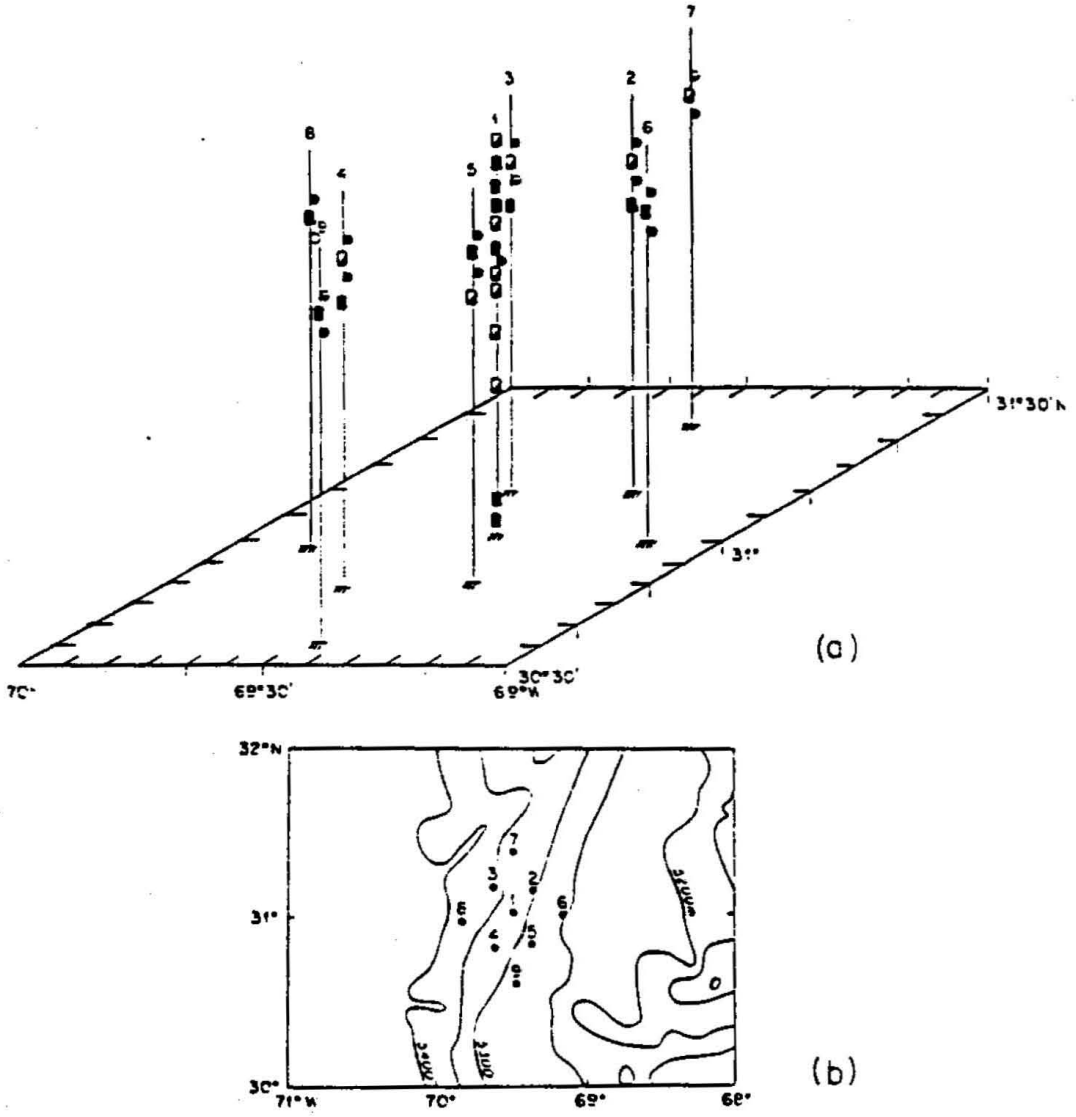

Figure 3.1

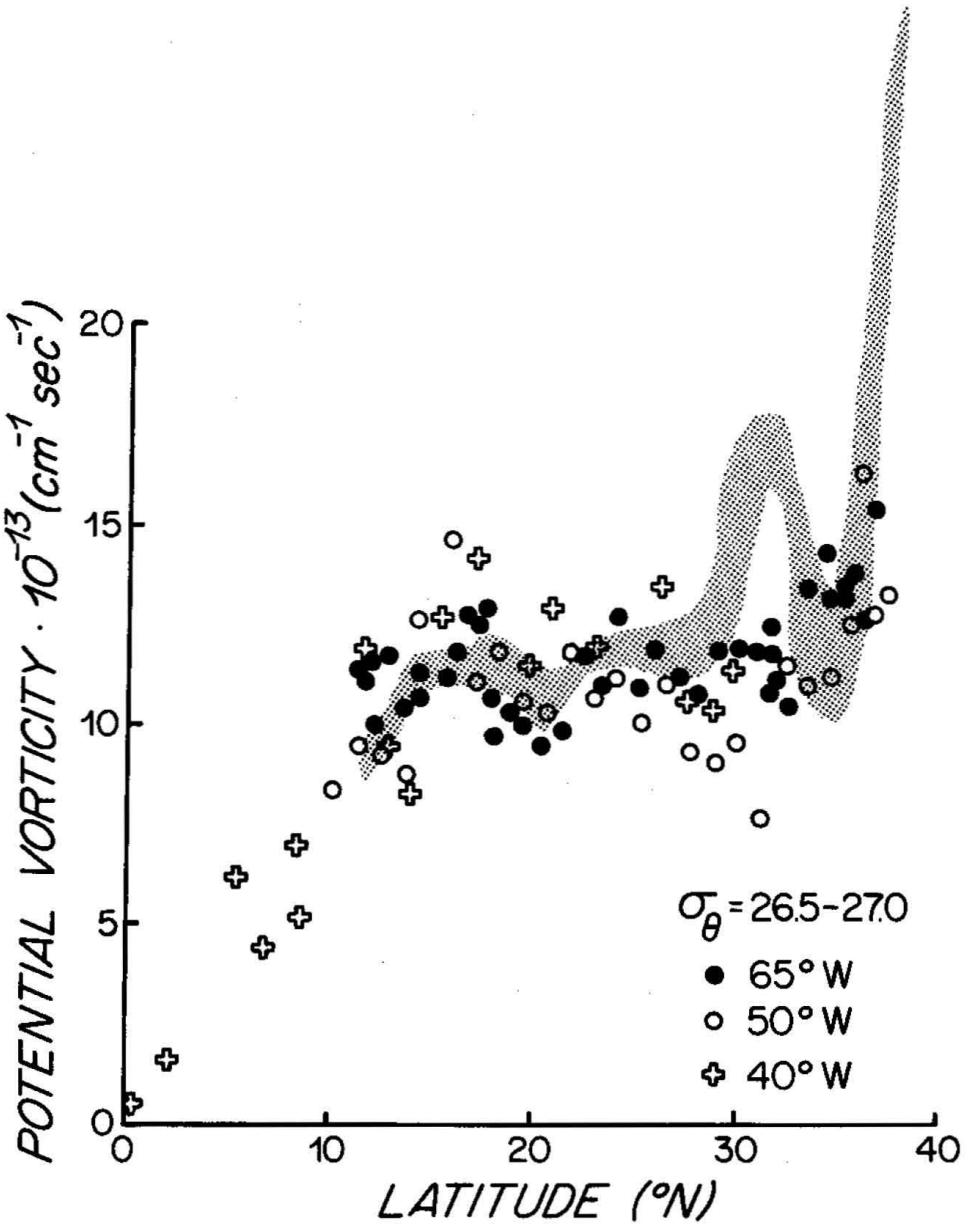
POTENTIAL VORTICITY · 10^{-13} (cm^{-1} sec^{-1})
LATITUDE (°N)
0
5
10
15
20
0
10
20
30
40
σ_θ = 26.5-27.0
65° W
50° W
40° W

Figure 3.2

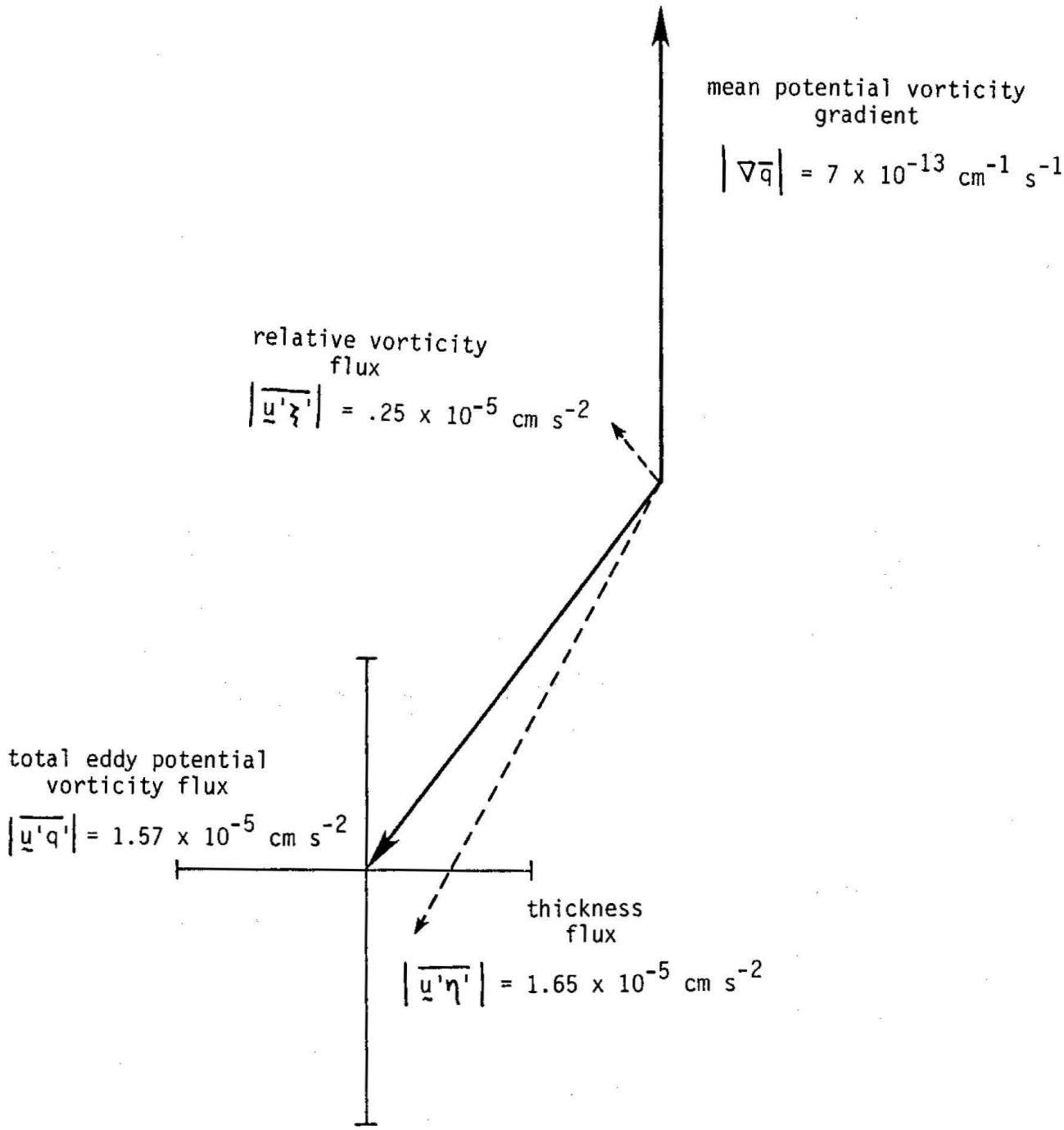
mean potential vorticity gradient
$|\nabla\bar{q}| = 7 \times 10^{-13}$ cm^{-1} s^{-1}
relative vorticity flux
$|\overline{\underset{\sim}{u}'\zeta'}| = .25 \times 10^{-5}$ cm s^{-2}
total eddy potential vorticity flux
$|\overline{\underset{\sim}{u}'q'}| = 1.57 \times 10^{-5}$ cm s^{-2}
thickness flux
$|\overline{\underset{\sim}{u}'\eta'}| = 1.65 \times 10^{-5}$ cm s^{-2}

Figure 3.3

CHAPTER 4

THE MEAN DYNAMICAL BALANCES IN THE LOCAL DYNAMICS EXPERIMENT: AN ALTERNATE MODEL

4.I. INTRODUCTION

The results of the previous two chapters of this thesis have strong implications for the mean dynamical balances at thermocline depths in the Local Dynamics Experiment (LDE). The scale analysis in Chapter 2 suggests that the eddy term has a negligible effect on the vorticity balance between mean planetary advection and vortex stretching. However, this analysis also shows that the eddy heat flux divergence in the mean heat balance might be as large as the mean horizontal temperature advection. These combined vorticity and heat balances imply that the relative vorticity flux in the mean potential vorticity balance should be negligible compared to the thickness flux. This has been demonstrated by the direct estimates in Chapter 3. Thus the results from both chapters suggest that the eddy term is negligible in the mean vorticity balance but may be important in the mean heat balance in the thermocline if the eddy heat fluxes are significant.

This chapter reexamines the mean dynamical balances for several averaging periods using the velocity measurements from nine depths on the LDE central mooring and the eddy heat fluxes in the thermocline from all nine moorings. A previous analysis of these data (McWilliams, 1983) suggested that the eddy relative vorticity flux divergence must be included in the depth-integrated vorticity balance in order to balance the topographically-induced vertical velocity. This vertical velocity inferred at the bottom from the

kinematic boundary condition is an order of magnitude larger than the Ekman velocity at the surface. We first show that the McWilliams' model vertical velocity at ~ 4000 m depth is an order of magnitude larger than the vertical velocity estimated directly from the mean heat equation. Since McWilliams' model is essentially determined by the bottom constraint, this discrepancy raises some question about the validity of his conclusions.

The statistical uncertainty in the measurements does not allow an absolute determination of the long-term mean vertical velocity even to within an order of magnitude. It is, however, possible to examine the consistency of balances for a finite averaging period. We use the method of Bryden (1980) to test the linear vorticity balance for the depth interval between the surface and the mid-thermocline. The depth-averaged mean planetary advection is compared to the vortex stretching between the surface and the mid-thermocline using the vertical velocity calculated from the sum of the mean horizontal temperature advection and the eddy heat flux divergence in the mean heat equation.

4.II. AN ALTERNATE MODEL

McWilliams (1983) evaluated the mean dynamical balances in the LDE using smoothed velocity and buoyancy profiles from the current meter and CTD data. McWilliams first examined the depth-integrated vorticity balance:

$$\int_{-H}^{0} [\beta \bar{v} + \bar{u} \cdot \nabla \bar{\zeta} + \nabla \cdot \overline{u'\zeta'}]dz = f(w_{Ek} - w_b) \qquad (4.1)$$

where w_{Ek} is the Ekman velocity at the surface and w_b is the vertical velocity at the bottom ($z = -H = -5355$ m). He found it necessary to include the eddy relative vorticity flux divergence term ($\nabla \cdot \overline{u'\zeta'}$) in order to

achieve a balance. The vertical velocity was then estimated as a function of depth by assuming the eddy relative vorticity flux divergence to be depth-independent. From this model the vertical velocity at all depths below 500 m was calculated to be an order of magnitude larger than the Ekman velocity. The inferred profile for vertical velocity together with the observed mean horizontal velocity and buoyancy profiles were then used to estimate the eddy term in the mean heat balance.

Because McWilliams' vorticity model was evaluated as a vertical integral over the entire depth, it depends almost entirely on the boundary conditions on the vertical velocity. For the LDE data set the first two terms in the integral in Equation (4.1) are negligible. The first of these terms, the depth-integrated planetary advection, is nearly zero because the southward flow above mid-depth cancels the northward flow below so that the integral $\int_{-H}^{0} \beta\bar{v}\, dz \sim 0$. The second term, the mean advection of vorticity ($\bar{u} \cdot \nabla\bar{\zeta}$), is also negligible as shown from the ratio:

$$\frac{\bar{u} \cdot \nabla\bar{\zeta}}{\beta\bar{v}} \sim \frac{U_o}{\beta L^2} \sim .025$$

evaluated with the parameters L = 200 km and U_o = 2 cm/sec. The third term, the eddy relative vorticity flux divergence, cannot be calculated directly from the data.

The terms on the right side of Equation (4.1) are the boundary conditions on the depth-integrated vorticity balance. At the bottom the mean velocity vectors are directed to the northeast, upslope of the topography. The value of the bottom vertical velocity w_b inferred from the kinematic boundary condition:

$$w_b = -\underset{\sim}{\bar{u}} \cdot \nabla h(x,y) \qquad (4.2)$$

at the bottom $z = -H + h(x,y)$ is an order of magnitude larger than the Ekman velocity at the surface. Since the depth integral of northward advection nearly vanishes, the eddy term must be included in this model balance in order to balance this strong topographic forcing. Thus the McWilliams' vorticity balance for the LDE is essentially:

$$\int_{-H}^{0} \nabla \cdot \overline{\underset{\sim}{u}'\zeta'} \, dz = w_{Ek} - w_b \sim -w_b \, .$$

However, we can show by scale analysis that the eddy term is at most depths negligible compared to the planetary advection. The magnitude of the eddy relative vorticity flux was estimated (Chapter 3) to be $.25 \times 10^{-5}$ cm/sec^2. If the eddy flux varies over the same scale (300 km) as the eddy energy (see Chapter 2), then the ratio:

$$\frac{\nabla \cdot \overline{\underset{\sim}{u}'\zeta'}}{\beta \bar{v}} \sim .2 \quad ,$$

assuming a mean velocity of $U_o \sim 2$ cm/sec. Yet in McWilliams' model the topographic forcing is balanced by the eddy relative vorticity flux divergence because the eddy term is assumed to be a depth independent constant. Therefore, the subsequent inferences of vertical velocity as a function of depth and of eddy heat diffusivity from this model are ultimately controlled by the bottom condition.

This chapter is an alternate analysis of the mean dynamical balances in the LDE. We first directly estimate the vertical velocity near the bottom

using the velocity point measurements and the mean heat balance. Below the thermocline the eddy heat fluxes are negligible and the vertical velocity is simply proportional to the mean horizontal temperature advection. Within the measurement errors the vertical velocity for the finite averaging period is shown to be an order of magnitude smaller than that predicted by the kinematic bottom boundary condition. There is sufficient uncertainty in the long-term mean velocity measurements to question the results of any model balance which depends so strongly on the boundary condition.

We then test the consistency of the linear vorticity balance for the depth interval between the surface and the thermocline by comparing the depth-averaged planetary advection to the vortex stretching using the method of Bryden (1980). This vertical integral is restricted to a depth interval over which the meridional velocity component does not change sign in order to reduce the experimental uncertainty and to allow a clear evaluation of the vorticity balance. The vortex stretching term is calculated from the difference in Ekman velocity (w_{Ek}) at the surface and the vertical velocity at mid-thermocline depth.

The vertical velocity (w) in the thermocline may depend on both the mean horizontal temperature advection (w_m) and the eddy heat flux divergence (w_e):

$$w = w_m + w_e \tag{4.3}$$

$$= \frac{-\bar{u} \cdot \nabla \bar{T}}{\bar{T}_z} + \left(- \frac{\nabla \cdot \overline{u't'}}{\bar{T}_z} \right)$$

where $\overline{T}_z$ is the mean vertical temperature gradient. The vertical velocity due to mean horizontal temperature advection (w_m) is calculated using the thermal wind relation by the vertical turning of the mean velocity vector through the thermocline. The balance between planetary advection and vortex stretching due only to mean temperature advection is tested for averaging periods of 225, 290, and 445 days. Because of instrument failures, the thermocline vertical velocity due to the eddy heat flux divergence can be calculated only for the shortest of these time periods. The eddy heat flux divergence estimated by finite difference from the heat fluxes in the nine mooring array is non-zero for this time period. By comparing the depth-averaged planetary advection to $f(w_{Ek} - w_m)/\Delta z$ we can test the linear vorticity balance and the importance of the eddy heat flux divergence during the experiment.

4.III. DATA AND STATISTICAL UNCERTAINTIES

The velocity measurements used to compute the mean dynamical balances are from the central mooring of the LDE array. This mooring was instrumented with current and temperature meters at 269, 394, 516, 616, 715, 839, 2008, 3004, 5250, and 5332 m depths. The method for correcting the temperature records for mooring motion are discussed in Mills et al. (1981). Because of instrument failures there are some gaps in the basic data set. The data return from the current meter at 715 m depth is only 138 days, so the data from this level are not used in this study. The direction of the velocity vector from the 394 m instrument has been rotated to correct for instrument direction error as noted in Owens et al. (1982). Finally, although there is a 445 day record length from the instruments at and above 839 m, there were instrument failures during the middle of the experiment at 2008 and 3004 meters. Since

the information at these depths is necessary for computing the balances below the thermocline, a uniform 290 day record is also examined for the nine instruments on the central mooring.

The mean velocity vectors from this 290 day period are compared with those from the 445 day period in Figure 4.1(a,b). In both cases the mean velocities are southeastward above mid-depth (~ 2000 m) and northeastward below. For the 290 day record between 269 and 839 m the mean velocity vectors point nearly in the same direction, while between 2008 m and the bottom there is counterclockwise veering in depth. For the 445 day record there is counterclockwise veering in depth between 269 and 839 m. The velocity vectors at the bottom for the 445 day record point ~ 30°clockwise with respect to the 290 day means, but both are directed upslope of the bottom topography.

The uncertainty in the long-term means based on a record of finite length T is given by (Flierl and McWilliams, 1977) as $\varepsilon_u = \sqrt{2\sigma^2\tau_u/T}$ where σ_u^2 is the variance, τ_u is the integral correlation time:

$$\tau_u = \int_0^\infty c_u(\tau)d\tau \quad ,$$

and $c_u(\tau)$ is the covariance function of the velocity component. In practice, this function is integrated over increasing time lags (τ) until its amplitude decreases below the 95 percent significance level. The average integral time scale for all the moorings at 600 and 800 m is 15 days for temperature and the meridional velocity component and 13 days for the zonal velocity component. At other depths on the central mooring the time scales vary between 8 and 20 days and decrease to about 10 days for all variables at 5000 m. Table 4.1 shows the mean velocity components from the uniform 290 day record

at the central mooring. None of the meridional components are significant at the 70 percent level ($\pm \varepsilon_v$), while all the zonal components except those at 2008 and 3004 m are significant. This result agrees with the uncertainty in the 445 day mean velocity components tabulated in Owens et al. (1982).

To evaluate the mean dynamical balances we must also consider the possible importance of the eddy terms. Table 4.2 shows the eddy heat flux components from the 290 day record as a function of depth on the central mooring. The temperature sensors on instrument 6401 failed so there are no temperature measurements at the shallowest depth. The uncertainty in the long-term eddy heat flux from a record of duration T is given by (Flierl and McWilliams, 1977)

$$\varepsilon_{vt} = \sqrt{\frac{2\sigma_v^2 \sigma_t^2 \tau_{vt}}{T}} \qquad (4.4)$$

where σ_t^2 is the eddy temperature variance and σ_v^2 is the velocity component variance. The integral correlation time τ_{vt} is defined as:

$$\tau_{vt} = \int_{-\infty}^{\infty} C_{vt}^2(\tau)\, d\tau$$

where $C_{vt}^2(\tau)$ is the square of the cross-covariance function between temperature and velocity. The integral time scale for the heat flux components varies between 12 and 22 days. On the central mooring (Table 4.2) the amplitude of the meridional heat flux component is non-zero at the 70 percent level ($\pm \varepsilon_{vt}$) only at 516 and 616 meters for both the 290 and 445 day records lengths. Table 4.2 also shows the correlation coefficients for the eddy heat flux components calculated using the average time scale for temperature and the velocity component. For the 290 day record the 516 and 616 m meridional

components with correlation coefficients significant at the 90 percent level have non-zero amplitudes. At 445 days the 394 and 839 m meridional heat flux components are also correlated, but the amplitudes are not significantly different from zero. Increasing the record length by 60 percent from 290 days to 445 days reduces the uncertainty in the heat flux amplitude by only about five percent.

As discussed in Chapter 3, the eddy term in the mean heat balance can be evaluated only at mid-thermocline depth because of the configuration of the instruments. We estimate the magnitude of the eddy heat flux divergence in the mean heat balance by calculating the horizontal gradients of the eddy heat fluxes from the nine mooring array. The longest uniform record length for the nine moorings is only 225 days, a period which has been shown in Chapter 3 to be adequate for estimating the eddy thickness flux. The values of these eddy heat flux components and the 70 percent errors as defined in Equation (4.4) are shown in Table 4.3 for the 225 day records. At six of the nine moorings the meridional heat flux correlation coefficients are significant, but none of the zonal components show correlation. For the five meridional heat flux components with non-zero amplitudes the uncertainties are at least 60 percent of the magnitude.

It is important in this analysis to distinguish definitions of uncertainty. The error estimates given in this section are estimates of the uncertainty in the long-term absolute means from finite data records. Given the 445 day variances and correlation times in the thermocline, an estimate of the amplitudes of the mean velocity components and the heat flux to 20 percent accuracy at the 70 percent level would require records 10 years long for the meridional heat flux and zonal velocity component and 30 years long for the

meridional velocity component. Faced with this sampling requirement it is unlikely that dynamical statements can be made about the long-term mean balances from current meter arrays. Instead, in this study we can only establish consistency of the balances during the finite measurement period.

4.IV. A DIRECT COMPARISON WITH THE KINEMATIC BOUNDARY CONDITION

The first part of this analysis is a comparison of the vertical velocity computed directly from the mean heat balance with that predicted by the kinematic bottom boundary condition. Since McWilliams' model is controlled by the large topographically-induced vertical velocity, this will be an important consistency test. The vertical velocity near the bottom is determined entirely by the mean advection of temperature because the eddy heat fluxes are not significant below the thermocline. Bryden (1976) has shown that using the thermal wind relation this term is proportional to the turning of the mean velocity vector in the vertical according to

$$w = -\frac{f}{N^2} R^2 \frac{\partial \phi}{\partial z} \tag{4.5}$$

where $N^2(z)$ is the square of the buoyancy frequency, R is the speed, and ϕ is the direction. As shown in Figure 4.1a, the velocity vectors turn counterclockwise in depth between 2008 and 5000 m for the uniform 290 day record. The vertical velocity is calculated from the change in direction between 2008 m and 5291 m by:

$$w_{3650} = -\frac{f}{N^2_{3650}} R^2_{3650} \frac{\Phi_{2008} - \Phi_{5291}}{3283 \text{ m}} ,$$

where the two records at 5250 and 5332 m have been averaged to 5291 m depth. The speed at 3650 m is interpolated from the speeds at 3004 and 5291 m. The buoyancy frequency N^2_{3650} is calculated from the averaged CTD profile from 13 casts during recovery and deployment as described in Mills et al. (1981). From the uniform 290 day record we estimate that the vertical velocity at 3650 m is upward with a magnitude of 2.28×10^{-4} cm/sec. The standard error in this value is estimated to be $.72 \times 10^{-4}$ cm/sec assuming a 2 degree (.035 rad) and a .25 cm/sec experimental error in direction and speed (Bryden, 1980). This value is similar to the vertical velocity ($w = 1.78 \times 10^{-4}$ cm/sec $\pm .83 \times 10^{-4}$ cm/sec) at 4150 m estimated from the turning and average speed between 3004 and 5291 m. Thus the mean heat equation predicts a vertical velocity of $O(1 \times 10^{-4}$ cm/sec) at ~ 4000 m depth based on the uniform 290 day data. This is substantially less than the value (20×10^{-4} cm/sec) predicted for this depth by McWilliams' (1983) model from the same 290 day record (see his Figure 7, profile U).

This discrepancy is caused by the dependence of McWilliams' model on the kinematic bottom boundary condition Equation (4.2). This boundary condition is evaluated using the mean velocity measurements at the central mooring and the local bottom depth $z = -H + h(x,y)$. The bottom topography in the LDE region slopes upward to the southeast. The value for the slope used in McWilliams' (1983) analysis:

$$\nabla h = (1.5,-.3) \times 10^{-3} \tag{4.6}$$

was calculated over a horizontal scale of about 100 km from the topographic charts of Pratt (1968). This is similar to the value

$$\nabla h = (1.27,.03) \times 10^{-3} \tag{4.7}$$

calculated by Bryden (personal communication) from a planar fit through the sounding depths during the array deployment. The Ekman layer thickness over the slope can be estimated assuming a dissipation time of τ = 500 days (Owens, 1975; Holland, 1978) or equivalently a vertical viscosity coefficient of 1 cm^2/sec. The Ekman number $E_v = (1/f\,\tau)^2$ then gives an Ekman layer thickness ($\delta_E = H\sqrt{E_v}$) of only a few meters using H = 5400 m. Therefore, the vertical velocity induced by the Ekman pumping should be two orders of magnitude less than that induced by the sloping bottom.

Since the bottom velocities are directed to the northeast, the bottom boundary condition predicts an upward vertical velocity of $w = 24.92 \times 10^{-4}$ cm/sec at 5291 m using the topography estimate (4.6) or $w = 25.91 \times 10^{-4}$ cm/sec using Equation (4.7). Both estimates are an order of magnitude larger than the vertical velocity calculated at 3650 m from the mean heat balance. Some of this discrepancy can be rationalized because the horizontal velocity components are bottom intensified. The largest estimate of vertical velocity at 5291 m from the heat balance would be based on a forward difference:

$$w = \frac{-f}{N^2_{5291}} R^2_{5291} \quad \frac{\phi_{3004} - \phi_{5291}}{2287\ m} \quad . \tag{4.8}$$

This estimate, $w = 7.65 \times 10^{-4}$ cm/sec $\pm$ 2.45×10^{-4} cm/sec, is still a factor of three less than that predicted by the kinematic boundary condition. Stated in another way, the angle between the 3004 and 5291 meter velocity vectors would be three times larger than the observed.

There are several plausible explanations for the discrepancy between the kinematic boundary condition and the mean heat balance. The simplest is

due to the statistical uncertainty in the velocity components. From the 70 percent uncertainty for the 290 day record (Table 4.1) the bottom vertical velocity in the kinematic boundary condition could vary between $O(1 \times 10^{-4}$ cm/sec) and $O(5 \times 10^{-3}$ cm/sec). At the 95 percent confidence level it is not even possible to state the sign of w. The second simple explanation is that the eastward upslope bottom velocities are forced by local topographic features and therefore are not representative of the large-scale mean circulation. The eastward bottom flow in the LDE is in the opposite direction from the flow along 70°W (Schmitz, 1977). Since the LDE bottom velocities are only from a single mooring, we cannot establish whether they reflect the mean circulation in this region. It is likely that spatially-averaged velocity components would give a smaller estimate of vertical velocity in the kinematic boundary condition.

The third possibility concerns the representativeness of the 290 day uniform record. The velocity records from this time period are dominated by two intense baroclinic jets (Owens et al., 1982) which are polarized in depth. For the longer 445 day record the 2008 and 3004 m mean velocity vectors could, therefore, be quite different. However, we will argue that this possibility still would not resolve the discrepancy between the depth-integrated vorticity balance and the boundary conditions even for the 445 day record. In Figure 4.1(a,b) it is shown that at 5000 m the 445 day records are approximately the same length as the 290 day means but rotated 30° clockwise. The kinematic boundary condition for the 445 day bottom velocities predicts a vertical velocity $w = 34.65 \times 10^{-4}$ cm/s which is fifty percent larger than the value predicted from the 290 day records.

Suppose that the 290 day mean velocity vector at 3004 m is rotated so that the vertical velocity in the mean heat balance matches the prediction of the kinematic boundary condition for the 445 day record. In writing the mean heat balance in Equation (4.3) we have assumed that local time changes in temperature are negligible. There are no trends in the temperature records over the measurement period (see Mills et al., 1981), but to estimate the local time change in temperature, McWilliams used the difference in average temperature for the two halves of the 445 day record. The upper bound for this term:

$$\left| \frac{\partial T}{\partial t} \right| < .1 \times 10^{-8} \ ^\circ C \ sec^{-1}$$

could induce a vertical velocity of $w < 5 \times 10^{-4}$ cm/sec based on a mean vertical temperature gradient of $\bar{T}_z = 2 \times 10^{-6}$ °C/cm at 5000 m from the average CTD profile. Thus to balance the kinematic boundary condition, the mean horizontal temperature advection must still account for a vertical velocity of about 30×10^{-4} cm/sec. The 3004 m vector would then point 26 degrees clockwise from east, nearly a 60 degree rotation from the 290 day vector. Although this possibility cannot be excluded, the 60° rotation is a factor of two larger than any other change in direction between the 290 and 445 day mean vectors.

This rotation of the mid-depth velocity vectors would shift the zero crossing in the meridional velocity component from ~ 2000 m depth to ~ 4000 m depth, so it has the effect of tending to balance the topographically forced vertical velocity with more southward planetary advection. However, this change is still not sufficient to achieve a balance between the depth-integrated planetary advection and the difference between the Ekman velocity

at the surface and the topographic condition. For this balance to hold, it would require that the meridional components of the velocity vectors at 2008 and 3004 meters increase to about -4 cm/sec for the 445 day record, assuming that the angle between the 2008 and the 3004 m vectors is preserved. Thus, it does not seem plausible that a depth-integrated vorticity balance can be rationalized for these velocity vectors if the vertical velocity is as large as predicted by the kinematic boundary condition.

It is this discrepancy which led McWilliams to invoke the importance of the eddy relative vorticity flux divergence. Yet simple scale analysis shows that in the thermocline the eddy term is not large compared to the mean planetary advection. Moreover, the eddy relative vorticity is likely to decrease in importance at depth where the eddy kinetic energy is less than in the thermocline. The most plausible explanation for the discrepancy with the local heat balance and the vertically-integrated vorticity balance is that local topographic features are controlling the bottom point measurements and that a spatially-averaged field must be used in the bottom boundary condition.

4.V. THE MEAN DYNAMICAL BALANCES FROM THE THERMOCLINE TO THE SURFACE

Despite the discrepancy in the mean balances below the thermocline, it is still possible to evaluate the terms in the linear vorticity balance for the depth interval between the surface and the thermocline. This region contains most of the instruments and there is less uncertainty because the meridional velocity component does not change sign. We estimate the planetary advection from the depth-averaged velocity and the vortex stretching from the difference in Ekman velocity at the surface and the vertical velocity in the thermocline. The vertical velocity is the sum of contributions from the mean

horizontal temperature (w_m) advection and the eddy heat flux divergence (w_e). Bryden's (1980) method is used to calculate the mean horizontal temperature advection from the turning of the mean horizontal velocity vectors for three averaging periods. The vortex stretching due to the difference between the Ekman velocity and the term w_m is compared to the planetary advection for the three periods. In addition, we evaluate the vertical velocity induced by the eddy heat flux divergence from the LDE array. From these comparisons we can show whether it is necessary to include the vertical velocity induced by the eddy heat flux divergence in order to obtain a balance between planetary advection and vortex stretching.

The northward advection of planetary vorticity over this depth interval is estimated by integrating the northward velocity component using the trapezoidal rule. These values are listed in the first column of Table 4.4 along with the standard error from the depth-integrated velocity component. The 95 percent confidence interval for the true planetary advection based on normally distributed data is less than two standard deviations. The depth-averaged meridional velocity components for the depth interval between 825 m and the surface are -.30, -2.90, -2.56 cm/sec for the 225, 290, and 445 day records respectively.

To test whether this southward transport could be balanced without the eddy terms in the mean heat equation, we first calculate the vortex stretching from the difference between the Ekman velocity at the surface and the contribution to the vertical velocity at 728 m due only to the mean advection of temperature. The Ekman velocity in the LDE region is estimated to be -1.5×10^{-4} cm/sec from Leetmaa and Bunker (1978). The mean horizontal temperature advection at 728 m depth is estimated from the turning of the mean velocity

vector between 616 m and 839 m. For the 225 day record there are velocity measurements at these depths from moorings 2 and 3 in addition to mooring 1, the central mooring. The average of these three values is listed in Table 4.4 for the 225 day record. The longer 290 and 445 day records are available only from the central mooring, so the errors are larger for these two cases. The standard error in the values of w_m are again estimated using a .035 radian error in direction and a .25 cm/sec error in speed. The vertical velocities (w_m) at 728 m due to mean horizontal temperature advection for the 225 and 290 day time periods are $.21 \times 10^{-4} \pm .06 \times 10^{-4}$ cm/sec and $-.14 \times 10^{-4} \pm .66 \times 10^{-4}$ cm/sec respectively. For the 445 day record the vertical velocity is an order of magnitude larger, $w_m = +1.64 \times 10^{-4} \pm .71\ 10^{-4}$ cm/sec, because there is substantial clockwise turning of the mean velocity vectors with depth.

Vortex stretching between the thermocline and the surface is first estimated by using only the mean contribution (w_m) to the vertical velocity in the thermocline. The second column of Table 4.4 shows this term computed for the three averaging periods. At the 225 and 290 day periods planetary advection does not balance $f(w_{Ek} - w_m)/\Delta z$ within two standard errors although the terms are of the same sign. However, a balance is possible for the 445 day record using two standard errors for both terms.

To investigate the possible contribution of the eddy term to the vertical velocity in the thermocline, the eddy heat flux divergence is calculated from the slope of a planar regression through the 225 day average heat fluxes at the nine moorings. The heat fluxes were first interpolated to a uniform 728 m depth using the average vertical gradient of the heat flux from moorings 1, 2, and 3. The gradients were then determined by fitting planar regressions

through the nine values. The divergence is estimated to be -1.26×10^{-7}°C cm/sec with an error of 1.04×10^{-7}°C cm/sec. This error is calculated by dividing the standard error in the 225 day heat flux -- .27°C cm/sec for $\overline{u't'}$ and .62°C cm/sec for $\overline{v't'}$ (Bryden, 1982) -- by the 70 km meridional and 50 km zonal horizontal scales of the mooring array. The vertical velocity induced by the eddy heat flux divergence is calculated by dividing the heat flux divergence by the mean vertical temperature gradient at 728 m estimated from the average CTD profile. The result, $w_e = 5.67 \times 10^{-4}$ cm/sec with a standard error of 3.35×10^{-4} cm/sec, is comparable to or larger than the vertical velocity due to mean advection for all three averaging periods.

The confidence limits for the true eddy heat flux divergence can be computed by standard regression techniques assuming that the eddy heat fluxes are normally distributed. A significance test with six degrees of freedom for a planar fit through the nine moorings shows that the total eddy heat flux divergence is non-zero only at the 75 percent confidence level. The horizontal gradients with 95 percent confidence limits are:

$$\frac{\partial}{\partial x}\overline{u't'} = 1.05 \times 10^{-7} \pm 1.24 \times 10^{-7}\text{°C/sec}$$

and

$$\frac{\partial}{\partial y}\overline{v't'} = -2.31 \times 10^{-7} \pm 2.00 \times 10^{-7}\text{°C/sec.}$$

Thus most of the uncertainty in the eddy heat flux divergence is due to the zonal heat flux components which are not statistically significant, as shown in Table 4.3.

Because there is large uncertainty in the eddy heat flux, we cannot independently test the significance of the linear vorticity balance and the significance of the eddy-induced vertical velocity. However, for both the 290

and 445 day records the planetary advection term is larger than $f(w_{Ek} - w_m)/\Delta z$. If we assume that the balance holds between planetary advection and the vortex stretching from the total vertical velocity at 728 m depth ($w_{728} = w_m + w_e$), then from the values in Table 4.4 we can infer the vertical velocity (w_e) induced by the eddy heat flux:

$$w_e = \frac{-\Delta z}{f} \left[\beta \bar{v} - f\left(\frac{w_{Ek} - w_m}{\Delta z}\right)\right]$$

This quantity is shown in the third column of Table 4.4. At 225 days the inferred value of w_e is not consistent with the direct estimate $w_e = 5.67 \times 10^{-4} \pm 3.35 \times 10^{-4}$ cm/sec, but at both 290 and 445 days the two estimates agree within one standard deviation. We conclude that for the 290 day record the linear vorticity balance is consistent only if the vertical velocity due to the eddy heat flux divergence is included at the thermocline. For the 445 day record, planetary advection could balance vortex stretching without the eddy term if both quantities are in error by two standard deviations. However, the inferred eddy-induced vertical velocity from this record length is also consistent with the direct estimate of w_e to within only one standard deviation.

4.VI. DISCUSSION

The uncertainty in the long-term measurements prevents us from making statistically significant statements about the mean dynamical balances in the LDE. However, we use consistency arguments to analyze two aspects of the mean balances. First, we show that McWilliams' (1983) model for the depth-integrated vorticity balance is not consistent with direct estimates of vertical velocity . The mean heat balance predicts a vertical velocity at ~ 4000 m depth which is an order of magnitude smaller than that in McWilliams'

model. This difference is due to the vertical velocity from the kinematic boundary condition. We argue that consistent dynamical balances cannot hold if the vertical velocity is as large as predicted by the local point measurements.

To minimize the uncertainty in the balances we calculate the planetary advection and vortex stretching for the depth interval between the surface and the thermocline using three averaging periods. For the shortest period no consistent balance is possible. For the 290 day period, the linear vorticity balance can hold only if the eddy-induced vertical velocity is non-zero. For the 445 day period, the linear vorticity balance between $\overline{\beta v}$ and $f(w_{Ek} - w_m)/\Delta z$ is consistent within two standard errors, but the eddy-induced vertical velocity could still be non-zero. Finally, we comment on the effect of including the eddy relative vorticity flux divergence ($\nabla \cdot \overline{u'\zeta'}$) in the vorticity balance. According to McWilliams' arguments, this term should be negative and from scaling it is of order 1×10^{-13} s^{-2}. If the relative vorticity flux divergence is included in the mean vorticity balance, then the eddy-induced vertical velocity must be even larger than in column 3, Table 4.4.

TABLES AND FIGURES

TABLE 4.1: 290 DAY RECORD MEANS

Instrument	Depth m	$\bar{U}$ cm/sec	$\bar{V}$ cm/sec
6401	269	-3.20* ± 2.42	-3.09 ± 4.43
6402	394	-3.07* ± 2.82	-3.03 ± 4.11
6403	516	-2.87* ± 2.51	-2.79 ± 3.73
6404	616	-2.42* ± 2.16	-2.52 ± 3.54
6406	839	-1.57 ± 1.57	-1.60 ± 2.61
640,10	2008	.17 ± 1.10	.00 ± 1.77
640,11	3004	.49 ± 1.35	.29 ± 1.71
640,12	5250	1.84* ± 1.27	1.62 ± 1.86
640,14	5332	2.16* ± 1.35	1.77 ± 1.97

* Amplitude significant at 70 percent confidence level

TABLE 4.2: 290 AND 445 DAY EDDY HEAT FLUXES

Instrument	depth (m)	290 day records °C cm/sec $\overline{u't'}$	ρ_{ut}	$\overline{v't'}$	ρ_{vt}	445 day records °C cm/sec $\overline{u't'}$	ρ_{ut}	$\overline{v't'}$	ρ_{vt}
6401	269	no temperature record							
6402	394	- .44± .83	-.15	- .88± .91	-.32	- .39± .66	-.17	- .78± .83	-.31**
6403	516	-1.32±1.71	-.24	-2.52*±2.11	-.46**	-1.17±1.37	-.26	-2.55*±1.98	-.49**
6404	616	-1.48±1.91	-.25	-2.89*±2.47	-.45**	-1.25±1.57	-.25	-2.91*±2.36	-.48**
6406	839	- .55±1.48	-.13	-1.77±1.92	-.36	- .40±1.24	-.11	-1.53±1.85	-.32**
64010	2008	- .02± .08	-.07	- .06± .13	-.16	----------			
64011	3004	.04± .06	.23	.03± .07	.14	----------			
64012	5250	- .01± .01	-.004	- .01± .03	-.002	.01± .01	.09	- .001±.03	-.004
64014	5332	.00± .03	-.01	- .01± .06	-.09	.00± .04	.01	.00± .04	.002

* 70 percent uncertainty

** Significantly correlated at 90 percent. The correlation coefficients ρ_{ut} and ρ_{vt} have been computed assuming time scales of 13 days and 15 days respectively.

TABLE 4.3: 225 DAY EDDY HEAT FLUXES

	Mooring	Depth	$\overline{u't'}$ °C cm/sec	ρ_{ut}	$\overline{v't'}$ °C cm/sec	ρ_{vt}
(1)	640	616	.50 ± 1.56	.12	-3.12*± 2.66	-.52**
		839	1.10 ± 1.26	.33	-1.92 ± 2.05	-.42
(2)	639	611	.37 ± 1.61	.08	-3.46*± 2.53	-.54**
		830	.52 ± 1.32	.15	-2.06*± 1.75	-.49**
(3)	641	619	.64 ± 1.64	.13	-2.88*± 1.94	-.49**
		839	.74 ± 1.22	.22	-2.24*± 1.68	-.51**
(4)	643	858	1.08 ± 1.32	.31	-1.47 ± 1.99	-.33
(5)	646	567	1.17 ± 1.64	.26	-2.22 ± 2.60	-.37
(6)	647	728	1.11 ± 1.36	.31	-1.72 ± 2.26	-.33
(7)	638	636	-.03 ± 1.34	-.01	-2.57*± 1.53	-.62**
(8)	642	617	.19 ± 1.64	.04	-2.17*± 1.94	-.42
	644	587	.74 ± 1.48	.18	- .83 ± 2.25	-.15

* Non-zero amplitude at 70 percent level.

** Significantly correlated at 90 percent level.

TABLE 4.4: TERMS IN THE VORTICITY BALANCE

Averaging Period (days)	$10^{-13} s^{-2}$ $\beta\bar{v}$	$10^{-13} s^{-2}$ $f\left(\frac{w_{Ek} - w_m}{\Delta z}\right)$	10^{-4} cm/sec w_e(inferred)
225	- .59 ± .16	-1.76 ± .06	-1.13 ± .17
290	-5.66 ± .45	-1.40 ± .68	4.15 ± .79
445	-5.00 ± .18	-3.24 ± .73	1.71 ± .73

$\beta = 1.95 \times 10^{-13}$ cm^{-1} s^{-1}

$f = 7.496 \times 10^{-5}$ s^{-1}

$\Delta z = 728$ m

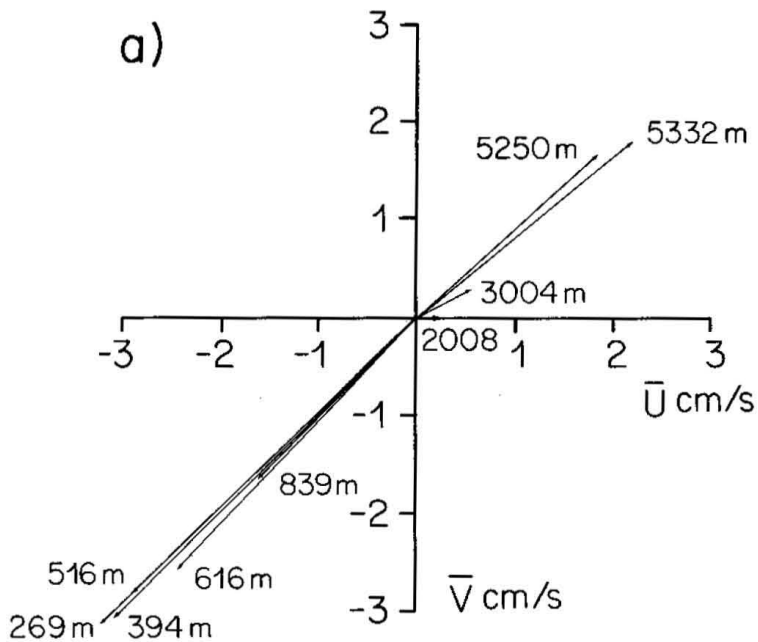

290 DAY RECORD

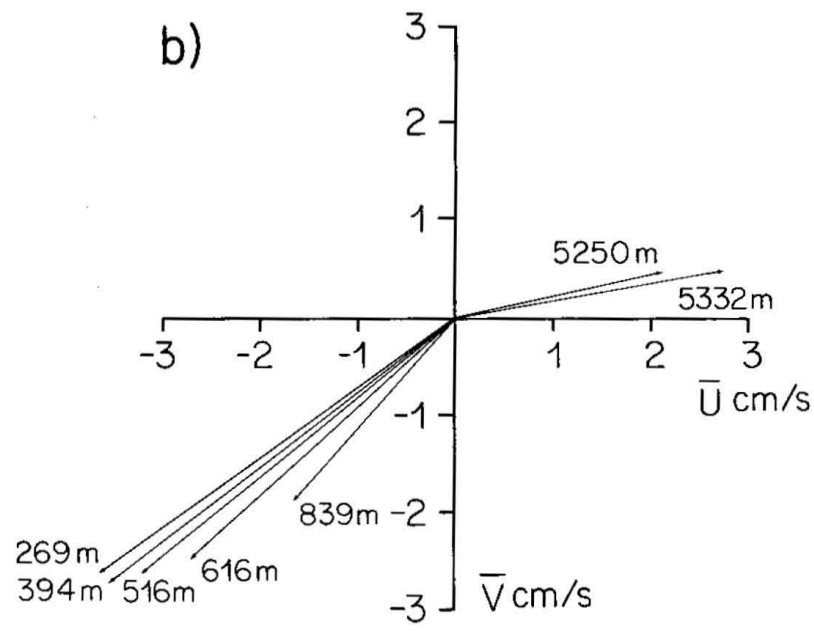

445 DAY RECORD

Figure 4.1

CHAPTER 5

A STABILITY MODEL COMPARISON WITH THE EDDY HEAT AND POTENTIAL VORTICITY FLUXES IN THE GULF STREAM RECIRCULATION

5.I. INTRODUCTION

Eddy potential vorticity fluxes may be generated by at least three processes -- spatial variations in the amplitude of wave packets (Rhines and Holland, 1979; Appendix), non-linear interactions, or instability. Observational evidence in support of baroclinic instability has been reported in two current meter arrays located in the Gulf Stream recirculation region - the Local Dynamics Experiment (Owens, 1984) at 31°N, 69.5°W and POLYMODE Array II (Hogg, 1984) along 55°W between 32°N and 38°N. These analyses compared the empirical orthogonal functions of the velocity and temperature cross-spectral matrix to the predicted structure for waves generated by baroclinic instability. Hogg (1984) compared the empirical orthogonal modes for the Array II data to Gill, Green, and Simmons' (1974) model for an unstable westward jet. The empirical modes show vertical phase propagation and phase relations between the meridional velocity component and temperature which cause a significant southward heat flux in the thermocline. Moreover, the observed wavefield agrees with the growth rates, phase speeds, and wavenumbers predicted by the model.

The comparison between stability theory and the data is less clear for the LDE data. Bryden (1982) demonstrated that there is conversion of mean available potential energy to eddy potential energy during the experiment. This suggests indirectly that the eddy field in the LDE is generated by

baroclinic instability. However, the direct evidence from the empirical mode analysis of the LDE velocity and temperature cross-spectral matrix is not completely in agreement with the general predictions of instability theory. Owens (1984) found that the empirical modes of the eddy variability decomposed most coherently if the zonal and meridional velocity components were rotated to the along-stream and cross-stream directions with respect to the mean flow. Most of the eddy heat flux was found to be in the along-stream component in the 64 to 32 day band, but the empirical modes showed no significant temporal phase changes with depth. Thus the LDE data does not quite fit the conventional picture of stability analysis.

Ideally one would like to compare the eddy potential vorticity fluxes generated by the unstable modes to the eddy fluxes from the Local Dynamics Experiment computed in Chapter 3. There are several objections to the use of this technique for analyzing the stability problem with the LDE data. First, all such comparisons suffer from the incorrect assumption that the observed mean velocity profile is the unperturbed basic state for the stability calculation. Second, the LDE velocity profile (Owens et al., 1982, Figure 2) from the record average at each current meter is not strictly zonal so the problem becomes mathematically much more complicated. Third, in the LDE there is no obvious choice for the mean velocity profile because of the gap in the data records at 2008 and 3004 m depth as described in Chapter 4. McWilliams (1983) has shown how the choice of record length changes the mean velocity profiles and potential vorticity gradients. Because of these ambiguities, it does not seem worthwhile to analyze the stability problem for the LDE data.

The eddy potential vorticity flux will instead be computed from Hogg's (1984) approximation to the mean velocity profile for the Array II data

because there is much stronger direct evidence for baroclinic instability from this data than from the LDE. The flow in this region along 55°W can be modeled approximately with a zonal profile. Since the basic state in the model is also assumed to have no meridional variation, the relative vorticity flux is identically zero and the total eddy potential vorticity flux is just the thickness flux. In order to compare the model more directly to the observations, we will also compute the vertical distribution of heat fluxes. This analysis is intended to be used as a guide for interpreting the observational results and for motivating further observational work.

5.II. HYPOTHESIS

Hogg (1984) has shown that the empirical orthogonal modes from the velocity and temperature cross-spectral matrix for the Array II data are consistent with the Gill, Green, and Simmons (1974, hereafter GGS) linear model for a wave field generated by baroclinic instability. An exponentially-varying westward shear profile was chosen for the basic state as an idealized approximation to the measured zonal velocity distribution from the point measurements at 600, 1000, 1500, and 4000 m depth. He found that the observed mesoscale eddy field is consistent with the predicted growth rate, horizontal wavenumber, and vertical phase changes for the baroclinic modes with the fastest growth rates. Given the uncertainty in the observational data, Hogg concluded that an exact calculation using the mean current meter velocities and hydrographic data would not significantly improve the model-data comparison.

The purpose of this chapter is to reassess this model by comparing the higher moments of the eddy variability -- the eddy heat and potential vorticity fluxes -- to the observations. One of the primary predictions of the GGS

model is that most of the eddy heat flux should occur in the upper 500 m or, in other words, shallower than the Array II instruments. We will show by comparing the vertical distributions of the model and the observed heat fluxes that the model prediction is much more surface intensified. The comparison shows that while the model accurately predicts basic properties like the growth rate and wavenumbers, there is substantial disagreement with the eddy heat fluxes.

5.III. THE GGS (1974)/HOGG (1984) INSTABILITY MODEL

GGS discussed the baroclinic instability problem for several zonal velocity profiles with and without bottom topography. It is assumed that the quasigeostrophic potential vorticity equation (Chapter 3, Equation 3.1) governs the stability problem for the zonal flow. The linearized stability problem for the unstable modes is given by the equation:

$$(\frac{\partial}{\partial t} + \overline{U}\frac{\partial}{\partial x})[\psi_{xx} + \psi_{yy} + \frac{f^2}{N^2}\psi_z)_z] + \psi_x\overline{Q}_y = 0 \qquad (5.1)$$

where $\psi(z)$ is the streamfunction for the perturbation eigenfunction,

$u = -\psi_y$, $v = \psi_x$,

$\overline{U}(z) = -\overline{\psi}_y$ is the basic state velocity profile,

and $\overline{Q}_y = \beta - (\frac{f^2}{N^2}\overline{U}_z)_z$ is the mean potential vorticity gradient. The boundary conditions require that the vertical velocity, $w = -f\psi_{zt}/N^2$ be zero at the surface [z=0] and that $w = -\underline{u}\cdot\nabla h$ at the bottom [$z=-H + h(x,y)$]. Since the basic state has no meridional variation, a normal mode form is assumed for the unstable modes

$$\psi(x,z,t) = \mathrm{Re}[\phi(z)e^{ik(x-ct)}] \tag{5.2}$$

where the phase speed $c = c_r + ic_i$ is the sum of a real part c_r and a complex part c_i. The equation governing the stability of these modes then becomes

$$(\overline{U} - C)[(\frac{f^2}{N^2}\phi_z)_z - k^2\phi] + \phi\overline{Q}_y = 0 \tag{5.3}$$

with the boundary conditions

$$\frac{\phi_z}{\phi} = \frac{\overline{U}_z}{\overline{U} - C} \tag{5.4}$$

at the surface z=0 and at the bottom z=-H in the absence of topography.

In order to simplify the mathematics, one of the basic velocity profiles was chosen to be an exponential of the form

$$\overline{U}(z) = U_0 e^{z/d}$$

with an e-folding scale of d=900 m and total depth H=-4500 m. Hogg (1984) compared the empirical orthogonal modes from the Array II data to the unstable modes for the westward zonal flow profile

$$\overline{U}(z) = -.05[1 + \exp\frac{z}{900}] \quad \mathrm{m/sec} \tag{5.5}$$

with no bottom topography. The uniform shift in the velocity profile just changes the real phase speed of the unstable modes without affecting their growth rates. His Figure 12 shows that the profile is a reasonable fit to the observed mean velocities from the current meter data. The chosen model buoyancy profile,

$$N^2/f^2 = 10^4 \, e^{z/d} \quad , \qquad (5.6)$$

is also exponential so that the mean potential vorticity gradient, Q_y, is simply β for this profile. The profile satisfies the necessary condition for instability, however, because the sign of Q_y is opposite to that of the mean vertical shear at the surface.

For this stability problem there are two peaks in the growth rate profile. The two modes with the fastest growth rates have been reproduced in Figure (5.1) using the shooting method to solve Equation (5.3) subject to the boundary condition, Equation (5.4). The most rapidly growing mode has a wavelength of 190 km (k=.033 km^{-1}), a real phase speed of -9.4 cm/sec, and an e-folding time of about 80 days. Its amplitude is surface-trapped with most of the phase change occurring above 400 m depth. The secondary peak in the growth rate curve is predicted at a wavelength of 320 km (k=.0195 km^{-1}), a phase speed of -9.5 cm/sec, and an e-folding time of 120 days. This mode has an amplitude distribution similar to the first baroclinic mode with a node at mid-depth and a deep amplitude equal to half the surface maximum. It differs from a quasigeostrophic dynamic mode because there is upward phase propagation in the upper half of the water column.

Hogg (1984) compared the empirical orthogonal functions for velocity and temperature in different frequency bands from the cross-spectral matrix of the Array II data. A single empirical function was found to account for more than fifty percent of the energy at periods between 120 and about 20 days. From the analysis of the empirical modes he found remarkable agreement with the model predictions for the wavelength, phase speed, and frequency of the two most rapidly growing unstable modes. The wavelengths were determined to be

350 and 190 km from a horizontally coherent subset of the moorings. The westward phase speed was then determined from a wavenumber-frequency plot to be about 11.5 km/day (slightly faster for shorter periods) so that the predicted periods for the two modes are about 30 and 12 days. These predicted periods correspond to significant peaks in the eddy kinetic energy spectra. The use of the linear model was justified because the phase speed of the waves is much greater than the particle speeds. Figure 5.2 reproduced from Hogg's paper shows the correspondence between the model and the empirical mode in the 30 day band. The direction of phase propagation in the empirical mode is upward for velocity and downward for temperature although most of the model phase change is predicted to occur above 600 m depth. On the basis of the properties sum- marized here, there is good agreement between the model and the empirical modes of the data.

5.IV. THE MODEL EDDY POTENTIAL VORTICITY FLUX

The eddy potential vorticity flux due to an unstable mode is calculated from $\overline{vq} = \frac{1}{4}(vq^* + v^*q)$ where $*$ denotes the complex conjugate and the overbar denotes the time average. Substitution of the relations

$$v = \Psi_x \quad \text{and} \quad q = \Psi_{xx} + \frac{\partial}{\partial z}\left(\frac{f^2}{N^2}\Psi_z\right) \tag{5.7}$$

gives the expression

$$\overline{vq} = \frac{1}{4}\, ik\left[\phi \frac{\partial}{\partial z}\left(\frac{f^2}{N^2}\phi^*_z\right) - \phi^* \frac{\partial}{\partial z}\left(\frac{f^2}{N^2}\phi_z\right)\right] e^{2kc_i t} \tag{5.8}$$

which can be rewritten using the real and complex forms of Equation (5.3). The final expression for the eddy potential vorticity flux reduces to

$$\overline{vq} = \frac{-kc_i}{2\left|\overline{U} - c\right|^2}\, \phi^2\, \overline{Q}_y e^{2kc_i t}\,, \tag{5.9}$$

so that the eddy flux due to an unstable mode is necessarily directed opposite to the mean potential vorticity gradient.

Since the stability problem has been linearized, the amplitude of the unstable modes must be specified. In the present analysis they are set equal to the amplitude of the empirical mode for the meridional velocity component at 600 m depth as calculated by Hogg (1984). His Figure 11b shows that this value is ~ 3 cm/sec at 600 m for the wave with the 30 day period (k = .0195 km^{-1}). The empirical mode in the 12 day band is not significant, but the amplitude for this mode is also set arbitrarily to 3 cm/sec. Since the square of the meridional wave velocity is equal to:

$$v^2(z) = k^2 \, |\phi(z)|^2 \exp 2kc_i t \quad , \tag{5.10}$$

the potential vorticity flux at 600 m is specified by

$$\overline{vq}\,(600) = \frac{-c_i}{2k \, |\overline{U}(600) - c|^2} \, \overline{Q}_y \, v^2(600) \tag{5.11}$$

so that at any depth

$$\overline{vq}(z) = \overline{vq}(600) \, \frac{|\phi(z)|^2}{|\phi(600)|^2} \, \frac{|\overline{U}(600) - c|^2}{|\overline{U}(z) - c|^2} \tag{5.12}$$

With this amplitude specification we can then calculate the eddy potential vorticity flux as a function of depth.

The eddy potential vorticity flux is plotted with amplitude normalized by the maximum value in Figure 5.3 (a,b) for the two most unstable modes of the zonal profile (5.5). Equation (5.11) predicts the magnitude of the potential vorticity flux at 600 m to be $-.59 \times 10^{-6}$ cm/sec^2 for the 30 day wave and $-.33 \times 10^{-6}$ cm/sec^2 for the 12 day wave, values which are about a

factor of 3 to 5 less than calculated from the LDE data (Chapter 3). However, most of the potential vorticity flux in the model is concentrated entirely above the shallowest of the Array II instruments. As seen from Equation (5.12), the maximum amplitude of the potential vorticity flux occurs at the depth of the steering level where the mean speed is equal to the real phase speed of the unstable modes, $U = c_r$. For the profile (5.5) this should occur near the surface at only about 100 m depth. Because the potential vorticity flux is trapped near the surface, the model predicts that the magnitude measured at 600 m would be several orders of magnitude less than the maximum.

It should be noted, however, that the eddy potential vorticity flux in the fluid interior is balanced by compensating fluxes at the boundaries (Bretherton, 1966). This balance is seen most simply from the necessary conditions for instability:

$$\int_{-H}^{0} \frac{Q_y |\phi|^2}{|\overline{U} - C|^2} \, dz = \frac{-f_o^2}{N^2} \frac{|\phi|^2}{|\overline{U} - C|^2} \, \overline{U}_z \Big|_{z=-H}^{z=0} \tag{5.13}$$

which is identical to the statement in Chapter 3, Equation 3.9, multiplied by the constant $(kc_i/2)\exp 2kc_i t$ and zonally-averaged. Thus there is actually no net meridional potential vorticity flux in the model.

5.V. THE NORMALIZED EDDY HEAT FLUX

Since the eddy heat flux is a lower order vertical derivative than the potential vorticity flux, its vertical distribution should be less trapped to the surface. Thus the eddy heat flux is more readily compared to the Array II measurements. On the basis of the stability model, Hogg concluded that most of the eddy heat flux in this region of the Gulf Stream Recirculation should

still occur at depths shallower than 600 m. We will show, however, that the zonal velocity profile, Equation (5.5), produces a much more surface intensified heat flux than is indicated by the data.

The eddy heat flux was calculated as a function of frequency from the Array II moorings 1, 2, 3, and 4 located near 36°N, 55°W. These moorings were chosen since they contain most of the variance in the empirical modes studied by Hogg. In addition, these were the set of moorings used to predict the frequency-wavenumber characteristics of the wave-field because they form a coherent array. The instruments on these moorings were located at 600, 1000, 1500, and 4000 m depths. The data records were divided into 120 day pieces which were then prewhitened, filtered using a hanning window, and fourier transformed. An ensemble average was formed over the four moorings for the eddy heat flux to obtain at least 35 degrees of freedom at each level. The heat fluxes are significant at the 99 percent level at all depths for the 30 day band and at all but the deepest level for the 120 day band. For the 12 day band the 600 m eddy heat flux is significant at the 99 percent level and the 1000 m value at the 95 percent level, but none of the values at the deeper instruments are significant.

The Array II heat fluxes in these three frequency bands are compared to the model prediction in Figure 5.4 where the normalized eddy heat flux defined as $f_o\overline{v't'}/\overline{T}_z$ is plotted. The mean vertical temperature gradient $\overline{T}_z$ was calculated from the CTD profiles taken during the deployment of moorings 1 through 4 (Tarbell et al., 1978). To convert the normalized quantity to heat flux, the values should be multiplied by a factor ranging between 2 and 4 from the shallow to the deep values.

For the stability model, the normalized eddy heat flux is calculated from

$$\frac{f^2}{N^2}\overline{\Psi_x\Psi_z} = \frac{f^2}{N^2}\frac{k\,A^2(z)}{2}\frac{d\theta}{dz}\exp 2kc_i t \ . \tag{5.14}$$

where the complex amplitude $\phi(z)$ has been written in terms of a real amplitude $A(z)$ and phase angle $\theta(z)$

$$\phi(z) = A(z)e^{i\theta(z)} \ . \tag{5.15}$$

The amplitude of the unstable modes is again specified using the observed amplitude of the empirical orthogonal function for the meridional velocity component at 600 meters so that the normalized heat flux at this level is

$$\frac{f^2}{N^2}\overline{\Psi_x\,\Psi_z}\,(600) = \frac{f^2}{N^2_{(600)}}\,\frac{1}{2k}\,v^2(600)\,\frac{d\theta}{dz}_{600} \tag{5.16}$$

The normalized eddy heat flux at any depth

$$\frac{f^2}{N^2}\overline{\Psi_x\,\Psi_z(z)} = \frac{f^2}{N^2}\overline{\Psi_x\Psi_z}\,(600)\,\frac{A^2(z)}{A^2(600)}\,\frac{\frac{d\theta}{dz}}{\frac{d\theta}{dz}(600)}\,\frac{N\,(600)}{N^2(z)}$$

is plotted in Figure 5.3 for the two most rapidly growing modes in the model at 30 day ($k=.0195\ km^{-1}$) and 12 day ($k=.033\ km^{-1}$) periods. These profiles are actually upper bounds on the model heat flux because the amplitude has been set by the empirical velocity mode. Figure 5.4 shows that the maximum amplitudes for the model eddy heat flux for both modes occur at the surface where they are strongly trapped. For the 12 day period wave the model predicts a negligible heat flux signature below 600 m depth. The wave with the 30 day

period should have a measurable heat flux at the Array II instrument locations, but at 600 m depth and below, it is only about 10 percent of the surface amplitude. Although the amplitude of the 30 day mode is significant below the thermocline, the model heat flux is negligible because there is no phase change below 2000 m. Thus, the model predicts that the eddy heat flux from the fastest growing unstable modes should occur above 300 m depth.

The data values, however, show considerably more heat flux below 500 m than predicted by the model. There are two major discrepancies. At the 30 day period the heat flux at 600 and 1000 m is about a factor of three larger than the model. Moreover, an even larger normalized eddy heat flux occurs at the 120 day period even though the energy spectrum for the meridional velocity component is peaked at 30 days.

5.VI. DISCUSSION

Although the stability model predicts the wavenumbers, growth rates, and phase speeds of the empirical modes for the Array II data, there are significant discrepancies in the higher moments of the eddy variability. In particular, the heat flux at 600 m in the 120 day band is an order of magnitude larger than the heat flux for the most unstable modes in the model. One possible explanation for the discrepancy is due to a difference between the modes in the data and in the model. An estimate for the vertical scale of an unstable mode is given by:

$$D \sim \frac{f^2 \overline{U}_z}{N^2 \beta}$$

which for the model profile should be less than 300 meters. Since the heat flux depends on the vertical derivative of the phase, it is particularly sensitive to this vertical scale.

The vertical scale depends on the slope of the isopycnals or, equivalently, on the ratio of the vertical shear to the square of the buoyancy frequency. A difference between either of these two quantities and the model could affect the scale of the observed modes. GGS examined the effect of changing the slope of the isopycnals near the surface in each of these two ways. First, they calculated the unstable modes from a model with a velocity profile (their profile 2) with less shear near the surface but with the same buoyancy profile as in Equation (5.6). They found that reducing the shear lowered the growth rates by 30 to 40 percent. Even this large a change is probably within the uncertainty of the fit to the empirical modes. Since the unstable modes from this other profile are also less surface-intensified with less vertical phase change between the surface and the thermocline, the heat flux from these modes would be less concentrated near the surface. GGS also examined the effect of reducing the buoyancy frequency above the thermocline on the stability of the profile in Equation (5.5) without changing the shear so that Q_y remained equal to β. They found that reducing N by a factor of 8 above 800 m depth also decreased the growth rates of the unstable modes without changing the location of the critical level.

Since the model has been fit to a data set without near-surface measurements, we can only speculate on the cause of the discrepancies. While these details of the model profile do not have much effect on the basic parameters like growth rate and wavenumber, the higher moments can be extremely model-dependent. Other data suggest that the apparent error in the model heat flux

may be due both to the difference in the buoyancy profile and to an overestimate of the surface shear. Richardson's (1983) surface drifter data show that surface velocities along 55°W between 35°N and 38°N are actually between +5 cm/sec and -.5 cm/sec rather than -10 cm/sec as used in the model. Figure 5.5 shows that the average $N^2(z)$ profile from the CTD data taken during the deployment and recovery of moorings 1 through 4 is also considerably less than the model profile below about 200 m. The heat flux is particularly sensitive to the effects of these differences between the data and the model. Although we cannot disprove the prediction that most of the eddy heat flux should occur above 600 m depth, the discrepancy between the model and the deeper eddy heat fluxes raises some doubt about this prediction.

FIGURES

Figure 5.1: Amplitude and phase for the two most rapidly growing unstable modes for the velocity profile in Equation (5.5). The dotted line is the wave with a 30 day period ($k = .0195\ km^{-1}$) and the solid line is the wave with a 12 day period ($k = .033\ km^{-1}$).

Figure 5.2: The empirical orthogonal modes (from Hogg, 1984) in the 30 day band for the velocity and temperature computed from Array II moorings 1 through 4. The amplitude and phase for velocity are also plotted for the GGS model (dashed line). The temperature mode is compared to the empirical mode calculated from the velocity structure of the model using the hydrostatic assumption.

Figure 5.3: Potential vorticity flux from the stability model with amplitude normalized to one for the 30 day (left) and 12 day (right) unstable modes.

Figure 5.4: Normalized meridional heat flux defined as $\overline{fv't'}/\overline{T}_z$ calculated from the instability model for the 30 day (dashed line) and the 12 day (solid line) unstable waves assuming a meridional velocity amplitude of 3 cm/sec at 600 m depth. The normalized heat fluxes from the Array II data are plotted as discrete points for the 120 day (circles), 30 day (crosses), and 12 day (diamonds) bands at 600, 1000, 1500, and 4000 meter depths.

Figure 5.5: The square of the buoyancy profile from the averaged CTD data measured at the deployment and recovery of Array II moorings 1 through 4. Also shown is the GGS model profile $N^2(z) = f^2 10^4 \exp(z/900\ m)$.

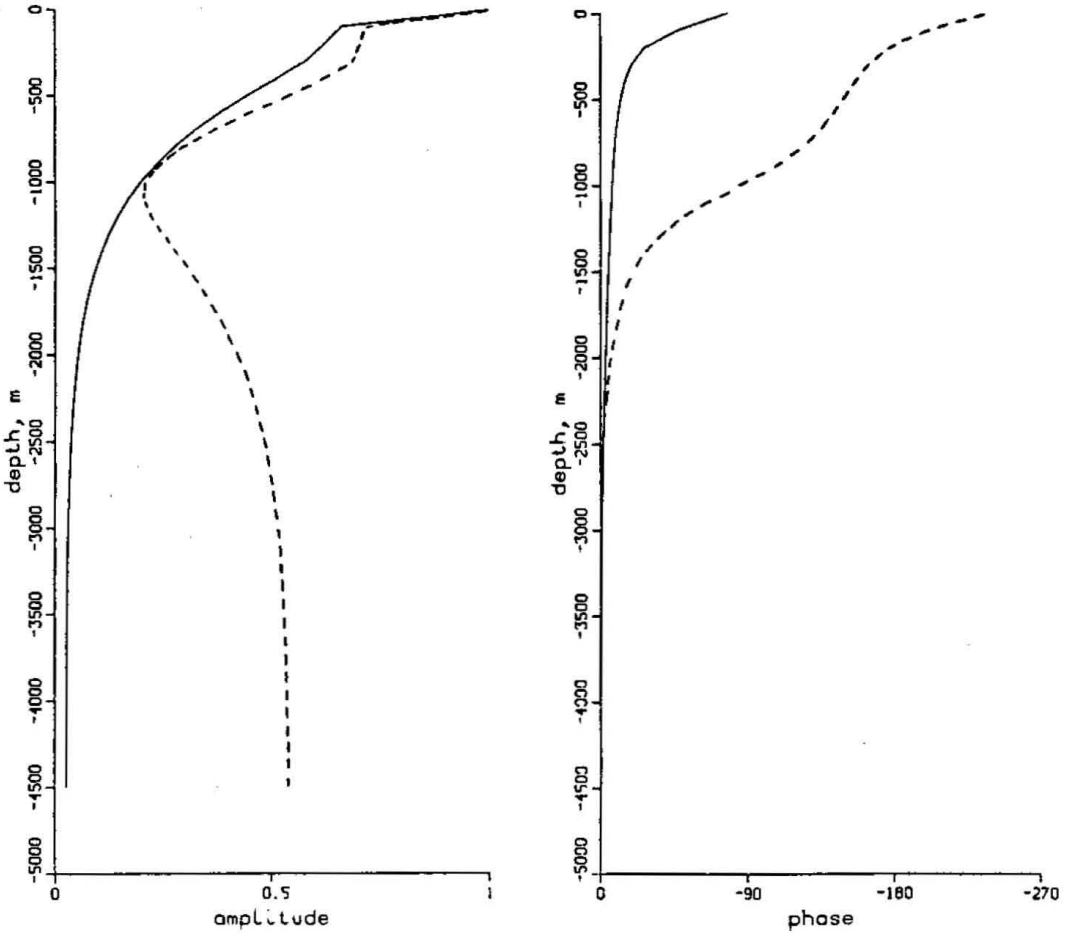
depth, m
0
-500
-1000
-1500
-2000
-2500
-3000
-3500
-4000
-4500
-5000
0
0.5
amplitude
depth, m
0
-90
-180
-270
phase

Figure 5.1

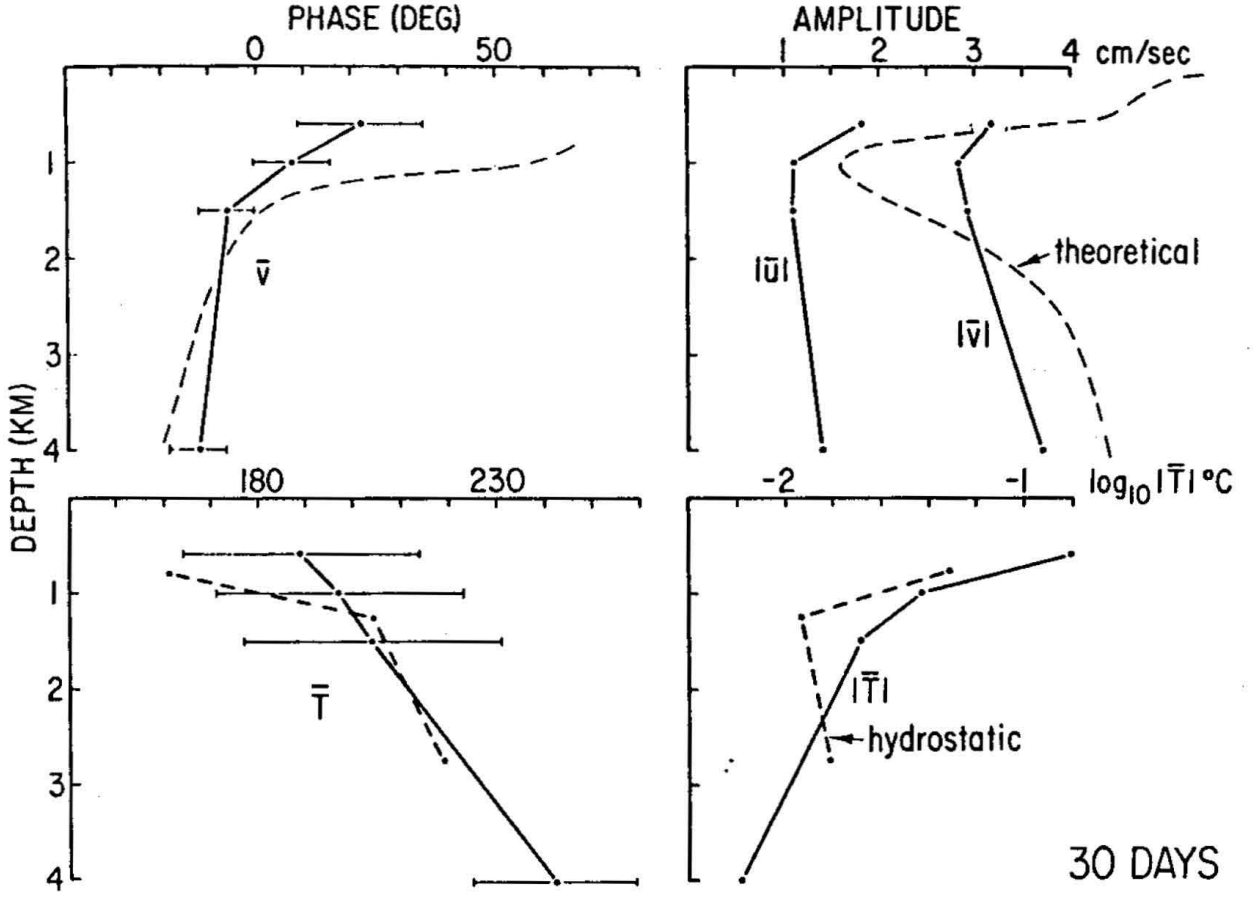
PHASE (DEG)
0
50
AMPLITUDE
1
2
3
4 cm/sec
DEPTH (KM)
1
2
3
4
$\bar{v}$
$|\bar{u}|$
$|\bar{v}|$
theoretical
180
230
-2
-1
$\log_{10}|\bar{T}|$ °C
$\bar{T}$
$|\bar{T}|$
hydrostatic
30 DAYS

Figure 5.2

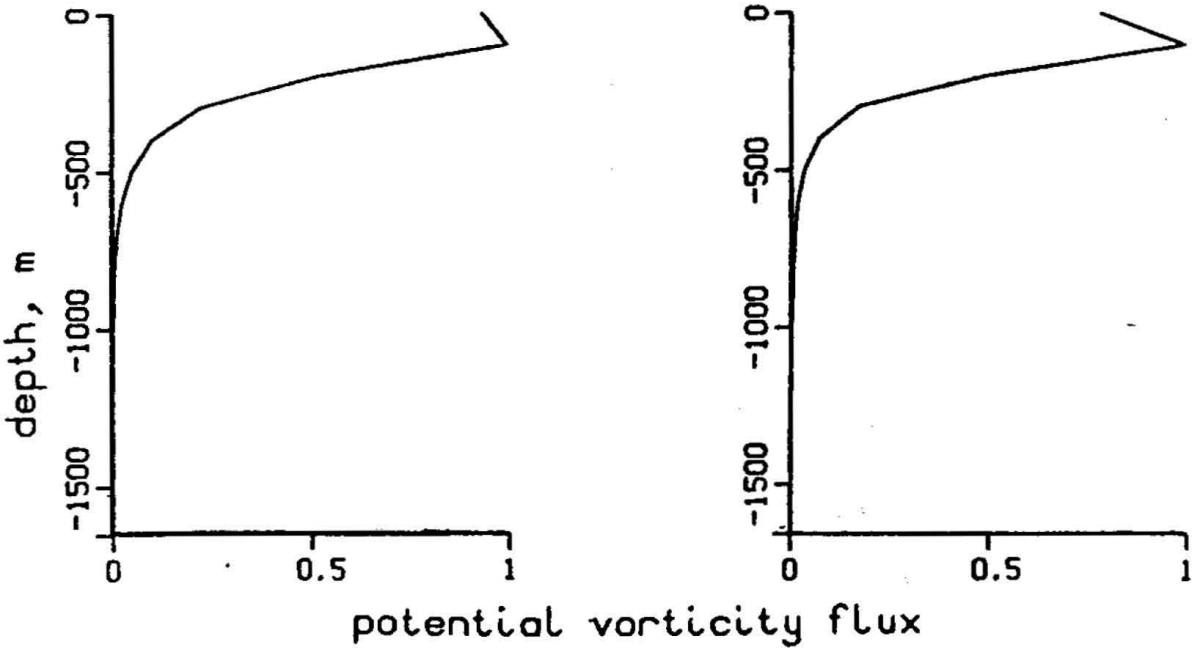

Figure 5.3

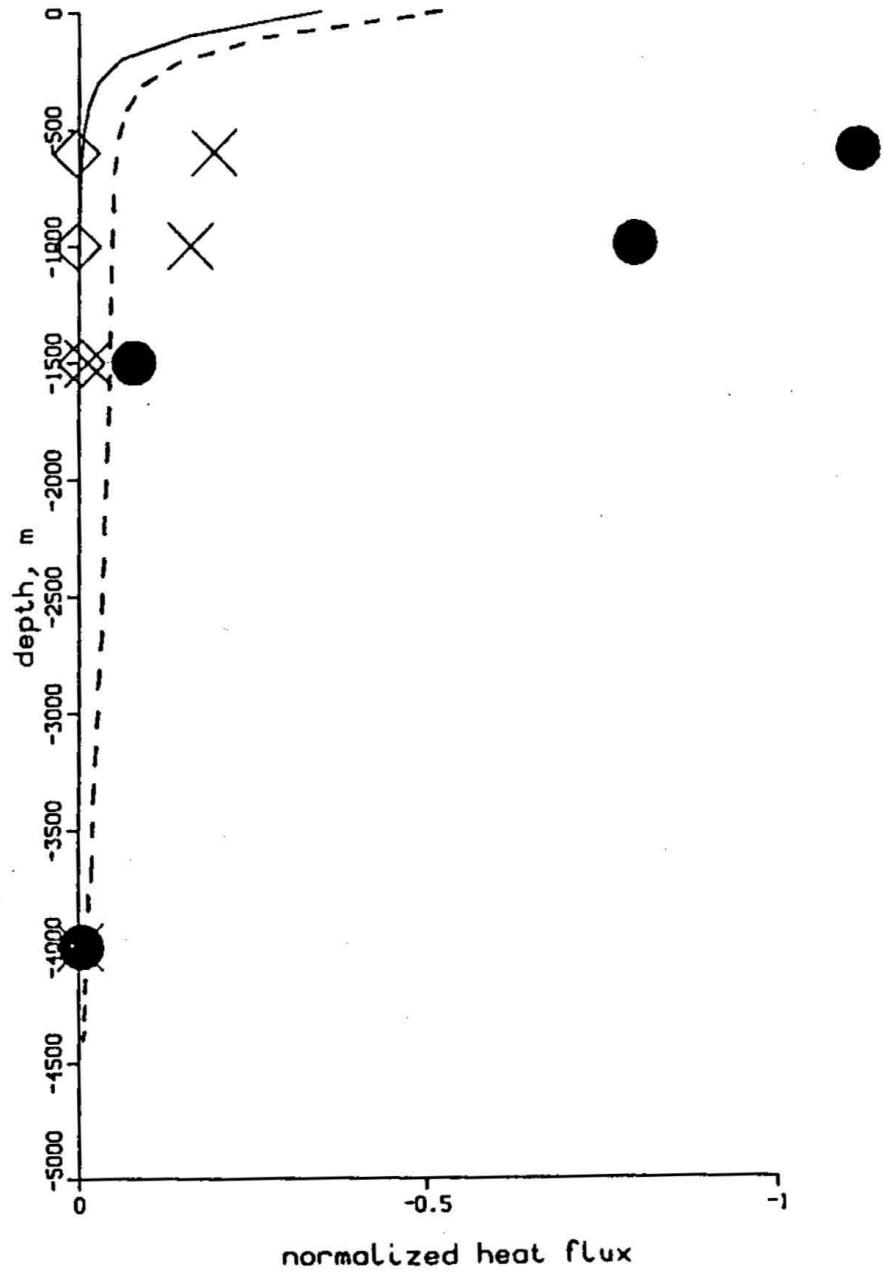
0
-500
-1000
-1500
-2000
-2500
-3000
-3500
-4000
-4500
-5000
depth, m
0
-0.5
-1
normalized heat flux

Figure 5.4

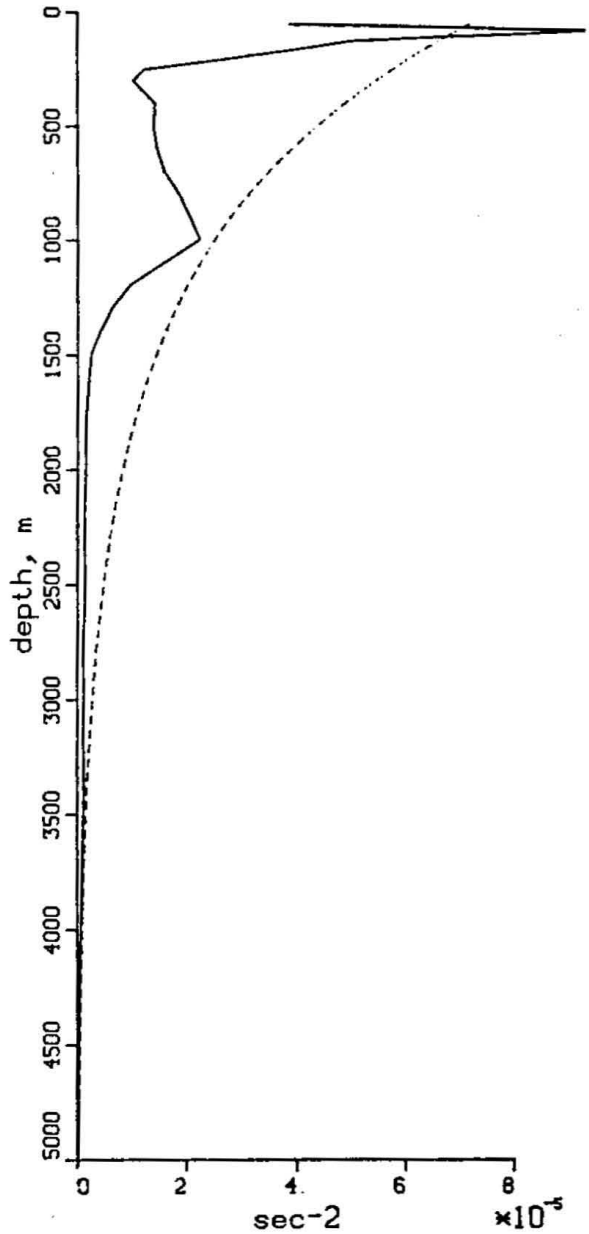
depth, m
0
500
1000
1500
2000
2500
3000
3500
4000
4500
5000
0
2
4
6
8
sec-2
×10-5

Figure 5.5

CHAPTER 6

THE VERTICAL STRUCTURE OF THE MESOSCALE EDDY FIELD IN THE GULF STREAM EXTENSION

6.I. Introduction

Much of the observational effort during the last decade has been directed toward relating properties of the low frequency eddy field to the mean flow in different geographical regions of the North Atlantic. One purpose of these studies is to assess the consistency of the observations with theoretical predictions about eddy-mean flow interactions. In most cases, the specific mechanism can only be inferred from the sign of momentum or energy transfer. Examples of this type of analysis are Schmitz (1976) and Bryden (1982). Schmitz (1976) suggested that the meridional distribution of eddy Reynolds stresses along 55°W from the POLYMODE Array II tends to accelerate the zonal Gulf Stream flow. Bryden (1982) showed that the direction of the heat fluxes with respect to the mean temperature gradient in the Local Dynamics Experiment indicates conversion from mean available potential energy to eddy potential energy. This led to the suggestion that eddies in the Gulf Stream recirculation region are generated by baroclinic instability. Although analyses like these cannot prove that a specific process actually occurs, they are a useful tool for comparing the observations to theory and to numerical model distributions (Schmitz and Holland, 1982).

One study of the eddy field in the Gulf Stream recirculation region provides a more direct comparison with theory. Hogg (1984) was able to relate the vertical structure of the eddy field in POLYMODE Array II to Gill, Green,

and Simmons' (1974) theory of eddy generation by baroclinic instability of the mean flow. The sense of vertical phase propagation for the complex velocity and temperature empirical orthogonal modes was found to agree with a model of a baroclinically unstable westward current. Furthermore, the theory predicted the wavenumber and growth rate of the observed waves. Although the empirical mode representation does not provide dynamical information about the eddy field, it is useful for characterizing the structure of the velocity and temperature variability.

Data from another geographical region of the North Atlantic, the Gulf Stream Extension (Figure 6.1), is analyzed in this chapter to relate the eddy structure to the local mean flow and to the eddy variability in other regions of the North Atlantic. The Gulf Stream Extension mooring array was designed to map the mesoscale eddy field in the region southeast of the Newfoundland Grand Banks between 37°- 41°N and 42°- 47°W. A summary of the data from the experiment which took place between September 1979 and November 1980 is given by Levy et al. (1982). Fofonoff and Hendry (1984) analyzed the space-time scales from more than a year of velocity data recorded at depths of 500, 1500, and 4000 m from the mooring array. Although the eddy field is very complex, their analysis suggested a change in eddy vertical structure from the vertically coherent and coplanar eddies observed in the North Atlantic POLYMODE experiments. This chapter compares this structure on the basis of the empirical orthogonal velocity and temperature modes.

6.II. Hypothesis

The analysis of Fofonoff and Hendry (1984), henceforth FH, is the starting point for this study of the mesoscale eddy field in the Gulf Stream

Extension (GSE) mooring array. Their paper gives a description of the eddy kinetic energy spectra, the spatial and temporal scales, the horizontal and vertical correlations, and the streamfunction maps. As reported by FH, there are significant geographic variations in eddy properties throughout the array. Eddy kinetic energy at 500 m decreases eastward from 340 cm^2/sec^2 at 39°N, 47°W to 54 cm^2/sec^2 in the mooring located furthest to the southeast at 37°N, 42°W.

Time scales were defined by integrating the eddy kinetic energy spectra over frequency and locating the period which contained 50 percent of the cumulative energy. In the GSE the time scales are longer than the 50-60 day periods calculated from the Array II data along 55°W. The time scale at 500 m increases from 120 days south of the Ridge to a maximum of ~ 200 days in the northeastern part of the array. At deeper levels, there is more energy at higher frequencies in the GSE instruments than in Array II possibly because of the increase in bottom slope approaching the Newfoundland Ridge.

The array moorings showed only marginal horizontal coherence so that the spatial scales of the eddy field were not well resolved. In particular, there is no coherence between moorings across the Ridge axis. Only the records from the three westernmost moorings - 678, 679, 680 - south of the ridge are horizontally coherent. Spatial scales were found by FH to be approximately 60 km based on the zero-crossing of the velocity transverse autocorrelation function. The character which emerges from the basic description is that the eddy field in this region is very inhomogeneous and quite different from the eddy field in the recirculation region.

The influence of topography on the horizontal and vertical eddy structure is not clear. Streamfunction maps from the velocity field at 500 m

depths show only intermittent evidence of organized wave propagation along the ridge axis. This contrasts with the coherent wave field observed by Luyten (1977) and Hogg (1981) along the continental rise at 70°W. FH suggested that wave refraction along contours of f/H might account for both the increase in time scales to the north and east of the Ridge and for the lack of wave propagation. The vertical structure of the GSE eddy field also seems influenced by the bottom topography. The principle axes of the low frequency fluctuations at 4000 m are closely aligned along bottom contours. This influence, however, is also seen at the shallower instruments. Figure 6.2 shows the principle axes at 1500 and 500 m depth superimposed on the bottom contours. The moorings located closest to the Ridge - 680, 678, 677, 675, 674 - all show an upslope rotation of between 9° and 38° between the 1500 m and the 500 m records. Part of the motivation of this analysis is to determine whether this rotation may reflect vertical phase propagation.

The GSE array was deployed to map the eddy variability in the region between the northern Gulf Stream recirculation region and the Newfoundland Basin. Fofonoff and Hendry's analysis suggested that the eddy structure in the Gulf Stream Extension region differs from vertically coherent and coplanar eddies like those observed in POLYMODE Array II. Much more is known about the vertical structure of the eddy field in the Gulf Stream recirculation where evidence of baroclinic instability is shown by vertical phase propagation. Eddies in the Newfoundland Basin have not yet been mapped with a current meter array, but Schmitz (1981) identified an energetic eddy field by large excursions of the 10°C isotherm as seen from XBT data. It was hypothesized that the lack of vertical coherence in the GSE data may also characterize the eddy field in the Newfoundland Basin.

This chapter presents a further study of the vertical eddy structure in the Gulf Stream Extension region using several types of empirical orthogonal functions. This technique incorporates the covariance information between all the measurement levels instead of using one series as a base reference. FH examined only one type of vertical structure allowing velocity veering between unidirectional flow at different levels. Empirical modes can similarly be used to represent modes for velocity veering, but the velocity components can also be treated as independent scalars to examine vertical temporal phase shifts in different frequency bands. In addition, temperature measurements can be combined using an appropriate normalization with the velocity data to examine evidence of baroclinic instability. Although some elements of FH's results carry through these techniques, the empirical mode analysis shows that the velocity variance in all the GSE moorings can in fact be described by a single coherent vertical mode. The complete velocity and temperature cross-spectral matrix is also examined for evidence of baroclinic instability.

6.III. Methodology

Empirical orthogonal functions are the linear combinations of the measurements which in a least squares sense best represent the structure of the covariance matrix. Several types of empirical modes (Davis, 1975; Richman et al., 1977; Owens, 1984) have been used to analyze the mesoscale eddy variability in the North Atlantic. Since the different modes show how well the structure is described under certain model assumptions, a comparison of different types of modes can be used to test hypotheses about the wave structure. The technique in its most general form is described by Wallace and Dickinson

(1972). For Fourier transformed velocity or temperature measurements $\hat{\zeta}_i$ located at the vertical level i, the cross-spectral matrix has the form

$$< \hat{\zeta}_i \hat{\zeta}_j^* >$$

where the brackets denote an ensemble average in frequency. The cross-spectral matrix is a symmetric complex Hermitian matrix with real eigenvalues λ_i which represent the percentage of the total variance accounted for by the ith empirical mode z_i. The significance of a given mode is determined from the ratio of the variances contained in the modes by an F-test (Bendat and Piersol, 1971). In practice, a given mode is significant if it contains more than twice the variance of the next mode. The empirical modes z_i are linear combinations of the measurements

$$z_i = \Sigma_j e_{ij} \zeta_j$$

and the squared coherence between the ith mode and the jth instrument is given by

$$\gamma_{ij}^2 = \frac{< \hat{\zeta}_j \hat{z}_i^* >^2}{< \hat{\zeta}_j^2 >< \hat{z}_i^2 >} = \frac{e_{ij}^2 \lambda_i}{< \hat{\zeta}_j^2 >} \quad .$$

The significance level for the coherence is determined by standard procedures (Julian, 1974).

Three types of empirical modes are discussed in this chapter. The simplest of these is the empirical mode analogue to FH's calculation of velocity veering and correlation with respect to the 500 m base record. The mode technique better represents the dominant wave structure because it incorporates the information from all vertical levels rather than using one series as

a base reference. However, this type of representation has the built-in assumption that the low frequency velocity at each level is unidirectional so that these empirical modes can only represent changes in direction of the velocity vector with depth.

This constraint on the unidirectional empirical mode representation can be relaxed to examine vertical temporal phase changes within narrower frequency bands. If the constraint of unidirectional flow is removed, then twice this number of modes are allowed. In this case, the coherence between the mode and the measurements is improved by rotating the velocity components to the upslope and alongslope directions of the local topography. This type of mode will describe vertical phase propagation between independent scalar velocity components in different frequency bands. If the combined temperature and velocity cross-spectral matrix is used to compute the modes, heat flux correlations in different frequency bands can also be examined. Since this matrix allows a total number of modes equal to three times the number of instruments, each mode accounts for less of the total variance. This type of analysis has been used by Hogg (1984) and Owens (1984) to compare the structure of empirical modes with that predicted for baroclinically unstable modes. The goodness of fit for each of these three representations of empirical modes is a test of how well the data fits a given hypothesis about the structure of the variability.

6.IV. Data Description

The ten mooring Gulf Stream Extension experiment (Figure 6.2) was deployed southeast of the Newfoundland Grand Banks from September 1979 to November 1980 as a joint experiment between the Woods Hole Oceanographic

Institution and the Bedford Institute of Oceanography. The data described in Levy et al. (1982) were recorded on two basic mooring configurations. Seven of the WHOI moorings (673 - 680) were instrumented with vector-averaging and Geodyne model 850 current meters at 500, 1500, and 4000 m depths. In addition, pressure and temperature were also measured at 800 m depths on those moorings. The Bedford Institute moorings 346/369 and 347/370 were instrumented at 500, 800, 1500, and 4000 m depths with Aanderaa current meters measuring speed, direction, temperature, and pressure.

The burst sampled data were low-pass filtered with a 24-hour Gaussian window and subsampled at daily intervals. In addition, the temperature records were corrected for the effects of mooring motion using a method demonstrated in the Local Dynamics Experiment (Mills et al, 1981). Mooring excursions were largest in the western part of the array where the eddy field was most energetic. The root-mean-square deviation of the instruments from nominal depth varied from a maximum of 60 m at the shallowest instrument on mooring 680 to a minimum of 2 m for the instruments on mooring 673. The method used to correct the temperature records for the effects of these depth excursions is discussed in Appendix B.

The vertical empirical modes are calculated from a subset of the recovered data summarized in Table 6.1. A uniform 380 day record length from November 3, 1979 to November 16, 1980 was used to compute the cross-spectral matrix from the WHOI data while the record length from the BIO mooring 347/370 is only 342 days from September 27, 1979 to September 2, 1980. The BIO mooring 346/369 could not be used in this study because of the short records at both 500 and 1500 m. The velocity modes are calculated from the 500, 1500, and 4000 m records at moorings 680, 678, 677, 674, 673, and 347/370. Because

of instrument failures at 4000 m in moorings 675 and 679, it is not possible to analyze the vertical empirical velocity modes for those cases. Temperature modes are calculated from the 500, 800, 1500, and 4000 m records at all moorings except 677 and 678 where the 1500 m and 500 m temperature records are of shorter duration. The complete velocity and temperature cross-spectral matrix can be calculated only at the four moorings 673, 674, 680, and 347 with measurements at three vertical levels -- 500, 1500, and 4000 m.

The choice of frequency bands for the empirical orthogonal function analysis is difficult because of the change in dominant time scales for the eddy variability throughout the array. In particular, we do not expect the 342-380 day record length to be a very good description east and north of the Ridge axis where 50 percent of the eddy energy is contained in periods longer than 150-200 days. For simplicity, however, the same frequency bands have been analyzed in all the moorings. This choice of bands is based on the usual compromise between resolution and statistical stability. Since the record lengths are relatively short compared to the wave periods, it has been necessary to choose broad frequency bands for the analysis in order to achieve statistically significant results. The cross-spectral matrix for the 380 day records was computed for a low band containing harmonics with periods between 285 and 70 days and a middle band between 70 and 30 days. The low frequency band includes at least 50 percent of the eddy kinetic energy present at the 500 m level at all moorings (see FH, Table 4). At deeper depths the low band contains less of the total energy because of the shift to higher frequencies. The middle frequency band containing 70-30 day periods was chosen to include the dominant periods found in the Array II region.

6.V. Data Analysis

FH examined the vertical structure at each of the GSE array moorings by computing the velocity veering and correlation for each instrument relative to the 500 m record. The veering angle

$$\theta_k - \theta_j$$

between the eddy velocity vectors

$$\underset{\sim}{u}_k = (u_k, v_k) \qquad \text{and} \qquad \underset{\sim}{u}_j = (u_j, v_j)$$

at depth z_k and depth z_j is given by the ratio of the cross product to the dot product:

$$\tan(\theta_k - \theta_j) = \frac{\underset{\sim}{u}_k \times \underset{\sim}{u}_j}{\underset{\sim}{u}_k \quad \underset{\sim}{u}_j} = \frac{\overline{u_k v_j} - \overline{v_k u_j}}{\overline{u_k u_j} + \overline{v_k v_j}} \tag{6.1}$$

with positive veering indicating that the velocity vector j is rotated clockwise with respect to k*. The elements of the form $\overline{u_k v_j}$ are the record average correlations between the velocity component time series from which the mean values have been removed. The square of the correlation between the velocity vectors at different depths is given by:

$$c_{ij}^2 = \frac{\overline{(\underset{\sim}{u}_k \times \underset{\sim}{u}_j)}^2 + \overline{(\underset{\sim}{u}_k \quad \underset{\sim}{u}_j)}^2}{\overline{|u_k|^2} \quad \overline{|u_j|^2}} \quad . \tag{6.2}$$

---

*FH measured positive direction as clockwise from north. We have reversed the angle convention to be positive counterclockwise from east.

On the basis of these parameters FH classified the moorings into three groups which seemed related to the local topography. In the moorings located on the northern flanks of the Ridge (674, 675) and to the south of the Ridge on the Sohm Abyssal Plain (679, 680) the eddy velocity variance at 1500 m and 4000 m was correlated with that at 500 m with no directional change in depth. The moorings 677 and 678 located on the southern flanks of the Ridge and 346/369 and 347/370 located to the east near the Mid-Atlantic Ridge showed no correlation between the 500 m and the deeper velocity records. FH suggested that higher frequency bottom-trapped waves degraded the vertical coherence between instruments on moorings 677 and 678. The incoherent vertical structure measured in 346/369 and 347/370 was interpreted as evidence that the vertically coherent North Atlantic eddies do not propagate northeast of the Ridge into the Newfoundland Basin. However, mooring 673 closest to the Mid-Atlantic Ridge showed both significant vertical correlation and significant clockwise veering in depth.

a) Veering modes

The simplest type of empirical orthogonal function shown here is the analogue to FH's representation of veering and correlation with respect to the 500 m basis record. The empirical mode formulation combines the information from all three depths to determine the best fit to the vertical cross-spectral matrix in different frequency bands. Furthermore, the modal decomposition explicitly allows for the presence of more than one mode which can degrade the vertical correlations used in FH's analysis. This type of empirical mode has been used previously by Fu et al. (1982) to analyze the data from POLYMODE Array III Clusters A, B, and C.

Veering modes represent vertically correlated rotations between unidirectional flows. At each vertical level, k, the velocity vector is written in complex notation

$$w_k = u_k + iv_k$$

where $u_k(t)$ and $v_k(t)$ are the real-valued time-dependent components of the horizontal velocity vector with the mean values removed. The cross-spectral matrix for the Fourier transformed velocity is then composed of elements of the form

$$\overline{\hat{w}_k \hat{w}_j} = \overline{\hat{u}_k \hat{u}_j^*} + \overline{\hat{v}_k \hat{v}_j^*} + i[\overline{\hat{v}_k \hat{u}_j^*} - \overline{\hat{u}_k \hat{v}_j^*}] \tag{6.3}$$

where the overbar denotes a sum over frequency harmonics of the complex Fourier elements $\overline{\hat{u}_k \hat{v}_j^*}$. A sum over all frequencies will just reproduce the purely real correlation matrix used in FH's computations. If the imaginary (quadrature) part of the Fourier elements $\overline{\hat{u}_k \hat{u}_j^*}$ is set equal to zero, then veering modes can also be computed within narrower frequency bands. In this form the veering of the complex velocity $\hat{w}_j$ relative to $\hat{w}_k$ is given by

$$\Delta\theta = \theta_k - \theta_j = \arctan \frac{I_m \overline{\hat{w}_k \hat{w}_j^*}}{\mathrm{Re}\ \overline{\hat{w}_k \hat{w}_j^*}} \tag{6.4}$$

which is identical to the veering angle in Equation (6.1) except for the reversal in sign convention. Therefore, veering modes are empirical orthogonal functions which represent the correlated changes between the velocity vector at different depths.

The two most energetic veering modes are shown in Figures 6.3 and 6.4 for the GSE moorings 680, 674, 678, 677, 347, and 673 for the frequency band containing variability at 285-30 day periods. The other moorings cannot be analyzed with this method because of absent records due to instrument failures. The amplitudes of the modes have been normalized by the surface amplitude and the deepest velocity vector has been rotated along the positive x axis because the absolute direction is arbitrary. The 95 percent significance level for the squared coherence is .26 for the 380 day record and .28 for the 342 day record (Julian, 1974). The total band used in this analysis differs slightly from that used in FH's analysis because it does not contain periods longer than 285 days or shorter than 30 days. Solid arrows in Figures 6.4 and 6.5 indicate significant coherence at the 95 percent confidence level between the empirical mode and the complex velocity at a given depth. Analysis of these two figures shows some similarities with the earlier results, but the empirical modes clearly decompose the vertical structure in those cases which were previously found to be vertically incoherent. In all cases the most energetic velocity veering mode is coherent at all depths and it contains more than twice the energy of the second mode.

The modal decomposition is sharpest at mooring 673. The first two modes account for 96 percent of the total variance with 85 percent in mode 1 and 11 percent in mode 2. The first velocity mode is strongly surface intensified and coherent at all depths with significant counterclockwise veering of $70^\circ \pm 14^\circ$ between 500 and 4000 m. By contrast, the second mode is not coherent with any of the instrument levels. Because most of the energy is in a single mode, its structure is similar to that found in FH's correlation analysis. The

velocity structure in mooring 673 is well represented by a single vertically coherent mode with significant counterclockwise veering with depth.

FH's analysis described the velocity structure in mooring 674 on the northern flank of the Ridge and in mooring 680 near the Sohm Abyssal Plain as vertically coherent but with no significant veering. The dominant empirical veering modes in both these cases are surface intensified and contain 81 percent of the variance. In mooring 674 this mode is also bottom intensified while in 680 there is no change in amplitude between 1500 and 4000 m. The 15° clockwise veering between 500 and 4000 m in mooring 674 is significant at the 90 percent level, but mooring 680 does not show any veering. The second mode at both moorings is coherent only at the shallowest and deepest levels.

The most complex vertical structure characterizes the modes from moorings located on the southern flank of the Ridge (677 and 678) and in those moorings (346 and 347) located nearest to the Newfoundland Basin. FH found that the velocity structure in these two groups of moorings was vertically incoherent. The empirical mode analysis shows that this lack of coherence is due to the presence of the second mode which contains between 22 and 30 percent of the variance and is not coherent at the 1500 m level. Mode 1 accounts for only 65, 75, 68 percent of the total variance at moorings 678, 677, and 347 respectively. The dominant modes are surface intensified and coherent at all depths. Mooring 677 also shows strong bottom amplitude intensification. The velocity veering angles between 500 and 4000 m are barely significant at the 95 percent level in all three cases.

From the analysis of veering alone the velocity vertical structure in the Gulf Stream Extension array is in some respects similar to that found in POLYMODE Clusters A, B, and C and in POLYMODE Array II. Fu et al. (1982)

showed that the dominant velocity mode in those three arrays is a single surface intensified baroclinic mode without much veering in depth. A single mode accounts for 96 percent of the variance in Clusters A and B while in Cluster C only 78 percent of the variance is described by the lowest mode. FH report that in Array II the variability for the total band is vertically correlated with less than 10 degrees of veering between 600 and 4000 m except for mooring 6 which was located near topographic features. The structure of the GSE complex velocity modes is similar to these other data because the total band can be represented predominately by a single mode.

(b) Independent velocity and temperature modes

To further investigate temporal phase changes it is instructive to remove the constraint that the velocity field be unidirectional at each level. In this case the east and north components are treated as independent scalars and the covariance matrix then allows twice as many possible modes as the number of instruments. These modes were calculated for low (275-70 days) and middle (70-30 days) frequency bands. Since topography has an important influence on the velocity orientation, the velocity components were rotated to the alongslope and upslope directions. The orientation of the bottom contours at each mooring is given in Table 2 of Fofonoff and Hendry (1984). This rotation improves the coherence between the modes and the data in the low frequency band, but it has no significant effect on the coherence of the middle frequency band.

The vertical structure in the low frequency band (Figure 6.5) can be adequately described by a single vertical mode at only three of the moorings. In these three moorings - 673, 677, and 678 - the dominant mode contains more

than twice the variance of the second mode. Mooring 673 contains 85 percent of the variance in a single mode showing upward temporal phase propagation. Both the upslope and the alongslope velocity components are coherent and in quadrature at all depths as would be expected for a quasigeostrophic mode. However, the mode shows a uniform vertical temporal phase change of nearly 90 degrees between the thermocline and the bottom. For mooring 677 located along the ridge crest the dominant mode with 73 percent of the variance shows upward phase propagation in the alongslope flow. The other three moorings - 347, 674, 680 - require more than the lowest mode to account for the variance with this representation. Therefore, the significance of these modes cannot be interpreted. The empirical modes for the middle frequency band are shown in Figure 6.6. A single mode describes most of the variance at moorings 673, 674, 677, and 680, but there is no common direction for phase propagation.

Empirical modes were also computed separately from the corrected temperature data for the low and middle frequency bands. These modes shown in Figure 6.7 were computed from the temperature at each level normalized by the ratio of the mean vertical temperature gradient to the buoyancy frequency. These modes are not significantly different from the modes computed from the matrix normalized by the variance. The first mode represents nearly all the energy at each mooring and the dominant mode in the low band accounts for more of the variance than in the middle band. The modes are coherent at most levels with no vertical temporal phase change except in the middle band at moorings 673 and 347 which show upward temporal phase propagation.

The temperature modes at moorings 677, 678, and 680 in the western part of the array are very surface intensified and the intensification decreases to

the west for both the temperature and the velocity modes in Figures 6.5 and 6.6. The structure of the modes may reflect the passage of warm anticyclonic rings or Gulf Stream meanders through the western part of the array. FH note that such events marked by the presence of water warmer than 14°C occur only for a total of about 40 days at mooring 679 and 680. The first mode in the middle frequency band is also strongly surface intensified in the western moorings - 677, 678, 680 - but this intensification elsewhere is less pronounced than in the low frequency band.

c) Cross-spectral velocity and temperature modes

The complete velocity and temperature cross-spectral matrix was computed using data from three depths at four of the moorings --347, 673, 678, 680. In each of these cases the dominant mode accounts for more than twice the variance of the second mode. However, the low coherence in both the low and the middle frequency bands does not indicate any significant relation between velocity and temperature at any of the moorings. In order to increase the number of degrees of freedom, the cross-spectral matrix was ensemble averaged over the available data from the three westernmost moorings -- 678, 679, and 680 which are horizontally coherent. The first empirical mode for the low frequency band (Figure 6.8) accounts for only 47 percent of the variance, but this is significantly more than the variance of the second mode according to an F-test (Bendat and Piersol, 1971). The dominant mode in the middle frequency band is not significant according to this test. The mode is coherent with both the meridional velocity component and temperature. This mode does not produce a significant heat flux because the variables are 270 degrees out

of phase at 1500 and 500 m depth. There is, however, a vertical phase change between the 1500 and 4000 m instruments.

6.VI. Discussion

The empirical mode representation is a compact way to compare the vertical structure in different frequency bands. If the variability in the Gulf Stream Extension is described by only velocity veering, then the structure at all the moorings is a single mode which is coherent in depth. In this representation the largest veering occurs in mooring 673 near the flanks of the Mid-Atlantic Ridge. If temporal phase changes are accounted for by treating the velocity variables as independent scalars, then this veering is shown to actually represent upward phase propagation in the low frequency band. Several other of the velocity modes also show upward phase propagation in this band, although the coherence at most depths is not high. The only temperature modes which show a uniform time lag with depth are in the middle frequency band at the easternmost moorings.

In order to improve the coherence between the modes and the data, the velocity and temperature cross-spectral matrix was ensemble averaged over three of the moorings in the eastern part of the array. The first empirical mode which represents nearly 50 percent of the variance in the low frequency band is coherent at all depths with temperature and the meridional velocity component. The meridional velocity and temperature are in quadrature and the phase decreases with depth between 500 and 1500 m. Between 1500 m and the bottom the velocity phase continues to increase while the temperature phase decreases. It is possible that these modes represent Gulf Stream meanders or

warm rings, although the temperature data show that such events occur during only forty days of the total 380 day record.

These data cannot be interpreted unambiguously in terms of models for wave generation by a mean flow. The data length is relatively short compared to the time-scale of the variability and since the fields are horizontally inhomogeneous, the data from all the moorings cannot be ensemble averaged to increase the degrees of freedom. There is some evidence of vertical phase propagation as would be expected for a wave field generated by baroclinic instability. However, the stream function maps calculated by Fofonoff and Hendry (1984) do not show much horizontal wave propagation. There is no strong evidence of baroclinic instability like that found in the Gulf Stream Recirculation region although it may be necessary to analyze the variability in narrower frequency bands. The present data are not sufficient to do this type of detailed analysis. It is also possible that the vertical phase changes in the empirical modes reflect a process of wave generation by the flow of the Gulf Stream over topography.

Tables and Figures

Table 6.1: Data record from the Gulf Stream Extension Experiment, adapted from Levy et al. (1982).

Figure 6.1: Mean velocity vectors at 4000 m superimposed on topographic contours. The significant part of the velocity vector is drawn as a solid line.

Figure 6.2: Principle axes of the eddy variance at 1500 and 500 m superimposed on topographic contours.

Figure 6.3: The first empirical veering mode computed for the total frequency band between 285 and 30 days. Coherence at the 95 percent significance level between the mode and the data is indicated by a solid arrow.

Figure 6.4: The second empirical veering mode computed for the total band. Coherence at the 95 percent significance level between the mode and the data is indicated by the solid arrow.

Figure 6.5: The first complex empirical mode computed with the velocity components as independent scalars. The velocity components have been rotated in the local alongslope (solid line) and upslope (dotted line) directions. Coherence at the 95 percent significance level between the mode and the data from a given depth is indicated by a solid circle. The percentage of the total variance accounted for by the first mode is also given.

Figure 6.6: The first complex empirical mode for the middle frequency band computed with the velocity components treated as independent scalars.

Figure 6.7: Complex empirical modes for corrected temperature data from 500, 1500, and 4000 m depths. Records from 800 m were also available at moorings 673, 674, and 680. The dominant modes are plotted for the low band (solid line) and the middle band (dotted line). The percentage of the total variance contained in these modes is also given. Coherence at the 95 percent significance level between the mode and the data at a given depth is indicated by the solid circle.

Figure 6.8: Empirical modes of the velocity and temperature cross-spectral matrix in the low frequency band ensemble averaged over moorings 678, 679, and 680. There are missing records for temperature at 500 m on mooring 678 and for all variables at 4000 m on mooring 679.

TABLE 6.1 (adapted from Levy et al., 1982)

Instrument	Depth (m)	Variables	Start Date	Record Length (days)
6731	641	u,v,t,p	Oct. 25, 1979	395
6732	938	t,p	Oct. 25, 1979	395
6733	1640	u,v,t,p	Oct. 25, 1979	394
6734	4053	u,v,t	Oct. 25, 1979	396
6741	550	u,v,t,p	Oct. 27, 1979	391
6742	852	t,p	Oct. 28, 1979	390
6743	1552	u,v,t,p	Oct. 27, 1979	390
6744	4029	u,v,t	Oct. 27, 1979	392
6751	569	u,v,t,p	Oct. 28, 1979	390
6752	866	t,p	Oct. 28, 1979	390
6753	1564	u,v,t,p	Oct. 28, 1979	390
6754	4037	u,v,t	Oct. 27, 1979	392
6771	560	u,v,t,p	Nov. 1, 1979	387
6772	858	t,p	Nov. 1, 1979	387
6773*	1497	u,v,t,p	Nov. 1, 1979	166
6774	4036	u,v,t	Oct. 31, 1979	389
6781*	516	u,v,t,p	Nov. 2, 1979	385 (t-154)
6782	809	t,p	Nov. 2, 1979	384
6783	1513	u,v,t,p	Nov. 2, 1979	383
6784	3995	u,v,t	Nov. 2, 1979	385
6791	519	u,v,t,p	Nov. 3, 1979	382
6792	817	t,p	Nov. 3, 1979	382
6793	1516	u,v,t,p	Nov. 3, 1979	382
6794*	4006	u,v,t	Nov. 3, 1979	81
			June 9, 1980	164
6801	521	u,v,t,p	Nov. 3, 1979	382
6802	822	t,p	Nov. 4, 1979	381
6803	1520	u,v,t,p	Nov. 3, 1979	382
6804	4016	u,v,t	Nov. 3, 1979	383
3461*	500	u,v,t,p	Sept. 28, 1979	214
3462/3692	800	u,v,t,p	Sept. 28, 1979	348 (351)
3463*	1500	u,v,t,p	Sept. 38, 1979	214
3464/3693	4000	u,v,t	Sept. 28, 1979	348 (351)
3471/3701	500	u,v,t,p	Sept. 27, 1979	345 (348 with 3 day interpolated gap)
3702*	800	u,v,t,p	May 3, 1980	129
3472/3703	1500	u,v,t,p	Sept. 27, 1979	345 (348)
3473/3704	4000	u,v,t	Sept. 27, 1979	345 (348)

*short record

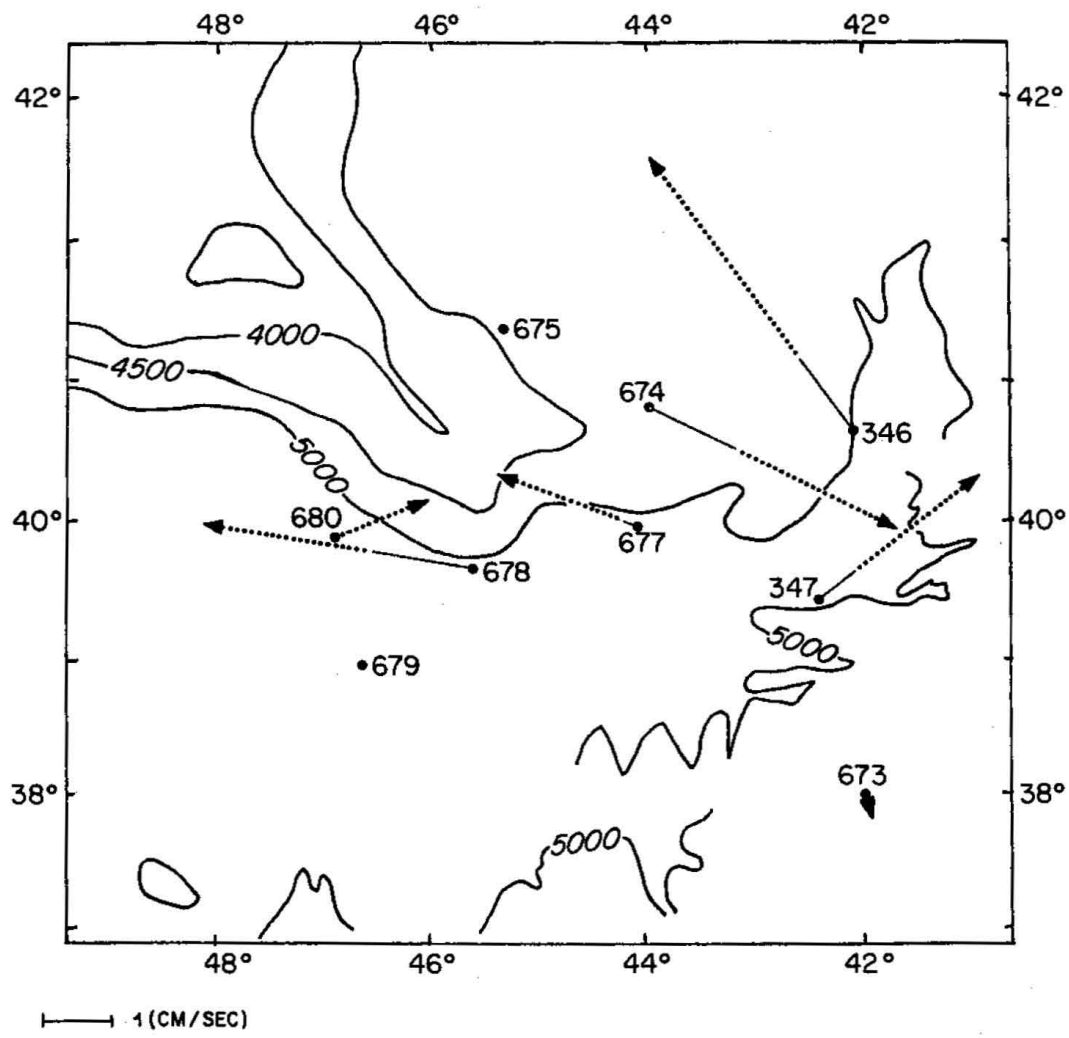
48°
46°
44°
42°
42°
40°
38°
4000
4500
5000
675
674
346
680
677
678
347
679
673
1 (CM/SEC)

Figure 6.1

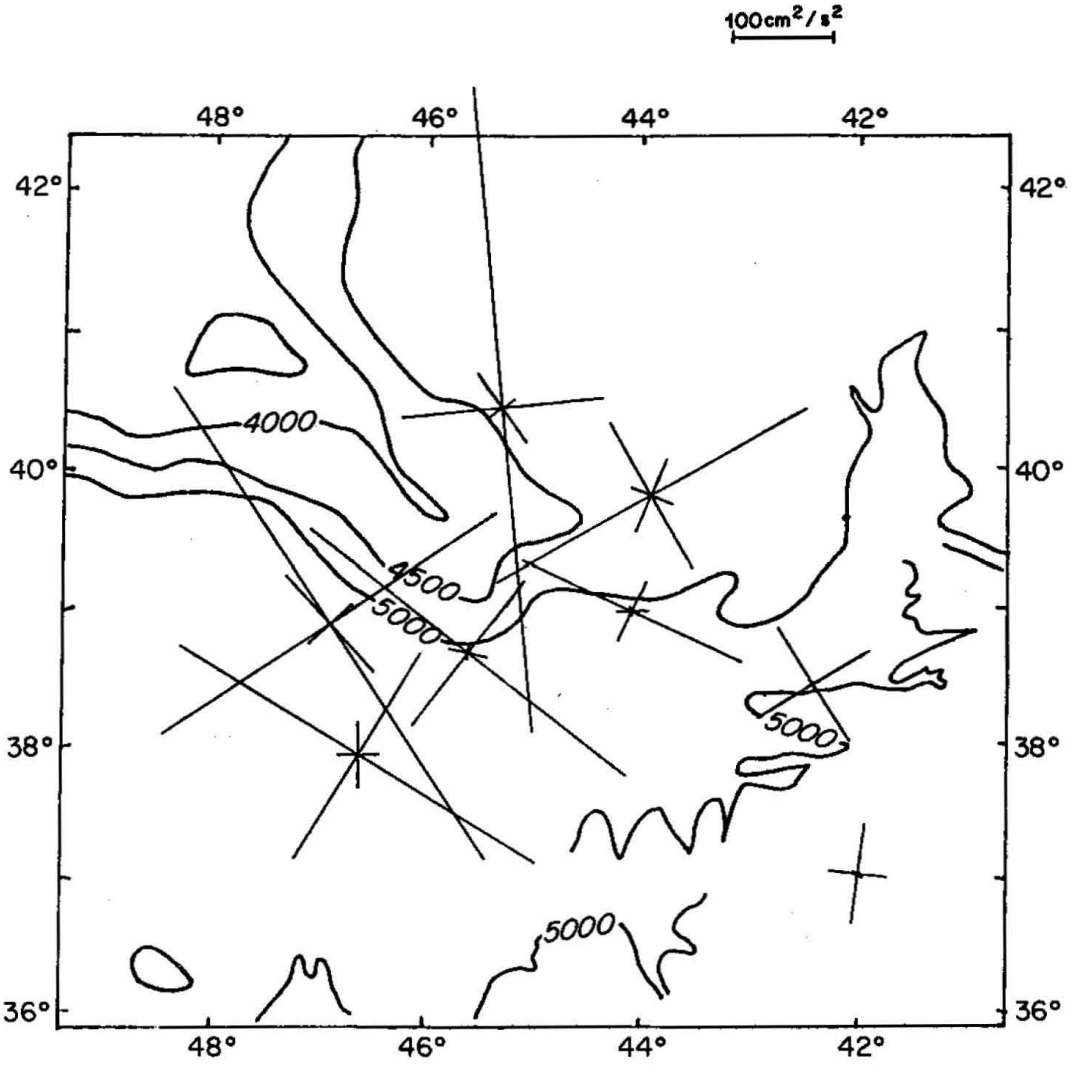

Figure 6.2

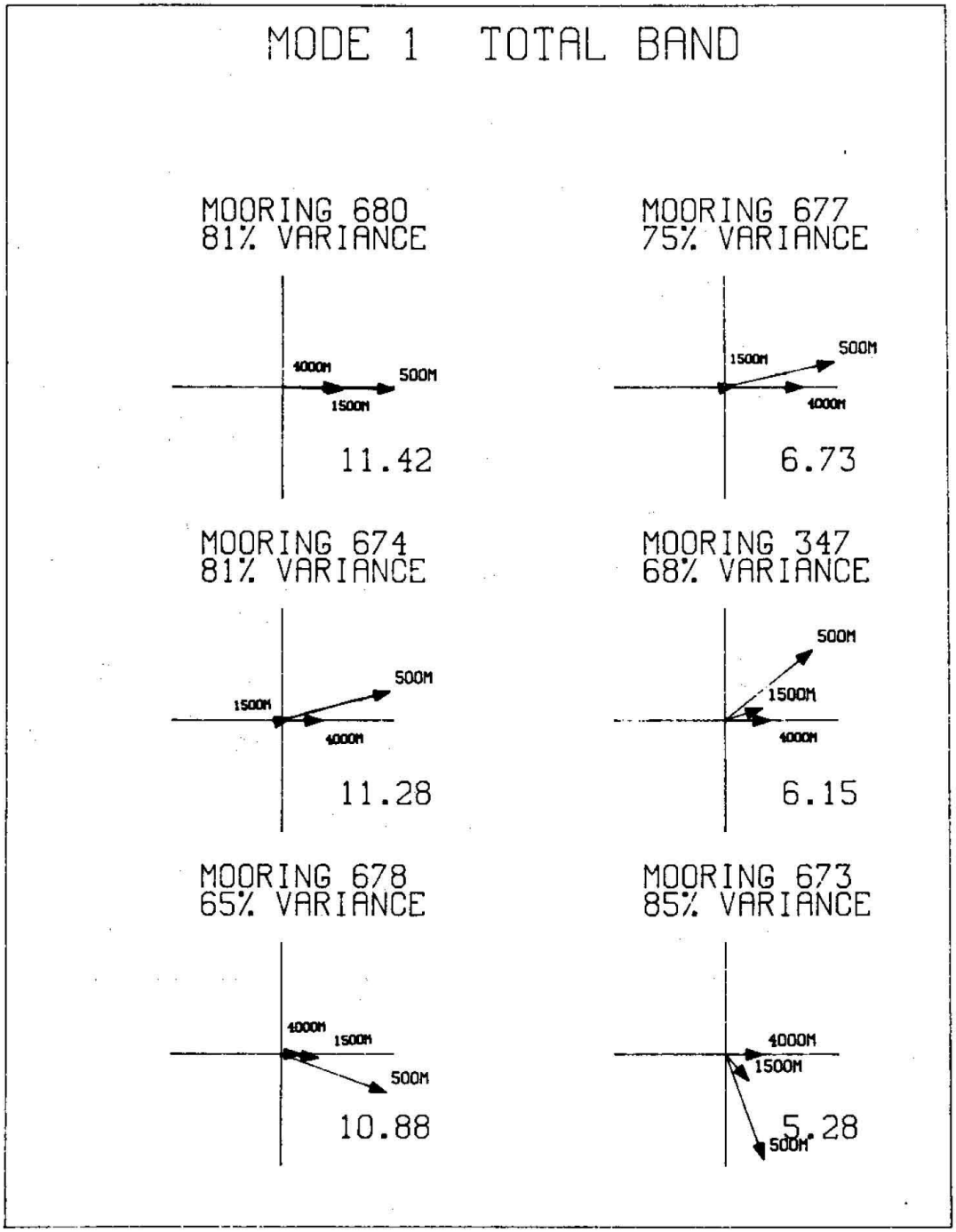
MODE 1 TOTAL BAND
MOORING 680
81% VARIANCE
4000M
500M
1500M
11.42
MOORING 677
75% VARIANCE
1500M
500M
4000M
6.73
MOORING 674
81% VARIANCE
500M
1500M
4000M
11.28
MOORING 347
68% VARIANCE
500M
1500M
4000M
6.15
MOORING 678
65% VARIANCE
4000M
1500M
500M
10.88
MOORING 673
85% VARIANCE
4000M
1500M
500M
5.28

Figure 6.3

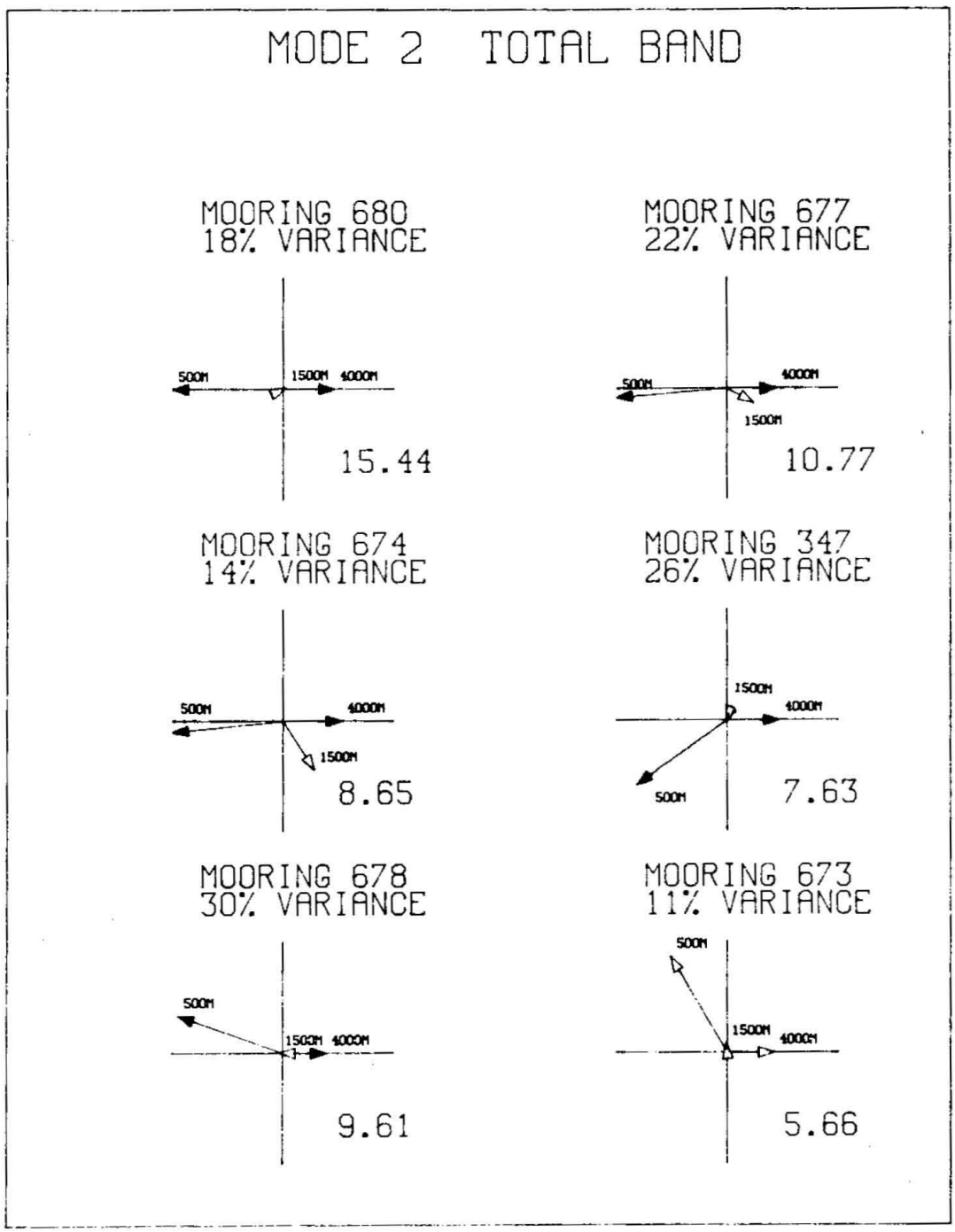
MODE 2 TOTAL BAND
MOORING 680
18% VARIANCE
500M
1500M
4000M
15.44
MOORING 677
22% VARIANCE
500M
4000M
1500M
10.77
MOORING 674
14% VARIANCE
500M
4000M
1500M
8.65
MOORING 347
26% VARIANCE
1500M
4000M
500M
7.63
MOORING 678
30% VARIANCE
500M
1500M
4000M
9.61
MOORING 673
11% VARIANCE
500M
1500M
4000M
5.66

Figure 6.4

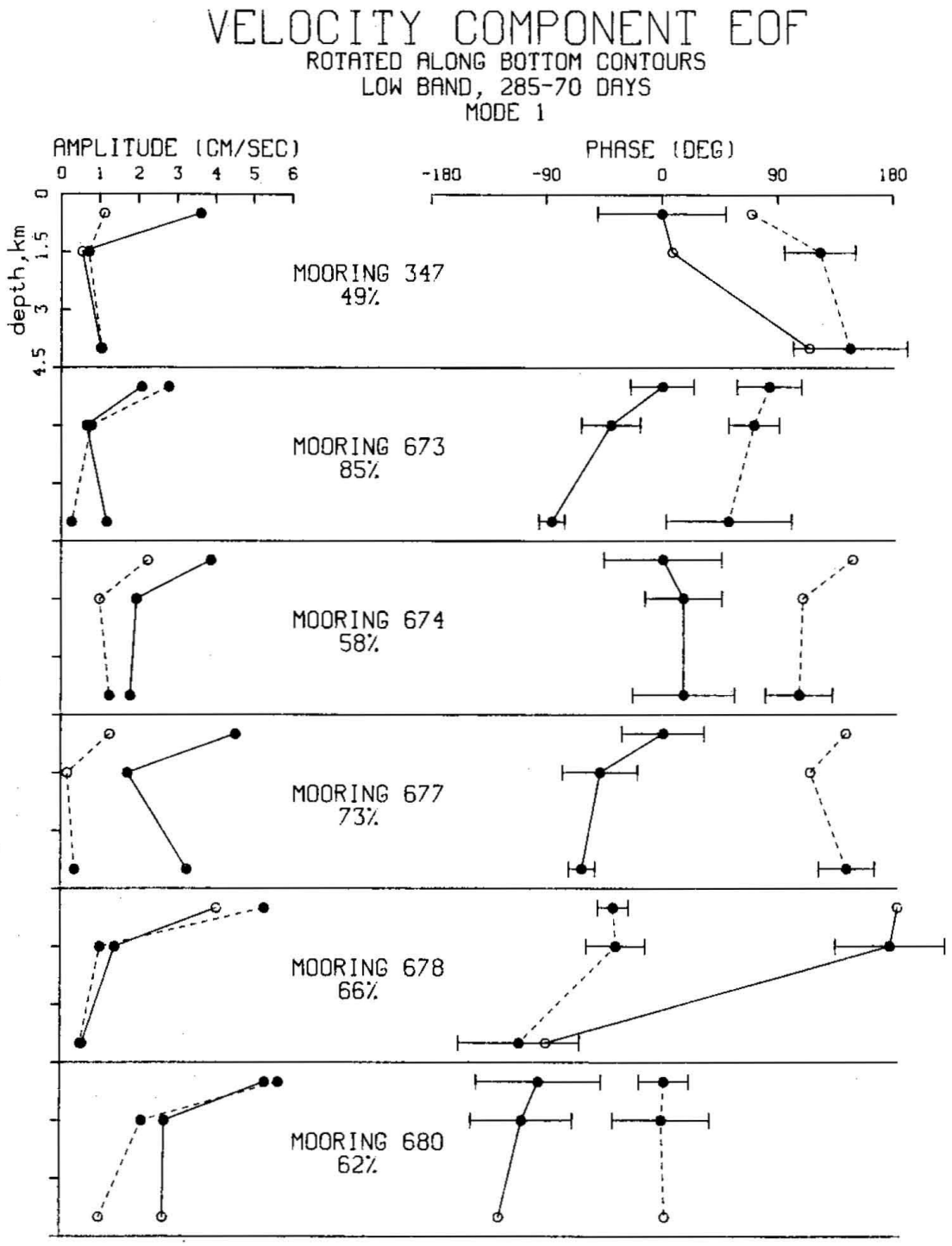
VELOCITY COMPONENT EOF
ROTATED ALONG BOTTOM CONTOURS
LOW BAND, 285-70 DAYS
MODE 1
AMPLITUDE (CM/SEC)
0 1 2 3 4 5 6
PHASE (DEG)
-180 -90 0 90 180
depth, km
0
1.5
3
4.5
MOORING 347
49%
MOORING 673
85%
MOORING 674
58%
MOORING 677
73%
MOORING 678
66%
MOORING 680
62%

Figure 6.5

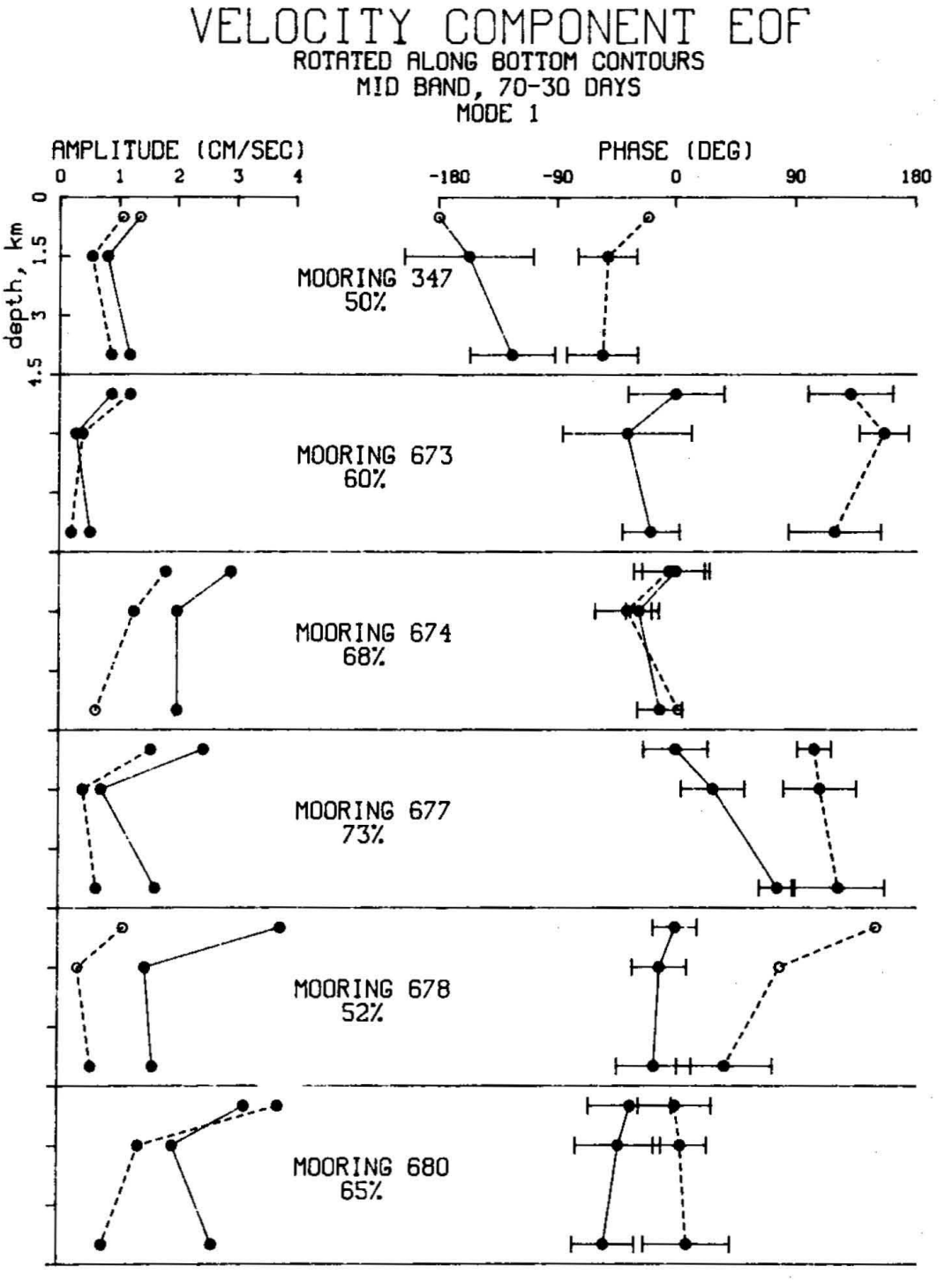
VELOCITY COMPONENT EOF
ROTATED ALONG BOTTOM CONTOURS
MID BAND, 70-30 DAYS
MODE 1
AMPLITUDE (CM/SEC)
0 1 2 3 4
PHASE (DEG)
-180 -90 0 90 180
depth, km
0
1.5
3
4.5
MOORING 347
50%
MOORING 673
60%
MOORING 674
68%
MOORING 677
73%
MOORING 678
52%
MOORING 680
65%

Figure 6.6

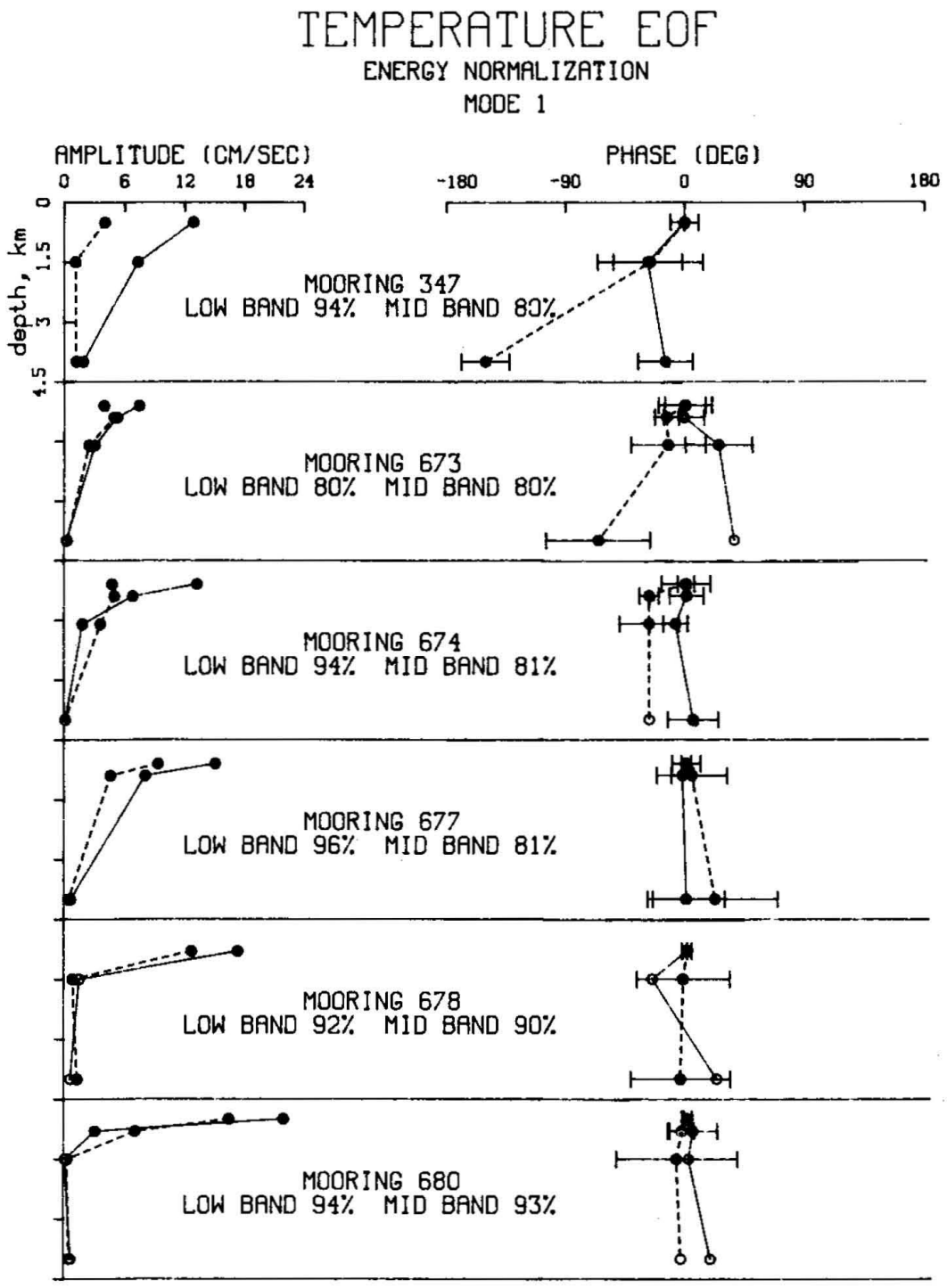
TEMPERATURE EOF
ENERGY NORMALIZATION
MODE 1
AMPLITUDE (CM/SEC)
0
6
12
18
24
PHASE (DEG)
-180
-90
0
90
180
depth, km
0
1.5
3
4.5
MOORING 347
LOW BAND 94% MID BAND 80%
MOORING 673
LOW BAND 80% MID BAND 80%
MOORING 674
LOW BAND 94% MID BAND 81%
MOORING 677
LOW BAND 96% MID BAND 81%
MOORING 678
LOW BAND 92% MID BAND 90%
MOORING 680
LOW BAND 94% MID BAND 93%

Figure 6.7

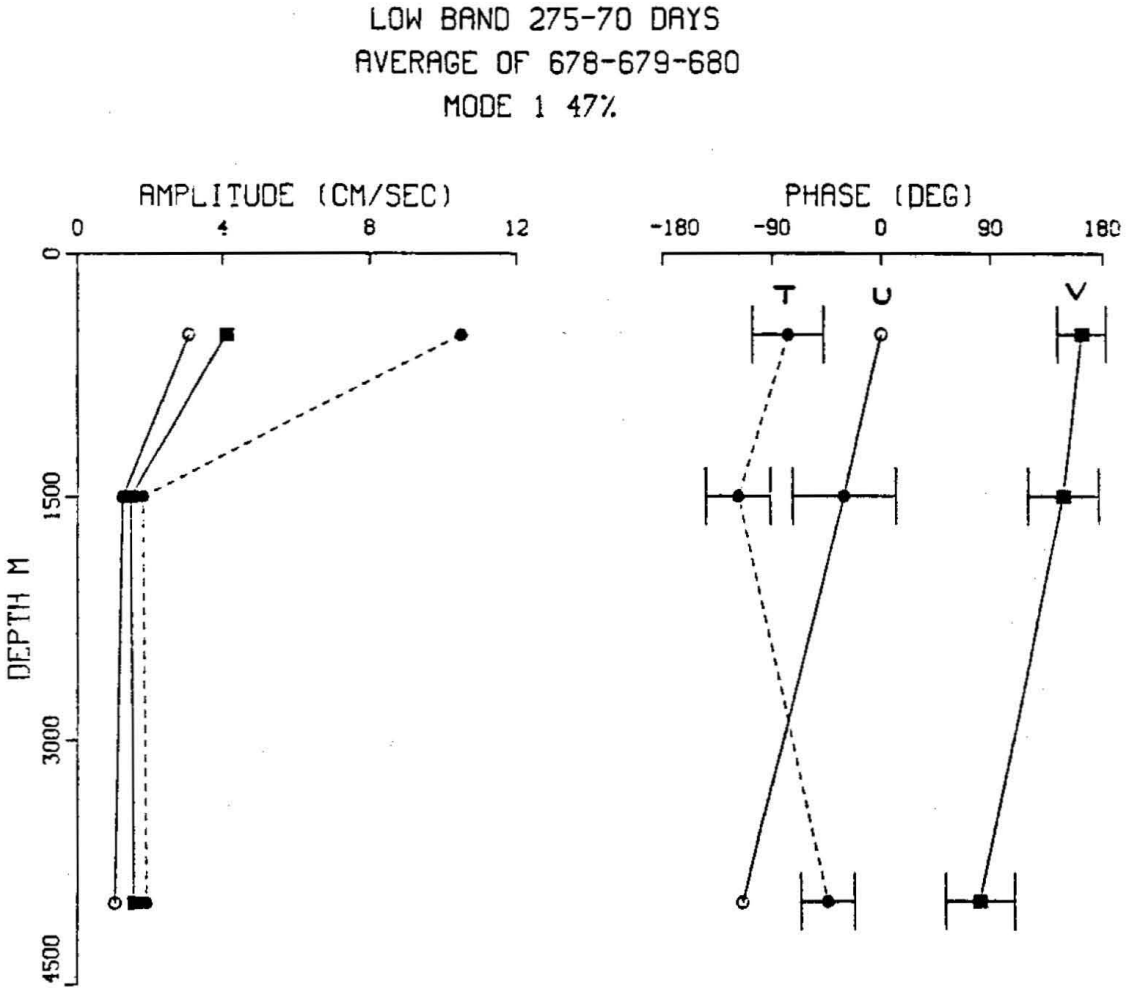
LOW BAND 275-70 DAYS
AVERAGE OF 678-679-680
MODE 1 47%
AMPLITUDE (CM/SEC)
0
4
8
12
PHASE (DEG)
-180
-90
0
90
180
T
U
V
DEPTH M
0
1500
3000
4500

Figure 6.8

APPENDIX B

The buoyancy distribution for the Gulf Stream Extension moorings was designed to be flexible enough to withstand the strong vertical shears in this region. Mooring motion is largest in the energetic western part of the array where excursions from the nominal instrument pressure are as large as one hundred db which is about a one degree temperature change near the mid-thermocline. These excursions occur typically over the one month time scale of energetic events. Moorings to the east and north of the Newfoundland Ridge show smaller depth excursions with mooring 673 showing depth variations of only a few meters.

Mooring excursions cause an error in the temperature measurements and therefore in the heat fluxes by inducing a spurious correlation between velocity and temperature fluctuations. The error is largest in the thermocline where there is the most variation in depth. At 4000 m this causes smaller errors because the vertical temperature gradient and the mooring excursions are smaller. The technique devised by Mills et al. (1981) has been used here to correct the temperature measurements at 500 m, 800 m, and 1500 m for the effect of mooring motion. The method consists of two steps - first, converting the pressure record to depth and, second, correcting the temperature measurements to a uniform depth.

The pressure to depth conversion is calculated from the hydrostatic relation using the method devised by Saunders and Fofonoff (1975). Pressure p and depth z are related by

$$\frac{dp}{dz} = \frac{g}{\alpha} \tag{B1}$$

where α is the in situ specific volume and g the gravitational strength is written as the sum of g_0, a function which depends on latitude and a linear function in depth

$$g = g_0 + \gamma z \qquad \gamma = 2.226 \times 10^{-4} \text{ dbar.} \tag{B2}$$

The depth is determined by integrating Equation (B1)

$$z = \frac{\int_0^p \alpha dp}{(g_0 + \frac{1}{2}\gamma p)} \tag{B3}$$

where depth has been replaced with pressure under the integral. Saunders and Fofonoff rewrite this using the expansion

$$\alpha = \alpha_0 + \delta \tag{B4}$$

where α_0 is the specific volume for a standard ocean and δ is the specific volume anomaly. The integral in equation (A3) can then be written as the sum

$$z = \frac{\int_0^p \alpha_0 dp}{g_0 + \frac{1}{2}\gamma' p} + \frac{\Delta D}{g_0 + \frac{1}{2}\gamma' p} \tag{B5}$$

where $\Delta D = \int_0^p \delta dp$ is the dynamic height. The first integral is evaluated analytically using the Knudsen-Ekman formula for α_0. The second term is calculated from the average CTD profile by a least squares fit of the form

$$\Delta D = c_1 p^{c_2} \tag{B6}$$

Figure A1 shows a scatterplot of the dynamic height versus pressure from the CTD stations reported in Levy et al. (1982). For the GSE profile the appropriate regression coefficients are

$$c_1 = .0149$$

$$c_2 = .6315$$

Thus, given the time series of pressure can be converted to depth using equation (A5).

Pressure and temperature were measured on all the GSE moorings only at the 500 m and 800 m levels. For the three moorings - 673, 674, 678 - without 1500 m pressure records, the excursion depths at 1500 m must be inferred from the pressure records at 800 m. In these cases the time series of 1500 m depth excursion are calculated by applying the weighting factor

$$w = \frac{H - zmf_{1500}}{H - zmf_{800}} \tag{B7}$$

where H is the total water depth,

zmf_{1500} is the most frequent depth of the 1500 m instrument, and zmf_{800} is the most frequent depth of the 800 m instrument. The most frequent depths of the instruments were determined from the histogram of the pressure time series. The depth series at 1500 m, $z_{1500}(t)$, was then calculated from the depth series at 800 m, $z_{800}(t)$, by

$$z_{1500}(t) = zmf_{1500} + w[z_{800}(t) - zmf_{800}] \tag{B8}$$

Corrected temperature is calculated in three steps from the observed temperature $T_o(t)$ and the observed depth $z_o(t)$. The method is based on the

assumption that the mean temperature profile describes the depth dependence in a given depth interval but can be shifted vertically. The observed temperature T_o and depth z_o is first moved adiabatically to the point T_1 , z_1 on the mean temperature profile F(z) by solving the simultaneous equation

$$T_1 = T_o - \beta(z_o - z_1) = F(z_1) \tag{B9}$$

where β is the adiabatic temperature gradient $\beta = 1.1 \times 10^{-4}$ C/m. The mean profile F(z) is defined by a cubic spline fit to the average CTD profile. The temperature is then adjusted along the mean profile F(z) by an amount equal to the excursion Δz from the most frequent depth:

$$T_2 = F(z_2)$$

where

$$z_2 = z_1 - \Delta z$$

The final corrected temperature is determined by adiabatically moving the temperature down a distance equal to the mooring dip

$$T_{corr} = T_2 + \beta(z_o - z_1) \tag{B10}$$

Figures B1 through B6 show some examples of the measured and corrected temperatures for the 1500 m and shallower instruments.

6751 Figure B1

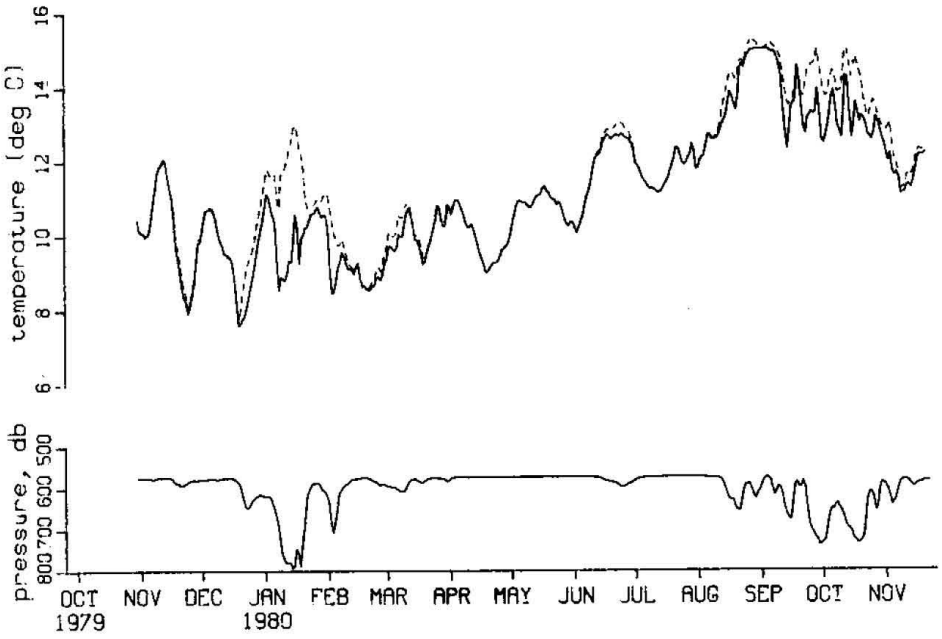

6741 Figure B2

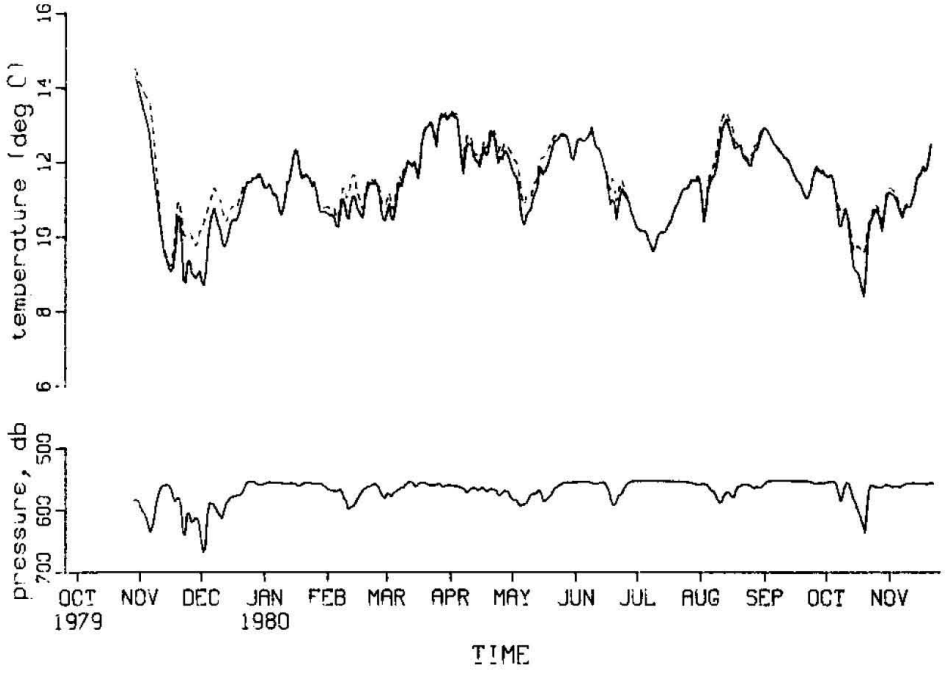

6782 Figure B3

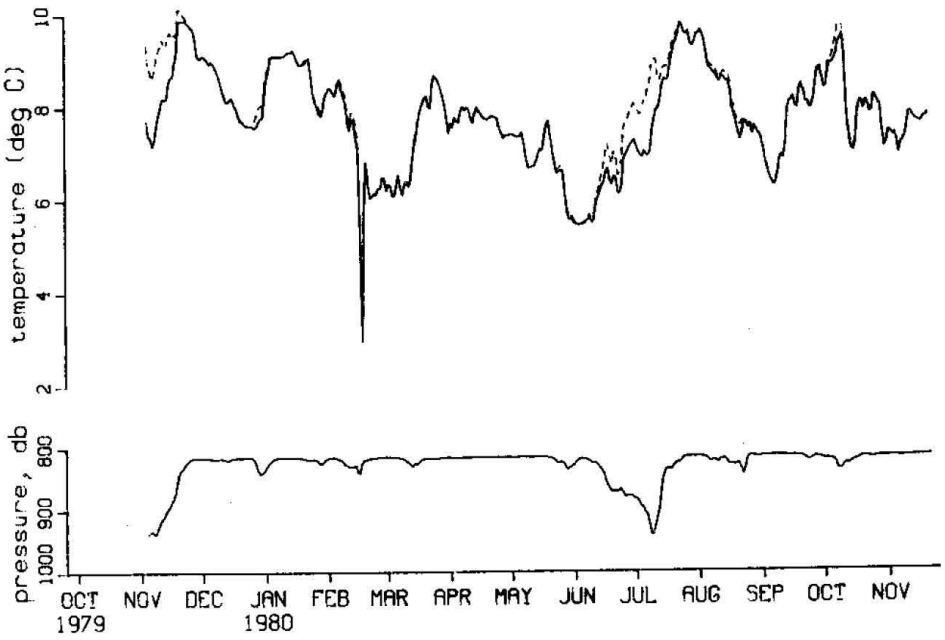

6771 Figure B4

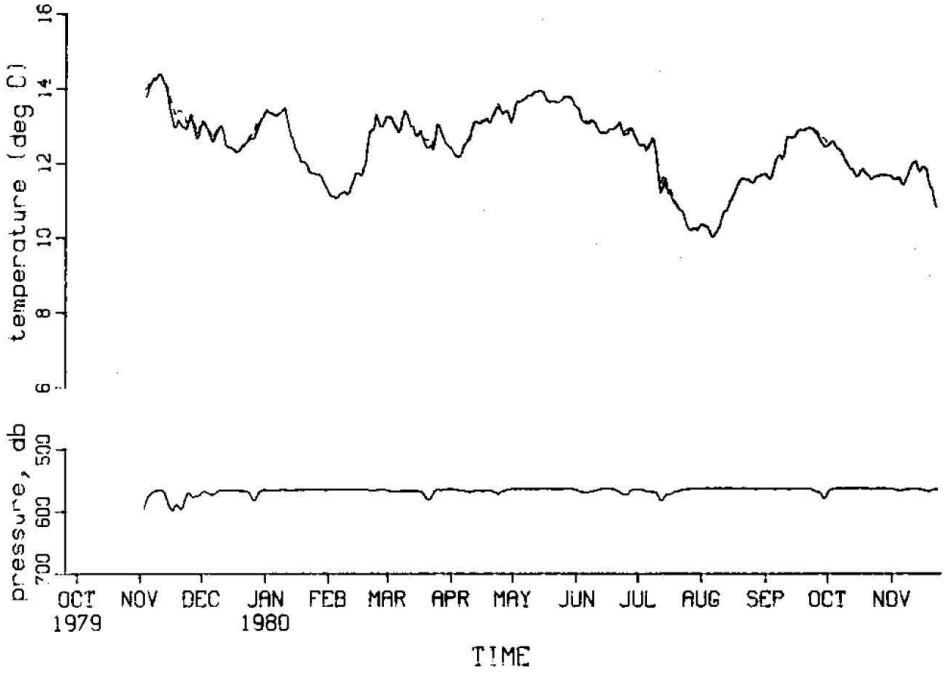

6801 Figure B5

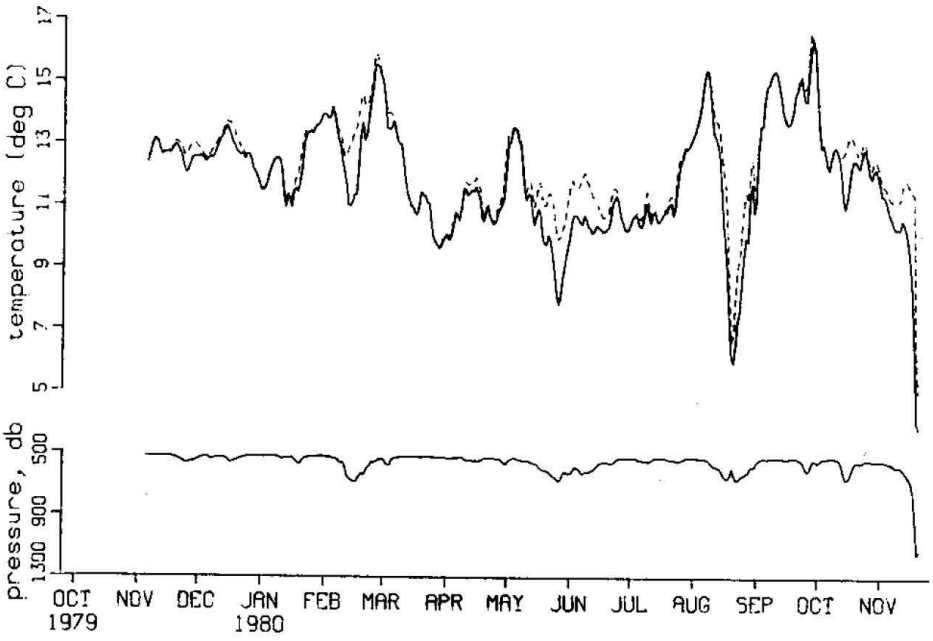

6791 Figure B6

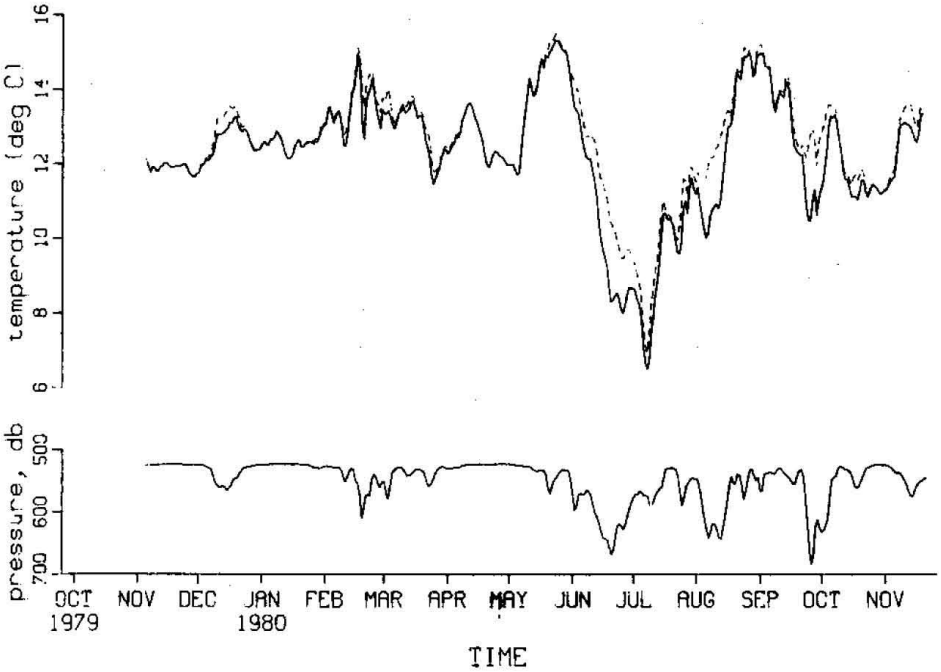

CONCLUDING REMARKS

During the early 1970's technological developments made possible long-term direct measurements of current and temperature fields. Since that time one important goal of oceanographic research has been to determine the effect of the low-frequency variability on the time-mean circulation. This research has to a large extent been motivated by studies of atmospheric dynamics in which time-dependent fields play an important role. However, it is unlikely that the oceanic "eddy problem" will be solved given the formidable sampling requirements for determining mean quantities. A measurement of the mean velocity or the eddy fluxes and their divergences to within about ten percent uncertainty would require about 10 years of data. Even with major innovations in data collecting programs, it will be at least a decade before this problem can be properly addressed.

Therefore, it is necessary to concentrate future observations in regions of the ocean where the eddy terms are largest in comparison to the mean. The scale analysis in Chapter 2 suggests that the eddy terms are most likely to be dynamically important in the mean vorticity and heat balances of the recirculation region. In the mid-ocean the vorticity balance is geostrophic and the heat balance is between mean horizontal and vertical temperature advection. On the southern edge of the Gulf Stream recirculation region near 30°N, 70°W the eddy terms are probably not important in the relative vorticity balance, but the eddy heat flux divergence is significant in the heat balance. Thus the eddy potential vorticity flux in the mean potential vorticity balance is dominated by the thickness flux which can be a significant term in the mean potential vorticity balance. In the region closest to the Gulf Stream axis, along 55°W between 35°N and 38°N, the eddy

terms may be important in both balances. The scale analysis of these three regions shows a geographic progression from the mid-ocean where the eddy terms are negligible to the near-field of intense zonal Gulf Stream flows where the eddy terms may be important in all of the balances.

Even with orders of magnitude more data, the present approaches towards assessing the effects of eddies on mean flows may still be ambiguous. Such problems have already been seen in analyses of numerical experiments. The numerical approach to the eddy problem has two major advantages over the direct observational approach. First, because large amounts of data are generated, all the terms in the dynamical balances can be calculated. Second, the model physics can be restricted in order to separately study the effects of different types of forcing on the model circulations. However, even with this brute force method for calculating the effects of time-dependent variability on model oceans, the results are often unclear. Two different interpretations have been presented for the same numerical data [see, for example, Holland and Rhines (1980) and Harrison and Holland (1981)]. The balances in these model oceans can differ depending on the regions of integration or on the choice of numerical parametrizations for physical processes. The problem then becomes one of relating the dynamics of these model oceans where the data base is enormous to the real ocean where the data base is comparatively meager.

Even in meteorology where the data base is orders of magnitude more extensive than in oceanography, direct calculations (Edmon et al., 1983) of the eddy-induced mean circulation have only recently been made. The studies of atmospheric dynamics have emphasized plotting vertical-meridional sections of the eddy potential vorticity flux as a means to visualize the mean circulation induced by the eddy field. The problem is quite a bit simpler for the zonally-averaged atmospheric flows than for spatially inhomogeneous oceanic

flows. The technique, however, has also been used to study the effect of an eddy field on the time-averaged atmospheric circulation (Hoskins et al., 1983). These types of analyses have a more promising practical application than the approaches used to analyze numerical model flows.

Although we cannot solve the "eddy problem", this thesis shows that several evaluations of the effect of eddies on the large scale flow can be made. In Chapter 4 the mean dynamical balances have been evaluated for a finite measurement period in order to assess the importance of the eddy term in the mean heat equation. The mean dynamical balances for the data from the Local Dynamics Experiment agree with the scale estimates in this region. The vorticity balance between vortex stretching and planetary advection is consistent within the measurement uncertainties provided that there is a significant eddy-induced vertical velocity. We also calculate a direct estimate of the eddy heat flux divergence in the thermocline from the LDE mooring array. Although the uncertainties are large, the vertical velocity due to the eddy heat fluxes could be comparable to that due to mean horizontal temperature advection.

Another approach taken in this thesis is the calculation of the eddy potential vorticity flux. In analyses of numerical models the flux is area-integrated because the divergence of this quantity is dynamically important in forcing the mean potential vorticity balance. The ocean data are sufficient only for calculating the flux in a small region of the ocean. The results of Chapter 3 show that during the Local Dynamics Experiment in the Gulf Stream recirculation region the flux is dominated by the thickness flux term which is directed opposite to the large-scale mean potential voricity gradient determined from hydrographic measurements. The eddy potential vorticity flux is non-zero and its sign is in accordance with the predictions

of instability theory. Moreover, it implies that there is a local cascade of enstrophy in the LDE region.

The potential vorticity flux is a fundamental quantity in stability theory as we have related in the model comparison in Chapter 5. In two-layer numerical model flows the divergence of eddy heat fluxes generated by baroclinic instability can drive a mean vertical velocity and so act as forcing for deep ocean circulation. For this reason, it is important to understand the process of baroclinic instability and the generation of eddy heat and potential vorticity fluxes eventhough these quantities are sensative to the specifics of the model profile. These types of analyses can be useful for directing the locations of new measurements. Previous analyses have identified the recirculation region as a likely region for baroclinic instability. The analysis in Chapter 6 shows that the Gulf Stream Extension region is probably not a site of active instability.

At present, the oceanic "eddy problem" can be addressed only peripherally. This thesis shows, however, that substantial progress can be made even without the orders of magnitude more data needed to fully analyze the problem. The questions which can be answered using ocean data are much more restricted than those using numerical models. However, these analyses are still useful for motivating future observational work and for providing a link between the numerical models and the real ocean.

References

Bendatt, J. S. and A. G. Piersol (1971). Random data: analysis and measurement procedures. John Wiley and Sons, New York, 407 pp.

Bretherton, F. P. (1966). Critical layer instability in baroclinic flows. Quarterly Journal of the Royal Met. Soc., 92, pp. 325-334.

Brown, E. D., and W. B. Owens (1981). Observations of the horizontal interactions between the internal wave field and the mesoscale flow. Journal of Physical Oceanography, 11, 1474-1480.

Bryden, H. L. (1980). Geostrophic vorticity balance in midocean. Journal of Geophysical Research, 85, 2825-2828.

Bryden, H. L. (1982). Sources of eddy energy in the Gulf Stream recirculation region. Journal of Marine Research, 40, 1047-1068

Davis, R. E. (1975). Statistical methods. In: Dynamics and the analysis of MODE-I: Report of the MODE-I Dynamics Group, Massachusetts Institute of Technology, Cambridge, Massachusetts, pp. 1-26.

Dickson, R. R. (1983). Global summaries and intercomparisons: flow statistics from long-term current meter moorings. In: Eddies in Marine Science. Springer-Verlag, New York, 609 pp.

Edmon, H. J., B. J. Hoskins, and M. E. McIntyre (1980). Eliassen-Palm cross sections for the troposphere. Journal of Atmospheric Sciences, 37, 2600-2616.

Fisher, A., Jr. (1977). Historical limits of the northern edge of the Gulf Stream. Gulfstream, 3, 6-7.

Flierl, G. R., and J. C. McWilliams (1977). On the sampling requirements for measuring moments of eddy variability. Journal of Marine Research, 35, 797-820.

Fofonoff, N. P. and R. M. Hendry (1984). Current variability near the Southeast Newfoundland Ridge. Journal of Physical Oceanography, submitted.

Fu, L., T. Keffer, P. P. Niiler, and C. Wunsch (1982). Observations of mesoscale variability in the western North Atlantic: A comparative study. Journal of Marine Research, 40, 809-848.

Fuglister, F. C. (1960). Atlantic Ocean Atlas of temperature and salinity profiles and data from the International Geophysical Year of 1957-1958. Woods Hole Oceanographic Institution Atlas Series I, 209 pp.

Gill, A. E., J. S. A. Green, and A. J. Simmons (1974). Energy partition in the large-scale ocean circulation and the production of mid-ocean eddies. Deep-Sea Research, 21, 499-528.

Guttman, I., S. S. Wilks, and J. S. Hunter (1971). Introductory Engineering Statistics. John Wiley and Sons, New York.

Harrison, D. E. (1979). Eddies and the general circulation of numerical model gyres: an energetic perspective. Rev. Geophys. Space Phys., 17, 969-979.

Harrison, D. E. (1980). Some Eulerian scale anaylsis results: eddy terms in the mean heat, momentum and vorticity equations. Journal of Physical Oceanography, 10, 1221-1227.

Harrison, D. E. (1982). On deep mean flow generation mechanisms and the abyssal circulation of numerical model gyres. Dynamics of Atmospheres and Oceans, 6, 135-152.

Harrison, D. E., and W. R. Holland (1981). Regional eddy vorticity transport and the equilibrium vorticity budgets of a numerical model ocean circulation. Journal of Physical Oceanography, 11, 190-208.

Harrison, D. E., and A. R. Robinson (1978). Energy analysis of open regions of turbulent flows: Mean eddy energetics of a numerical ocean circulation experiment. Dynamics of Atmospheres and Oceans, 2, 185-211.

Hogg, N. G. (1981). Topographic waves along 70°W on the Continental Rise. Journal of Marine Research, 39, 627-649.

Hogg, N. G. (1983). A note on the deep circulation of the western North Atlantic: its nature and causes. Deep-Sea Research, 30, 945-961.

Hogg, N. G. (1984). Evidence for baroclinic instability in the Gulf Stream recirculation. Progress in Oceanography, in press.

Holland, W. R. (1978). The role of mesoscale eddies in the general circulation of the ocean: Numerical experiments using a wind-driven quasi-geostrophic model. Journal of Physical Oceanography, 8, 363-392.

Holland, W. R., and L. B. Lin (1975). On the origin of mesoscale eddies and their contribution to the general circulation of the ocean. I. A preliminary numerical experiment. Journal of Physical Oceanography, 5, 642-657.

Holland, W. R., and P. B. Rhines (1980). An example of eddy-induced ocean circulation. Journal of Physical Oceanography, 10, 1010-1031.

Hoskins, B. J., I. N. James, and G. H. White (1983). The shape, propagation, and mean-flow interaction of large-scale weather systems. Journal of Atmospheric Sciences, 40, 1595-1621.

Julian, P. (1974). Comments on the determination of significance levels of the coherence statistics. Journal of the Atmospheric Sciences, 32, 836-837.

Leetmaa, A., and A. Bunker (1978). Updated charts of the mean annual wind stress convergences in Ekman layers, and Sverdrup transports in the North Atlantic. Journal of Marine Research, 36, 311-322.

Levitus, S. (1982). Climatological Atlas of the World Ocean. NOAA Professional Paper 13. U.S. Government Printing Office, Washington, D.C., 173 pp.

Levy, E., S. A. Tarbell, and N. P. Fofonoff (1982). A compilation of moored instrument data and associated oceanographic observations, volume XXX. (Gulf Stream Extension and Norwegian Sea Overflow Intrusion Experiments). WHOI Technical Report.

Luyten, J. (1977). Scales of motion in the deep Gulf Stream and across the continental rise. Journal of Marine Research, 35(1), 49-74.

McDowell, S., P. Rhines, and T. Keffer (1982). North Atlantic potential vorticity and its relation to the general circulation. Journal of Physical Oceanography, 12, 1417-1436.

McWilliams, J. C. (1983). On the mean dynamical balances of the Gulf Stream recirculation zone. Journal of Marine Research, 41, 427-460.

McWilliams, J. C., W. B. Owens, and B.-L. Hua (1983). An objective analysis of the POLYMODE Local Dynamics Experiment. I. General formalism. Journal of Physical Oceanography, accepted.

Mills, C. A., S. A. Tarbell, and R. E. Payne (1981). A compilation of moored instrument data and associated hydrographic observations, Volume XXVIII (POLYMODE LOCAL DYNAMICS EXPERIMENT, 1978-1979).

The MODE Group (1978). The Mid-Ocean Dynamics Experiment. Deep-Sea Research, 25, 859-910.

Neumann, G., and W. J. Pierson (1966). Principles of Physical Oceanography. Prentice-Hall, Inc., New Jersey, 545 pp.

Owens, W. B., and F. P. Bretherton (1978). A numerical study of mid-ocean mesoscale eddies. Deep-Sea Research, 25, 1-14.

Owens, W. B. (1984). A synoptic and statistical description of the Gulf Stream and subtropical gyre using SOFAR floats. Journal of Physical Oceanography, 14(6), 104-113.

Owens, W. B. (1984). A statistical description of the vertical and horizontal structure of eddy variability on the edge of the Gulf Stream recirculation.

Owens, W. B., J. R. Luyten, and H. L. Bryden (1982). Moored velocity measurements on the edge of the Gulf Stream recirculation. Journal of Marine Research, Supplement to 40, 509-524.

Pedlosky, J. (1979). Geophysical Fluid Dynamics. Springer-Verlag, New York, 624 pp.

Rhines, P. B., and W. R. Holland (1979). A theoretical discussion of eddy-driven mean flows. Dynamics of Atmospheres and Oceans, 3, 289-325.

Richardson, P. L. (1983). Eddy kinetic energy in the North Atlantic from surface drifters. Journal of Geophysical Research, 88(C7), 4355-4367.

Richardson, P. L. (1984). Average velocity and transport of the Gulf Stream near 55°W. Journal of Marine Research, submitted.

Richman, J. G., C. Wunsch, and N. G. Hogg (1977). Space and time scales of mesoscale motion in the western North Atlantic. Reviews of Geophysics and Space Physics, 15, 385-420.

Robinson, A. R., D. E. Harrison, Y. Mintz, and A. J. Semtner (1977). Eddies and the general circulation of an idealized oceanic gyre: A wind and thermally driven primitive equation numerical experiment. Journal of Physical Oceanography, 7, 182-207.

Saunders, P. M. and N. P. Fofonoff (1976). Conversion of pressure to depth in the ocean. Deep-Sea Research, 23, 109-111.

Sgouros, T. A., and T. Keffer (1983). The CAMS Interactive Atlas Package. A computerized program for the archiving and presentation of oceanographic data. Technical Report WHOI-83-39.

Schmitz, W. J., Jr. (1976). Eddy kinetic energy in the deep western North Atlantic. Journal of Geophysical Research, 81, 4981-4982.

Schmitz, W. J., Jr. (1977). On the deep general circulation of the western North Atlantic. Journal of Geophysical Research, 81, 4981-4982.

Schmitz, W. J., Jr. (1978). Observations of the vertical distribution of low frequency kinetic energy in the western North Atlantic. Journal of Marine Research, 36, 295-310.

Schmitz, W. J., Jr. (1980). Weakly depth-dependent segments of the North Atlantic circulation. Journal of Marine Research, 38, 111-133.

Schmitz, W. J., Jr. (1981). Observations of eddies in the Newfoundland Basin. Deep-Sea Research, 28, 1417-1421.

Schmitz, W. J., Jr., and W. R. Holland (1982). A preliminary comparison of selected numerical eddy-resolving general circulation experiments with observations. Journal of Marine Research, 40, 75-117.

Tarbell, S. A., A. Spencer, and R. Payne (1978). A compilation of moored current meter and associated oceanographic observations. Vol XXII POLYMODE Array 2 data), Tech. Rep. 78-49, Woods Hole Oceanographic Inst.

Thompson, R.O.R.Y. (1977). Observations of Rossby waves near site D. Progress in Oceanography, 7, 135-162.

Wallace, J. M., and R. E. Dickinson (1972). Empirical orthogonal representation of time series in the frequency domain. Part I: theoretical considerations. Journal of Applied Meteorology, 11, 887-892.

Webster, F. (1965). Measurements of eddy fluxes of momentum in the surface layer of the Gulf Stream. Tellus, 17, 239-245.

Wunsch, C. (1984). On North Atlantic Sverdrup balance. (unpublished manuscript).

Wyrtki, K., L. Magaard, and J. Hager (1976). Eddy energy in the oceans. Journal of Geophysical Research, 81, 2641-2646.

ACKNOWLEDGEMENTS

I would like to thank my advisor, Breck Owens, for his patience in supporting me as a graduate student in the Joint Program. With his direction and encouragement, I have learned the rewards as well as the limitations of oceanographic analyses. This thesis has built on the earlier work of many scientists at WHOI and MIT. Nicholas Fofonoff kindly provided the data for the analysis in Chapter 6. I would especially like to thank the other members of my thesis committee -- Joe Pedlosky, Ed Harrison, and Harry Bryden -- for their many helpful suggestions for improving the clarity of the text and the ideas. Harry Bryden in particular provided many insights and acted as a limitless source of enthusiasm.

Many others contributed to the production of this thesis. Mary Ann Lucas typed the difficult parts of the manuscript. My friends in Cambridge and Woods Hole put up with my complaints and provided a lot of moral support in the home stretch. Finally, I am indebted to my family for their unfailing love and support throughout my years of schooling.

This research has been conducted under NSF contract numbers OCE 77-19403, ATM 79-21431, and OCE 82-00154.